

Tracking Movements of Threatened Migratory *rufa* Red Knots in U.S. Atlantic Outer Continental Shelf Waters



OCS Study
BOEM 2018-046

**US Department of the Interior
Bureau of Ocean Energy Management
Office of Renewable Energy Programs**



Tracking Movements of Threatened Migratory *rufa* Red Knots in U.S. Atlantic Outer Continental Shelf Waters

July 2018

Authors:

Pamela H. Loring, U.S. Fish and Wildlife Service (USFWS), Division of Migratory Birds
James D. McLaren, Environment and Climate Change Canada, Science and Technology Branch
Paul A. Smith, Environment and Climate Change Canada, Science and Technology Branch
Lawrence J. Niles, Conserve Wildlife Foundation of New Jersey
Stephanie L. Koch, USFWS, Eastern Massachusetts National Wildlife Refuge Complex
Holly F. Goyert, University of Massachusetts Amherst, Department of Environmental Conservation
Hua Bai, University of Massachusetts Amherst, Department of Electrical and Computer Engineering

Prepared under BOEM Intra-Agency Agreement No. M16PG00016

By

U.S. Department of Interior
U.S. Fish and Wildlife Service
Division of Migratory Birds
300 Westgate Center Dr.
Hadley, MA 01035



**US Department of the Interior
Bureau of Ocean Energy Management
Office of Renewable Energy Programs**

BOEM
BUREAU OF OCEAN ENERGY MANAGEMENT

DISCLAIMER

This study was funded, in part, by the US Department of the Interior, Bureau of Ocean Energy Management (BOEM), Environmental Studies Program, Washington, DC, through Intra-Agency Agreement Number M16PG00016 with the US Department of Interior, US Fish and Wildlife Service, Division of Migratory Birds, Hadley, MA. This report has been technically reviewed by BOEM, and it has been approved for publication. The views and conclusions contained in this document are those of the authors and should not be interpreted as representing the opinions or policies of the US Government, nor does mention of trade names or commercial products constitute endorsement or recommendation for use.

REPORT AVAILABILITY

To download a PDF file of this report, go to the US Department of the Interior, Bureau of Ocean Energy Management [Data and Information Systems webpage](http://www.boem.gov/Environmental-Studies-EnvData/) (<http://www.boem.gov/Environmental-Studies-EnvData/>), click on the link for the Environmental Studies Program Information System (ESPIS), and search on 2018-046. The report is also available at the National Technical Reports Library at <https://ntrl.ntis.gov/NTRL/>.

CITATION

Loring PH, McLaren JD, Smith PA, Niles LJ, Koch SL, Goyert HF, Bai H. 2018. Tracking movements of threatened migratory *rufa* Red Knots in U.S. Atlantic Outer Continental Shelf Waters. Sterling (VA): US Department of the Interior, Bureau of Ocean Energy Management. OCS Study BOEM 2018-046. 145 p.

ABOUT THE COVER

Cover photo by Yves Aubry, Canadian Wildlife Service.

ACKNOWLEDGMENTS

For study administration, guidance, and oversight, we thank the following individuals from the Bureau of Ocean Energy Management: David Bigger, Mary Boatman, Tim White, Jim Woehr (retired) and Paula Barksdale, as well as Scott Johnston, Caleb Spiegel, and Pamela Toschik from the US Fish and Wildlife Service (USFWS). We thank Annelee Motta, Laurie Racine, and Laurie McDermott (USFWS) administrative support.

Field work at the Mingan Islands, Quebec, Canada, was led by Yves Aubry of the Canadian Wildlife Service, with assistance from Yann Rochepault and Christophe Buidin. We also acknowledge the assistance of numerous volunteers as well as the staff of Parks Canada Agency and the Mingan Islands National Park Reserve. Tagging at James Bay, Ontario, Canada, was led by Christian Friis of the Canadian Wildlife Service, with help from Ross Wood, Allie Anderson, Amie MacDonald, Rod Brook, Sarah Hagey, Bernie McLeod, and numerous volunteers.

For field support with capturing and tagging birds in Massachusetts, we thank Monomoy National Wildlife Refuge staff for equipment and logistical support, and especially Kate Iaquinto for helping to lead the field effort. We also thank our many cooperators who provided landowner permission and field support, including: Towns of Chatham, Orleans, and Eastham; National Park Service; Massachusetts Audubon Society; Goldenrod Foundation; Biodiversity Works; and New England Wildlife Center. We also thank the numerous other USFWS staff and volunteers who assisted with field work and made the capture and tagging efforts a success.

For summer, fall capture and tagging in New Jersey we thank New Jersey Division of Fish and Wildlife especially Amanda Dey, Stephanie Feigin of Conserve Wildlife Foundation, Humphrey Sitters of International Wader Study and Joe Smith. For spring capture and tagging we also thank New Jersey Division of Fish and Wildlife, New Jersey Natural Land Trust, Conserve Wildlife Foundation of New Jersey and the entire Delaware Bay Shorebird Project and the volunteers and groups supporting the project, chief among them Citizens United to Protect the Maurice River. Finally, we thank to Michelle Poulououlos and Joe Atzert for keeping track of the birds and towers.

For field and logistical support with automated radio telemetry towers operated for this study, we thank our many cooperators from following entities: UMass Amherst-USGS Cooperative Fish and Wildlife Unit, USFWS Southern New England-New York Bight Coastal Program, University of Rhode Island, Cape Cod National Seashore, Eastern MA National Wildlife Refuge (NWR) Complex, Waquoit Bay National Estuarine Research Reserve, US Army Corps of Engineers/Cape Cod Canal Field Office, Rhode Island NWR Complex, Shearwater Excursions, Nantucket Islands Land Bank, Nantucket Conservation Foundation, Napatree Point Conservation Area, CT Department of Energy & Environmental Protection, American Museum of Natural History/Great Gull Island Project, Plum Island Animal Disease Center, Block Island Southeast Lighthouse Foundation, Camp Hero State Park, Fire Island National Seashore, Gateway National Recreation Area, Wildlife Conservation Society/New York Aquarium, Rutgers University Marine Field Station, Conserve Wildlife Foundation of New Jersey, New Jersey Division of Fish and Wildlife, Avalon Fishing Club, DE Department of Natural Resources/Cape Henlopen State Park, The Nature Conservancy Virginia Coast Reserve, Chincoteague NWR, Eastern Shore of VA NWR, Back Bay NWR, Diamond Shoals Light Station. We also thank the many partners operating automated radio telemetry stations throughout the Western Hemisphere as part of the Motus Wildlife Tracking System. For technical assistance with data management and analysis, we thank Stu Mackenzie and Zoe Crysler (Motus Wildlife Tracking System, Bird Studies Canada); Phil Taylor and John Brzustowski (Acadia University); Ramakrishna Janaswamy and Paul Sievert (UMass Amherst); and Kaycee Coleman (USFWS).

This study was funded in part by the US Department of the Interior, Bureau of Ocean Energy Management, Environmental Studies Program, Washington DC, through Intra-Agency Agreement Number M16PG00016 with the Department of Interior, Fish and Wildlife Service. Additional funding and in-kind support was provided by the USFWS, CWS-Ontario Region, CWS-Quebec Region, Ontario Ministry of Natural Resources and Forestry, Parks Canada Agency, and Trent University.

Summary

The Bureau of Ocean Energy Management (BOEM) is responsible for managing renewable energy development on the Outer Continental Shelf (OCS) of the United States. The OCS extends from the boundary of each state's jurisdictional waters (generally 3 nautical miles offshore) to the outer boundary of the US Exclusive Economic Zone (approximately 200 nautical miles offshore). In the Atlantic OCS, over 5,596 km² is under lease agreement for development of commercial-scale offshore wind energy facilities and with additional areas in the planning stages for potential lease (BOEM 2017a). Development in the United States to date (April 2018) is limited to a 30-MW, five turbine demonstration-scale facility in state waters off the coast of Block Island, Rhode Island. Herein, BOEM Lease Areas, BOEM Planning Areas, and the Block Island Wind Farm are broadly referred to as Wind Energy Areas (WEAs).

With large areas of the Atlantic OCS under consideration for development of offshore wind energy facilities, information on offshore movements and flight altitudes of high-priority bird species is needed for estimating exposure of birds to collision risks in WEAs and for developing strategies to manage adverse effects (BOEM 2017b). Adverse effects of offshore wind turbines to birds vary by species, and include direct mortality from collisions with infrastructure, and indirect effects of disturbance and habitat loss (Fox et al. 2006). Understanding the species-specific, cumulative adverse effects to bird populations resulting from exposure to multiple, commercial scale wind energy facilities throughout their migratory range will be increasingly important as offshore wind energy development advances in US waters (Goodale and Milman 2016).

This study provides new information on the movements and flight altitudes of a Federally-threatened subspecies, the *rufa* Red Knot (*Calidris canutus rufa*) within the Atlantic OCS. The *rufa* Red Knot is a long-distance migratory shorebird that breeds in Arctic Canada and winters from the coast of the southern United States to southernmost South America. During spring and fall, the *rufa* Red Knot migrates over the Atlantic OCS and uses select stopover sites along the US Atlantic coast to rest and refuel (Burger et al. 2012). More detailed information on the routes, altitudes, timing, and environmental conditions associated with flights over the Atlantic OCS is needed to refine assessments of exposure to offshore WEAs and to improve estimates of collision risk with offshore wind turbines (Burger et al. 2011, Gordon and Nations 2016, O'Connell et al. 2011).

In this study, *rufa* Red Knots (n=388) were fitted with digital VHF transmitters at major stopover areas in Canada and the US Atlantic coast during southbound migration. Tagged Red Knots were tracked using an array of automated radio telemetry stations within a Study Area encompassing a portion of the US Atlantic, extending from Cape Cod, Massachusetts to Back Bay, Virginia. We developed novel movement modeling techniques to assess the frequency and extent of offshore movements over Federal waters and WEAs within the Study Area. Our specific objectives were to: 1) develop spatially-explicit, 3-dimensional models of *rufa* Red Knot movements; 2) estimate the exposure of *rufa* Red Knots to each WEA within the Study Area during southbound migration; 3) assess WEA exposure and migratory departure movements into Federal waters relative to meteorological conditions (e.g. wind speed, wind direction, barometric pressure, temperature, visibility, precipitation), temporal effects (time of day, date) and demographic factors (age, sex).

Red Knots tagged within the Study Area had a high likelihood of being detected in the receiver array (>75%), demonstrating that tag loss and tag failure rates were low. Despite this, only 3-22% of birds tagged at stopover sites in Canada (James Bay and Mingan Islands) were detected within the Study Area, and only two individuals tagged in Canada were exposed to WEAs while transiting the Study Area. The James Bay and Mingan Islands stopover sites collectively may harbor up to a third of the *rufa* population,

and that only a small portion of these populations used the US Atlantic Coast during southbound migration suggests that this segment of the population had relatively low exposure to WEAs in the US Atlantic OCS in 2016.

Comparatively, 54% of birds tagged in Massachusetts and New Jersey stopover areas were detected passing through Federal waters of the Atlantic OCS in the Study Area, and 11% were exposed to one or more WEAs both during shorter-distance flights on staging grounds and longer-distance migratory movements. For Red Knots tagged in Massachusetts, flights across WEAs largely occurred during November, when seven individuals departed from staging areas on Cape Cod and flew southwest across the mid-Atlantic Bight. Five Red Knots tagged in New Jersey departed in late August and flew directly offshore to WEAs in adjacent Federal waters. Two individuals departed from New Jersey in November and followed a more coastal route that intersected with WEAs in Delaware, Maryland, and/or Virginia. During fall migration, flights across WEAs occurred primarily at night during favorable weather conditions (little to no precipitation, moderate winds, clear skies). The majority (77%) of flights across WEAs were estimated to have occurred in the rotor swept zone of offshore wind turbines (20 to 200 m), with a mean altitude of 106 m (range 22 m to 882 m). However, these estimates were subject to large error bounds (typically 100 to 200 m) and should be interpreted with caution.

A total of 59 Red Knots tagged at staging areas in Massachusetts and New Jersey were tracked by the array in migration over Federal waters. Offshore migratory departures primarily occurred within several hours of civil dusk, with a smaller peak close to dawn. Most adult birds migrated earlier (mid-August), relative to juveniles, who all migrated in mid-November. Departures into Federal waters were associated with stronger winds blowing towards the south, corresponding with conditions for a supporting tailwind in flight. As with WEA exposure events, migratory departures into Federal waters occurred during good weather conditions, including clear skies, moderate wind speeds, and little to no precipitation.

In this study, digital VHF telemetry was an effective method of tracking small bodied birds at local to regional spatial scales. However, there exist tradeoffs in the design of automated radio telemetry station arrays to maximize the detection or resolution of movement patterns, and these tradeoffs vary by species, geographic area, and study objective. Estimating bird locations through triangulation of the detecting towers requires strategic placement of towers at relatively high densities in areas of high ecological importance. Along straight coastlines that lack islands or peninsulas, we recommend assembling towers on offshore infrastructure, such as buoys or wind turbines, where possible. The geographic coverage and scope of digital VHF telemetry can be further extended through the coordinated efforts of the Motus Wildlife Tracking System. Future studies have the potential to integrate this network with other forms of developing technology (e.g. radar, high definition imagery) for collecting detailed movements of birds in offshore environments.

Key findings:

- Of the 388 tagged birds, 8% were detected passing through one or more WEAs during fall migration.
- During fall migration, flights across WEAs occurred under clear skies with little to no precipitation.
- Most birds departed on migration prior to dusk and crossed offshore WEAs at night. The majority of tagged adults migrated in early fall, with lesser numbers migrating in late fall. All tagged hatch year birds migrated during late fall.
- Three quarters of the flights across WEAs were within rotor swept zone (20 to 200 m) of a wind turbine; however, the error around the estimated flight heights was very large (typically 100 to 200 m).

- Birds departing to the southeast from stopover areas in Massachusetts, USA are most likely traveling to South America, while birds departing to the southwest are most likely traveling shorter distances to more northerly wintering areas such as the southeast US coast and/or the Caribbean.

Contents

Summary.....	i
List of Figures.....	vii
List of Tables.....	x
List of Abbreviations and Acronyms.....	xi
1 Introduction	1
1.1 The <i>rufa</i> Red Knot: Population Trends and Threats	2
1.2 Migration Routes of the <i>rufa</i> Red Knot.....	3
1.3 Risk Assessments of Offshore Wind Energy	4
1.4 VHF Technology to Study Movements	5
2 Methods	7
2.1 Study Area.....	7
2.2 Study Species	9
2.3 Digital VHF Transmitters	9
2.4 Capture and Tag Attachment Summaries by Site.....	9
2.5 Capture and Tag Deployment	11
2.6 Automated Radio Telemetry Stations	14
2.7 Frequency Coordination	16
2.8 Post-processing of Telemetry Data.....	17
2.9 Movement Models	17
2.9.1 Background and Motivation of Approach	17
2.9.2 Formulation	21
2.9.3 Near-simultaneous Detections	21
2.9.4 Single Detections	22
2.9.5 Determination of Non-stop Flight	22
2.9.6 Behavioral Flight Constraints	23
2.9.7 Temporal Interpolation Using Brownian Bridge Movement Model.....	23
2.9.8 Calibration and Validation	23
2.9.9 Including Sensor-gnome Receiving Stations	27
2.10 Assessment of Occurrence in Federal Waters and WEAs	27
2.11 Meteorological Conditions.....	27
2.12 Covariate Analysis of Exposure to WEAs	28
2.13 Covariate Analysis of Migratory Departures into Federal Waters.....	29
3 Results	30

3.1	Movement Model.....	30
3.2	Probability of Detection	31
3.3	Demographic Variation in Movements and WEA Exposure Summary	32
3.3.1	James Bay, Canada.....	32
3.3.2	Mingan Islands, Canada	33
3.3.3	Massachusetts, USA.....	33
3.3.4	New Jersey, USA	34
3.4	Timing, Meteorological Conditions, Altitude of Flights Across Offshore WEAs	36
3.4.1	Temporal Variation	36
3.4.2	Meteorological Conditions	37
3.4.3	Altitude of Flights Across WEAs.....	43
3.5	Covariate Analysis of Migratory Movements in Federal Waters	45
3.5.1	Temporal, Demographic, and Meteorological Variation.....	45
3.5.2	Multivariate Boosted GAM Analysis	54
3.5.3	Effects of Temperature, Pressure, Visibility and Precipitation	55
3.5.4	Altitude of Migratory Departure Flights Over Federal Waters.....	60
4	Discussion.....	61
4.1	Movement Models.....	61
4.2	Demographic Variation in Movements and WEA Exposure	62
4.3	Timing, Meteorological, Conditions, and Altitude of Flights Across Offshore WEAs	64
4.3.1	Timing.....	64
4.3.2	Meteorological Conditions	64
4.3.3	Altitude	64
4.4	Covariate Analysis of Migratory Movements in Federal Waters	67
4.4.1	Temporal, Spatial, and Demographic Variation	67
4.5	Meteorological Conditions.....	67
5	Future Directions.....	68
6	References.....	72
7	Appendix A. Metadata for all Red Knots included in this study.	79
8	Appendix B. Metadata for BOEM automated radio telemetry stations in 2016	81
9	Appendix C. Detection probability of BOEM automated radio telemetry stations	83
10	Appendix D: Summary of data from nano-tagged birds that were tagged by partners in the Motus network and detected by BOEM radio telemetry stations in 2016.....	88
11	Appendix E. Summary of geospatially referenced detection data from all Red Knots in this study submitted to BOEM as a supplemental material to this report.....	94

12	Appendix F. Maps of flights that intersected one or more WEAs in Atlantic OCS. Inset plots show estimated altitude (pts) and error quartiles (bars, in m) over time (in min, Eastern Standard Time) during WEA exposure event. Shading shows altitude range in Rotor Swept Zone of offshore wind turbines (20 to 200 m).	96
13	Appendix E. Summary of supplemental data from Red Knots tagged during spring of 2016 in Delaware Bay, USA	124
13.1	Tag deployment and movement summaries	124
13.2	Discussion	125

List of Figures

Figure 1. Map of the 2016 study area extending from Cape Cod, MA and to the southern border of VA... 8	8
Figure 2. Map showing locations of Red Knot tagging sites and active automated radio telemetry stations in eastern North America in 2016	10
Figure 3. Photos of Red Knot capture and transmitter deployment.....	14
Figure 4. Automated radio telemetry station on Nantucket NWR (Great Point), Nantucket, MA	15
Figure 5. Radiation pattern of antenna beam	19
Figure 6. Results of model calibration survey conducted during September 2014 adjacent to two automated radio telemetry towers on Monomoy NWR, MA, USA	25
Figure 7. Model estimated mean and standard deviation of altitude (m, ASL) over time (min) of VHF-tagged kite during September 2014 calibration survey.....	26
Figure 8. Frequency distribution of estimated flight altitudes.....	31
Figure 9. Detection probability of kite in relation to receiver location and transmitter alignment.....	32
Figure 10. Frequency distribution in calendar of WEA exposure events (n=26) in 2016 by location of tag deployment.....	36
Figure 11. Diel variation (hrs, in EST) in timing of WEA exposure events (n=26), categorized by daylight using timing of local sunrise and sunset	37
Figure 12. Frequency distribution of wind speed (m/s) during WEA exposure events (n=26)	38
Figure 13. Circular histogram of wind direction (degrees clockwise from N)) during WEA exposure events (n=26), by location of tag deployment.....	39
Figure 14. Frequency distribution of wind support (m/s) during WEA exposure events (n=26)	40
Figure 15. Frequency distribution of crosswind (m/s) during WEA exposure events (n=26).....	40
Figure 16. Frequency distribution of visibility (m) during WEA exposure events (n=26)	41
Figure 17. Frequency distribution of barometric pressure (Pa) during of WEA exposure events (n=26) ...	41
Figure 18. Frequency distribution of precipitation air temperature (K) during of WEA exposure events (n=26).....	42
Figure 19. Frequency distribution of precipitation accumulation (kg/m ²) during of WEA exposure events (n=26).....	42
Figure 20. Frequency distribution of model-estimated altitude (m) during WEA exposure events (n=26). 44	44
Figure 21. Frequency distribution of uncertainty (interquartile range) of altitude estimates (m) during WEA exposure events (n=26).	44
Figure 22. Diel variation (hrs, in EST) in timing of migratory initiation for flights (n=59) into Federal waters of the Study Area	46

Figure 23. Demographic variation in dates of migratory initiation for flights (n=59) into Federal waters of the Study Area	47
Figure 24. Distributions of meteorological and temporal covariates	48
Figure 25. Angular distribution of track directions (degrees clockwise from N).....	49
Figure 26. Angular distribution of track directions (degrees clockwise from N).....	50
Figure 27. Distributions of meteorological conditions and day of year among staging locations (at civil dusk and dawn) versus initiation of migratory departure flights into Federal waters	52
Figure 28. Predicted influence of covariates on relative likelihood of initiating migratory flights into Federal waters	56
Figure 29. Predicted strength of marginal response to covariates in increasing likelihood of migratory departure into Federal waters	57
Figure 30. Predicted strength of marginal response to covariates in increasing likelihood of migratory departure into Federal waters by AHY females.	58
Figure 31. Predicted strength of marginal response to covariates in increasing likelihood of migratory departure into Federal waters among AHY males	59
Figure 32. Predicted strength of marginal response to covariates in increasing likelihood of migratory departure into Federal waters among HY individuals	60
Figure 33. Predicted flight altitudes on initiation of migratory flights over Federal waters (n=59).	61
Figure 34. Distribution of flight height by taxa for 225 observations of shorebirds recorded during offshore surveys in the US Atlantic, from 2003 to 2017.....	66
Figure 35. Block Island offshore wind turbines	71
Figure C-1. Two-dimensional radiation pattern of 9-element Yagi antenna	84
Figure C-2. Coverage map from 2016 BOEM-funded towers showing the probability of detecting a bird flying at (a) 20m, (b) 200m, or (c) 1000m.	87
Figure F-1. Estimated flight path of Red Knot ID 316, Hatch Year (HY) male, tagged in the Mingan Islands, Canada.	98
Figure F-2. Estimated flight path of Red Knot ID 328, After Hatch Year (AHY) male, tagged in the Mingan Islands, Canada.	99
Figure F-3. Estimated flight path of Red Knot ID 471, HY female, tagged in Massachusetts, USA.....	100
Figure F-4. Estimated flight path of Red Knot ID 464, SY female, tagged in Massachusetts, USA.....	100
Figure F-5. Estimated flight path of Red Knot ID 453, SY female, tagged in Massachusetts, USA.....	101
Figure F-6. Estimated flight path of Red Knot ID 453, SY female, tagged in Massachusetts, USA.....	102
Figure F-7. Estimated flight path of Red Knot ID 453, SY female, tagged in Massachusetts, USA.....	103
Figure F-8. Estimated flight path of Red Knot ID 453, SY female, tagged in Massachusetts, USA.....	104

Figure F-9. Estimated flight path of Red Knot ID 434, Second Year (SY) female, tagged in Massachusetts, USA.....	105
Figure F-10. Estimated flight path of Red Knot ID 454, SY male, tagged in Massachusetts, USA.....	106
Figure F-11. Estimated flight path of Red Knot ID 437, SY male, tagged in Massachusetts, USA.....	107
Figure F-12. Estimated flight path of Red Knot ID 449, SY female, tagged in Massachusetts, USA.....	108
Figure F-13. Estimated flight path of Red Knot ID 449, SY female, tagged in Massachusetts, USA.....	109
Figure F-14. Estimated flight path of Red Knot ID 470, HY female, tagged in Massachusetts, USA.....	110
Figure F-15. Estimated flight path of Red Knot ID 470, HY female, tagged in Massachusetts, USA.....	111
Figure F-16. Estimated flight path of Red Knot ID 458, HY female, tagged in Massachusetts, USA.....	112
Figure F-17. Estimated flight path of Red Knot ID 458, HY female, tagged in Massachusetts, USA.....	113
Figure F-18. Estimated flight path of Red Knot ID 458, HY female, tagged in Massachusetts, USA.....	114
Figure F-19. Estimated flight path of Red Knot ID 451, SY male, tagged in Massachusetts, USA.....	115
Figure F-20. Estimated flight path of Red Knot ID 451, SY male, tagged in Massachusetts, USA.....	116
Figure F-21. Estimated flight path of Red Knot ID 47, age and sex unknown, tagged in New Jersey, USA.	117
Figure F-22. Estimated flight path of Red Knot ID 101, AHY male, tagged in New Jersey, USA.	118
Figure F-23. Estimated flight path of Red Knot ID 478, AHY female, tagged in New Jersey, USA.	119
Figure F-24. Estimated flight path of Red Knot ID 48, HY female, tagged in New Jersey, USA.....	120
Figure F-25. Estimated flight path of Red Knot ID 48, HY female, tagged in New Jersey, USA.....	121
Figure F-26. Estimated flight path of Red Knot ID 47, age and sex unknown, tagged in New Jersey, USA.	122
Figure E-1. Estimated flight path of Red Knot ID 310 (AHY, unknown sex), tagged in Delaware Bay, USA during May 2016.	127
Figure E-2. Estimated flight path of Red Knot ID 354 (AHY, unknown sex), tagged in Delaware Bay, USA during May 2016.	128
Figure E-3. Estimated flight path of Red Knot ID 354 (AHY, unknown sex), tagged in Delaware Bay, USA during May 2016.	129
Figure E-4. Estimated flight path of Red Knot ID 169 (AHY, unknown sex), tagged in Delaware Bay, USA during May 2016.	130

List of Tables

Table 1: Model workflow: steps 1-3 govern localization estimation, step 4 interpolates covariate data, and step 5 estimates exposure to Federal waters and WEAs	20
Table 2. The number of VHF-tagged Red Knots that were detected crossing each BOEM Lease Area and BOEM Planning Area by tagging site during fall migration 2016. Sample size (N) of birds tagged at each site appears in top row.	35
Table 3. Summary statistics of meteorological conditions during WEA exposure events (n=26) for Red Knots tracked during fall migration 2016.....	43
Table 4. Summary of meteorological covariates by demographic cohort among migratory departures into Federal waters.	51
Table 5. Summary of meteorological covariates among migratory departures into Federal waters versus staging locations (twice-daily) at civil dawn and dusk.....	53
Table D-1. Total number of nano-tagged individuals per species detected by BOEM-funded radio telemetry stations in 2016, including sex and age data where available	89
Table D-2. Projects with nano-tagged birds detected by BOEM radio telemetry array in 2016.	91

List of Abbreviations and Acronyms

AHY	After Hatch Year
ASY	After Second Year
asl	above sea level
EST	Eastern Standard Time
OCS	Outer Continental Shelf
BOEM	Bureau of Ocean Energy Management
dBm	decibel-milliwatts
DOI	US Department of the Interior
ESA	US Endangered Species Act
ESP	Environmental Studies Program
GMT	Greenwich Mean Time
GW	gigawatts
ft	foot/feet
BGAM	Boosted Generalized Additive Model
HY	Hatch Year
K	Kelvin
kg	kilogram
km	kilometer
m	meter
MBTA	Migratory Bird Treaty Act
min	minute(s)
Motus	Motus Wildlife Tracking System
MW	megawatts
NARR	North American Regional Reanalysis
NEPA	National Environmental Policy Act
NWR	National Wildlife Refuge
Pa	Pascal
PI	Principle Investigator
PO	Project Officer
SD	Standard Deviation
SY	Second Year
US	United States
USFWS	US Fish and Wildlife Service
USGS	US Geological Survey
UTM	Universal Transverse Mercator
VHF	Very High Frequency
WEA	Wind Energy Area

1 Introduction

The Bureau of Ocean Energy Management (BOEM) is responsible for managing energy and mineral resources on the Outer Continental Shelf (OCS) of the United States. The OCS extends from the outer limit of each state's jurisdictional waters (approximately 3 nautical miles or 5.6 km offshore) to the outer limit of the US Exclusive Economic Zone (approximately 200 nautical miles or 370 km offshore).

Since 2009, BOEM's Office of Renewable Energy Programs has issued thirteen commercial wind energy leases and one research lease in the Atlantic OCS, from Nantucket Sound, MA to waters offshore of North Carolina, totaling approximately 5,566 km². Assuming a standard capacity density of 3 megawatts (MW)/km², this equates to 17.6 gigawatts (GW) of potential capacity (Musial et al. 2017). Additional areas offshore of New York (166 km²), Massachusetts (1,572 km²), North Carolina (750 km²), and South Carolina (4,002 km²) are in the planning stages for future designation as lease areas (BOEM 2017a, Musial et al. 2017). Herein, Wind Lease Areas and Wind Planning Areas are collectively referred to as Wind Energy Areas (WEAs).

Concurrently, several Atlantic coast states are developing plans to site additional wind energy facilities within their jurisdictional waters. The first offshore wind energy facility in the US, consisting of 5 turbines (30-MW) within state waters off the coast of Block Island, RI, officially began operation in December of 2016. Additional areas have been leased in state waters within Maine (Department of Energy's Advanced Technology Demonstration Program) and New Jersey (Atlantic City Windfarm). Several states have passed legislative requirements for power purchase agreements to procure energy from offshore wind (e.g., 5 GW capacity by 2030 in Maine, 1.6 GW capacity by 2027 in Massachusetts, 2.4 GW capacity by 2030 in New York, 1.1 GW capacity by 2028 in New Jersey), or to mandate that a proportion of electricity come from renewable sources (e.g., 25% by 2025 in New Hampshire, 38.5% by 2035 in Rhode Island, 25% by 2025 in Delaware, 25% by 2020 in Maryland, 15% by 2025 in Virginia, 12.5% by 2021 in North Carolina; Musial et al. 2017).

With large areas of the Atlantic coast and OCS under consideration for development, both site specific and regional-scale studies are critical for understanding potential exposure of migratory birds to WEAs (BOEM 2017b). Current understanding of the effects of offshore wind turbines on birds comes primarily from studies in western Europe, where large-scale offshore wind energy facilities have been in operation for over a decade (Langston 2013). These studies have broadly categorized adverse effects to birds from offshore wind turbines as: 1) acting as barriers to movement (e.g. between foraging and roosting sites, along migration routes); 2) destruction, modification, or displacement of habitat; and 3) direct mortality from collisions with infrastructure or pressure vortices (Drewitt and Langston 2006, Exo et al. 2003, Fox et al. 2006). However, the magnitude of these effects are highly species and site specific, highlighting the importance of conducting fine-scale movement studies on priority species in areas of wind energy potential (Furness et al. 2013, Green et al. 2016).

In the Federal waters of the US, evaluations of the potential effects of development on migratory birds and their habitats are conducted in accordance with the National Environmental Policy Act (NEPA) and the Migratory Bird Treaty Act (MBTA). In addition, information regarding potential adverse effects to

species listed as “Threatened” or “Endangered” under the US Endangered Species Act (ESA) is needed for risk assessments and Section 7 consultations between BOEM and the USFWS.

Preliminary assessments have identified three ESA-listed bird species that occur in the Atlantic OCS and could be adversely affected by wind energy development: the Roseate Tern (*Sterna dougallii*) of the Federally-Endangered northeastern US breeding population, the Piping Plover (*Charadrius melodus*) of the Federally-Threatened US Atlantic coast breeding population, and the Red Knot (*Calidris canutus rufa*) of the Federally-Threatened *rufa* subspecies that is the focus of the present study (Burger et al. 2011, O’Connell et al. 2011). The *rufa* Red Knot is a long-distance migratory shorebird that occurs along the US Atlantic coast and OCS during spring and fall migration between breeding areas in the Canadian Arctic and non-breeding areas that extend to southern latitudes of South America (Burger et al. 2011). It was listed as “Threatened” under the ESA in 2014 (USFWS 2014) and is also listed as “Endangered” under Canada’s Federal Species at Risk Act (Environment and Climate Change Canada 2016).

1.1 The *rufa* Red Knot: Population Trends and Threats

The ESA listing of the *rufa* Red Knot was based on a series of significant declines in abundance between the 1980s and the early 2000s. This loss was first observed at the species’ primary stopover site at Delaware Bay, where numbers estimated by aerial surveys peaked at 91,000 (Clark et al. 1993), fell to less than 50,000 by 2001 then finally to a low of 15,000 in 2005 (Niles et al. 2008). This trend was mirrored by large declines at the principal wintering areas in Tierra del Fuego, including Bahía Lomas, Chile, and Rio Grande, Argentina (Morrison and Ross 1986, Morrison et al. 2005).

Population declines of the *rufa* Red Knot coincided with a decline of foraging conditions at the Delaware Bay stopover site, where the densities of horseshoe crab (*Limulus polyphemus*) eggs, a primary food at stopover, have declined due to harvest pressure that intensified in the mid-1990s (Atlantic States Marine Fisheries Commission 2016, Smith et al. *in prep*). Although harvests have since been curtailed, the current population of horseshoe crabs is still only a third of carrying capacity (McGowan et al. 2011). Using band-resighting data, Baker et al. (2004) demonstrated that a decline in rates of mass gain in Delaware Bay was associated with a reduced apparent survival rate, potentially linking the population declines to failing foraging conditions at the Delaware Bay stopover site. In a subsequent study, Duijns et al. (2017) used digital VHF telemetry to demonstrate that Red Knots leaving Delaware Bay with low body condition have reduced migratory performance, and potentially a lower likelihood of breeding and surviving through to fall migration.

Throughout its hemispheric range, the species is exposed to additional threats including: shorebird hunting in the Leeward islands of the Caribbean and northern South America (especially French Guiana and Brazil), disturbance by humans at all southbound stopovers in the US (Burger and Niles 2013) and northbound stopovers in South America (Fedrizzi 2008), and habitat loss in areas such as San Antonio Este and Rio Grande, Argentina (P. González pers. comm.), Florida’s gulf coast (Niles et al. 2006), and Lagoa do Peixe, Brazil. Climate change represents another potential threat, with impacts that remain largely unknown. Red Knot’s subtropical wintering areas and Arctic breeding areas are more than 10,000 km apart, so asynchronies resulting from climate change are nearly inevitable. Whether timing of breeding “mismatch” is hampering reproductive success remains unknown. Potentially significant habitat

shifts in Arctic breeding areas, as a consequence of future climate change, have been demonstrated by Lathrop et al. (2016). Moreover, many of the climate-related threats to Red Knots observed to date were unexpected, such as the delayed spawning of horseshoe crabs resulting from unusually cool bay water temperature (Smith *pers. comm.*), that limits egg availability during the brief migration period. The full impacts of climate change on Red Knot populations are difficult to measure and predict.

The risk of mortality or disturbance to *rufa* Red Knots from the development of wind energy facilities in coastal and offshore areas is not well understood. Although Red Knots pass over several existing onshore wind facilities during migration (Diffendorfer et al. 2017), there are no records of knots colliding with turbines. Similarly, in a study of 177 bird species that use the Atlantic OCS, the Red Knot was among 72 species with a “Medium Collision Sensitivity” to offshore wind turbines, based on assumptions about its flight behavior and basic population parameters (Robinson Willmott et al. 2013). However, carcass surveys may greatly underestimate turbine mortality (Huso 2010, Kerns et al. 2005, Korner-Nievergelt et al. 2011), and unknown flight parameters for Red Knots and other shorebirds mean that assessments of collision risk based on literature values have substantial uncertainty. For example, the assignment of “Medium Collision Sensitivity” for Red Knots in Robinson Willmott et al. (2013) is based in part on an assumption of <5% of time spent in the rotor swept zone (while in the Atlantic OCS), with “supporting evidence sparse or absent”. Moreover, even modest mortality risks must be identified for an ESA-listed species like the Red Knot. The degree of Red Knot exposure to risk from wind energy facilities depends on the flight behavior and routes taken during migration, both of which can vary over time and among individuals.

1.2 Migration Routes of the *rufa* Red Knot

The Red Knot is well known for its long migration between breeding and wintering areas. However, recent studies using tracking technologies demonstrate a highly variable migratory ecology, influenced by individuals’ body condition and weather (Duijns et al. 2017). Most *rufa* Red Knots nest in the Canadian Arctic Archipelago, from northern Baffin Island to Victoria Island, with the highest densities on Southampton and King William Islands (Niles et al. 2009). After nesting, the timing of departure from the breeding site depends on sex (females leave first in mid-July), age (juveniles leave in late August), and breeding success (failed breeders leave in early to mid- July, while successful breeders remain until late July or August; Harrington 2001). The routes taken to exit the breeding grounds are fairly well described, with most birds flying through stopovers on Hudson Bay, Manitoba, and James Bay, Ontario, or through the Mingan Archipelago, Quebec (Morrison and Harrington 1992). From these key northern stopovers, Red Knots flying to different wintering areas use different routes. Birds from each wintering area are physiologically and morphologically distinct.

Red Knots traveling the longest distances to winter in Tierra del Fuego (Chile and Argentina), as well as those traveling mid-distances to winter in northern Brazil, must significantly increase their mass before departure from the northern stopovers. These individuals will retain their flight feathers until arrival in their respective wintering areas (Sitters 2017). Red Knots traveling the shortest distances (wintering in the southeastern US and the Caribbean Islands) maintain relatively low weights and initiate molt earlier (Harrington et al. 2010, Niles et al. 2006).

All three groups use the northern stopovers in James Bay and Mingan Islands, Canada, as well as more southerly stopovers including Cape Cod, Massachusetts, and Stone Harbor, Avalon and Brigantine Islands, New Jersey, but in different proportions and at different times. Those Red Knots using the Mingan Islands will primarily migrate long-distances to winter in South America. They begin to arrive at the stopover in mid-July and most have left by early October (Buidin et al. 2010). Juveniles can occur as late as early November, although cold weather usually decreases habitat suitability before then. At Cape Cod, Massachusetts, a large number of Red Knots occur in the USFWS Monomoy Refuge (Harrington et al. 2012) and nearby areas. Red Knots at this site may migrate long, mid, or short distances to winter in any of the three regions. They begin to arrive to Cape Cod in mid-July, and the long and mid-distance migrants typically leave before mid-September. The short-distance migrants, along with the juveniles, linger in the area until at least early November when cold weather diminishes the stopover's suitability. The key fall stopovers in New Jersey are similar to those in Massachusetts, except that a later onset of harsh winter weather allows short-distance migrants and juveniles to linger into January in some years (A. Dey *pers. comm.*).

The three segments of the *rufa* population, the long, mid, and short-distance migrants, display strikingly different migratory behavior. The following discussion is based on results from recaptured geolocators reported in Niles et al. (2010) and Burger et al. (2012a, 2012b), as well as previously unpublished geocator tracking data. During southward migration, most Red Knots make their first stop at Hudson or James Bay, or to a lesser extent, the Mingan Islands. After leaving these northern stopovers, some individuals fly directly to their respective wintering areas, although many will make a stop along the Atlantic coast of the United States. Short distance migrants typically fly along the Atlantic coastline to winter in areas as far north as Maryland and as far south as the Venezuelan coast. Large numbers of these wintering short-distance migrants occur on the Gulf and Atlantic Coasts of Florida, as well as Georgia (Niles et al. 2006, Lyons 2017). Long-distance and mid-distance migrants typically fly directly from Mingan Islands, Cape Cod, or Atlantic New Jersey stopovers to their wintering grounds in South America (Morrison and Ross 1986, Morrison et al. 2004, Niles and Aubry 2014).

1.3 Risk Assessments of Offshore Wind Energy

Assessments from conceptual risk models and tracking data from geocator studies indicate that offshore wind facilities on the Atlantic OCS may pose some risk to Red Knots during migration (Burger et al. 2011, Burger et al. 2012). These assessments indicated that exposure to offshore wind energy facilities may be highest in waters south of Cape Cod, MA, in the fall, and from Delaware Bay to North Carolina during spring (Normandeau Associates 2011). However, because geolocators record only two locations per day and are routinely subject to errors of >100 km, these devices do not offer the high spatiotemporal resolution required to track movements across specific lease areas. Geolocators also do not provide direct estimates of altitude, which is needed to determine if Red Knots that are crossing the Atlantic OCS are within the rotor swept zone of offshore wind turbines (typically 20 to 200 m; Burger et al. 2011). Therefore, more detailed data on migratory routes and flight altitudes of Red Knots in the Atlantic OCS are needed to improve estimates of exposure to offshore WEAs. Wind and weather conditions play a crucial role in the migratory performance of *rufa* Red Knots (Duijns et al. 2017), and flight altitudes might vary with weather as birds search to find suitable tailwinds (Shamoun-Baranes et al. 2010). Altitude may also depend on the length of the flight and distance from shore. Offshore radar studies have

recorded Red Knots and other species of shorebirds migrating at altitudes exceeding 1 to 2 km (Richardson 1976, Williams and Williams 1990), whereas nearshore studies documented local and migratory flights of shorebirds occurring at altitudes <100 m (Dirksen et al. 2000).

However, few direct measurements of flight altitudes are available for Red Knots (O'Connell et al. 2011). Red Knots flying at migratory altitudes are likely to be above the rotor swept zone, but they may occur within rotor swept altitudes during ascent or descent from long distance flights or during short distance flights between coastal areas used for feeding and roosting (Burger et al. 2011, Burger et al. 2012, this study). Although not directly observed for Red Knots, migratory birds may also descend into the rotor swept zone during periods of limited visibility, low cloud ceiling, and/or inclement weather (Langston et al. 2004, Hüppop et al. 2006). In addition, for other species, the risk of collision with offshore wind turbines was elevated during night or other periods of low visibility (Dirksen et al. 2000), or inclement weather conditions such as fog, precipitation, or high wind speeds (Exo et al. 2003). Therefore, information on movement patterns of Red Knots in relation to diel variation and meteorological conditions is needed to improve assessments of collision risk (Gordon and Nations 2016).

1.4 VHF Technology to Study Movements

For relatively small-bodied species such as the Red Knot, VHF technology remains one of the sole options for tracking movements of individuals at high spatial and temporal resolution over extended durations, with heavier (>2 g) units capable of operating for multiple years. Conventional VHF telemetry has been a standard technique in wildlife tracking studies for decades (Cochran et al. 1965) and involves affixing individuals with lightweight radio transmitters (minimally <1 g), and tracking their signals with specialized antennas and receiving units (Kenward 1987). Conventional VHF technology is based on a system where each transmitter operates on a unique frequency and receivers are programmed to cycle through frequencies sequentially, resulting in a trade-off between overall sample size and detection probability of individual transmitters (Kenward 1987).

Recent advances in the development of digital VHF technology now make it possible to simultaneously monitor thousands of uniquely coded transmitters on a single VHF frequency (Taylor et al. 2017). The use of digital VHF transmitters with automated radio telemetry stations allows large numbers of individuals to be monitored continuously and autonomously. Configurations of automated radio telemetry stations are customizable and thus vary widely, but in general consist of one or more receiving antennas elevated on a structure (typically a stand-alone mast) and connected to an automated receiving unit that records detection data from all transmitters within range of the station (typically within 15 km; Taylor et al. 2017). Detection range of automated radio telemetry stations generally increases with the height and gain of the transmitting and the receiving antennas (Cochran 1980), and since VHF waves emitted by transmitters travel within line-of-sight, factors such as topography, vegetation, and electronic noise may block, reflect, or attenuate the signal (Kenward 1987).

In 2013, a pilot study was initiated to test digital VHF technology for tracking shorebirds and terns offshore (Loring et al. 2017). Between 2013 and 2015, an array of 22 automated radio telemetry stations was established at key coastal and island sites distributed from Cape Cod, Massachusetts to Long Island, New York. Sites were selected that were: 1) in close proximity to key areas used by focal species within

the Study Area; 2) adjacent to BOEM Lease Areas and Planning Areas within the Study Area; 3) in direct line of sight to offshore waters to maximize reception; 4) within detection range of one or more adjacent towers to facilitate triangulation, a technique to estimate 2-dimensional (x, y) animal locations using signal strength and bearings from signals received by directional antennas from multiple towers simultaneously.

This effort is conducted in partnership with Motus Wildlife Tracking System (Motus; www.motus.org), a collaboration of researchers using digital VHF transmitters and automated radio telemetry stations to track the movements of birds and bats from the Canadian High Arctic to South America. Motus provides a system to coordinate data sharing among automated radio telemetry studies on a common frequency, allowing all tagged individuals to be detected by all stations in the network (Taylor et. al 2017). In 2016, the Motus network included over 300 automated radio telemetry stations distributed across the western Hemisphere that were operated in collaboration among 120 different research efforts (Taylor et al. 2017).

Our current study builds on the success of the Motus network and previous work by expanding the telemetry array to include 10 new stations along the mid-Atlantic coast, and by tagging *rufa* Red Knots at fall migratory stopover sites that are adjacent to WEAs in Federal waters off the coasts of Massachusetts and New Jersey. In partnership with Environment and Climate Change Canada, and with data coordination through Motus, our analysis also includes tracking data from Red Knots captured at two major fall staging sites (James Bay, Ontario, Canada and the Mingan Archipelago, Quebec, Canada) for *rufa* Red Knots that collectively hold a large proportion of the population. This partnership therefore provides us with an opportunity to examine movements of *rufa* Red Knots that are more randomly sampled from the population, augmenting our sample of *rufa* Red Knots that are captured near the US Atlantic OCS.

The aim of this expanded work is to provide a spatially-explicit, empirical assessment of the degree to which Red Knots use targeted areas of the Atlantic OCS, from Cape Cod, MA to coastal VA, that are under consideration for the development of offshore wind energy facilities. As part of this study, we expanded upon existing, 2-dimensional movement modeling techniques developed for our pilot work with Common Terns (Janaswamy et al., *in review*) to include estimates of altitude when signals are received simultaneously by multiple receiving stations. We then assess offshore movements relative to meteorological, temporal, and demographic covariates to address key information gaps and inform future collision risk and exposure assessments of *rufa* Red Knots to offshore WEAs in the Atlantic OCS.

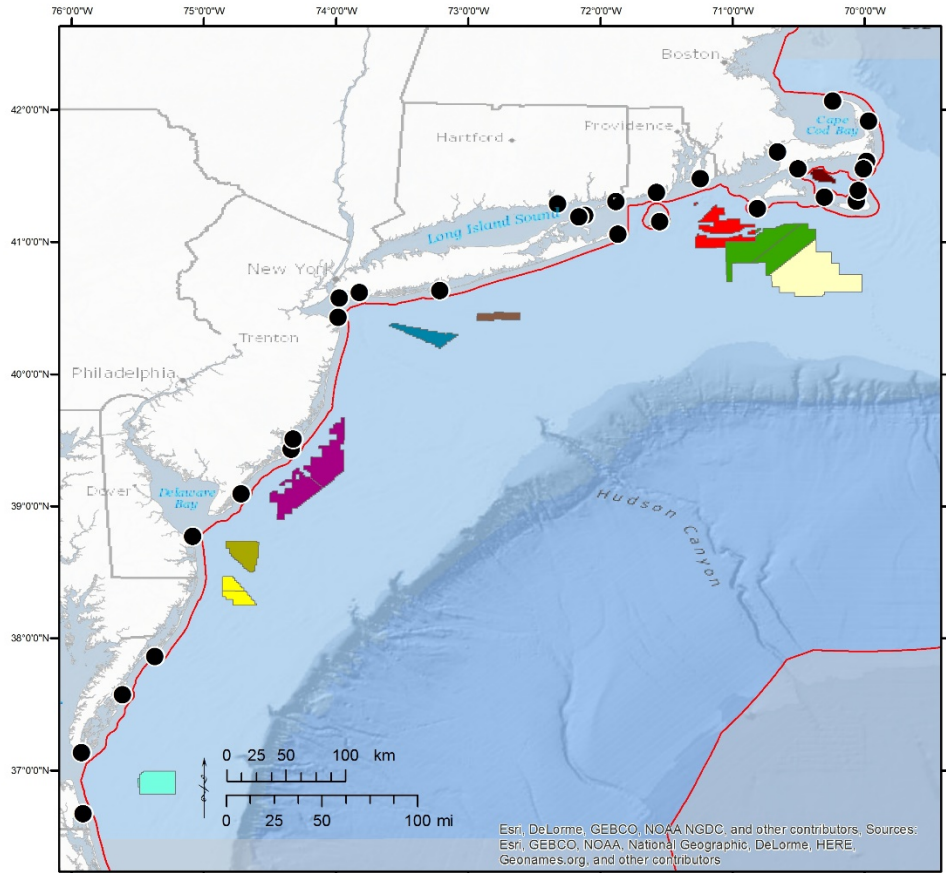
Our specific objectives were to: (1) develop spatially-explicit, 3-dimensional models of *rufa* Red Knot movements along the Atlantic OCS from Massachusetts to Virginia; (2) relate offshore movements of *rufa* Red Knots to meteorological conditions (e.g., wind speed, wind direction, barometric pressure, temperature, visibility, precipitation), temporal variation (time of day, date), and demographic factors (age, sex, staging site); and (3) estimate the exposure of *rufa* Red Knots to each BOEM Lease Area and BOEM Planning Area within the Study Area during fall migration.

2 Methods

2.1 Study Area

The Study Area extends along the US Atlantic Coast and adjacent OCS waters, and is bounded by Cape Cod, MA to the north and Back Bay, VA to the south. This Study Area was selected because it includes major stopover areas along the US Atlantic coast for *rufa* Red Knots during fall migration, specifically in Cape Cod, Massachusetts and coastal New Jersey (Brigantine Natural Area and Hereford Inlet, Stone Harbor, New Jersey).

To date (April 2018), there are a total of 12 BOEM Commercial Renewable Energy Lease Areas within the Study Area, as well as one Research Renewable Energy Lease Area (Fig. 1). These BOEM Renewable Energy Lease Areas are located in Nantucket Sound, MA (119 km²), Rhode Island Sound and adjacent offshore waters of Massachusetts (2,101 km²), New York Bight (321 km²), and adjacent waters offshore of New Jersey (1391 km²), Delaware (390 km²), Maryland (323 km²) and Virginia (465 km²). In total, their combined area covers 5,111 km² of the Atlantic OCS. Additional BOEM Planning Areas (under consideration for designation as lease areas) are located within the Study Area in Federal waters off the coast of Massachusetts (1,573 km²) and New York (166 km²). Immediately to the south of the Study Area, an additional 495 km² lease area is located in Federal waters off the coast of North Carolina.



Legend

- | | |
|------------------------------|---|
| BOEM Wind Lease Areas | BOEM Wind Planning Areas |
| MA OCS-A 0478 | MA Wind Energy Area |
| RI/MA OCS-A 0486 and 0487 | NY Proposed Commercial Lease |
| MA OCS-A 0500 and 501 | |
| NY OCS-A 0512 | U.S. Federal Waters |
| NJ OCS-A 0498 and 0499 | — 3 - 200 nautical mile boundary |
| DE OCS-A 0482 | State Wind Lease Areas |
| MD OCS-A 0489 and 0490 | Block Island Renewable Energy Zone |
| VA OCS-A 0483 and 0497 | ● BOEM Automated Radio Telemetry Stations |

Figure 1. Map of the 2016 study area extending from Cape Cod, MA and to the southern border of VA

US Federal waters are delineated by the red boundary (3 to 200 nautical miles). Waters beyond the Study Area are in grey. Black points show the locations of BOEM automated radio telemetry stations. Polygons show the locations of BOEM Wind Lease Areas, BOEM Wind Planning Areas, and the Block Island Renewable Energy Zone in state waters of Rhode Island

2.2 Study Species

The Red Knot is a mid-sized (135 g) *Calidris* sandpiper with a Holarctic breeding distribution and wintering range that extends to southern latitudes of South America (Baker et al. 2013). The *rufa* subspecies occurs in the Western Hemisphere and migrates along the US Atlantic coast and OCS (Niles et al. 2010, Burger et al. 2012). Under the US ESA, the *rufa* subspecies of Red Knot is listed as Threatened (USFWS 2014). The subspecies is also listed as Endangered under the Species at Risk Act (S.C. 2002, c.29) in Canada (Environment and Climate Change Canada 2016).

2.3 Digital VHF Transmitters

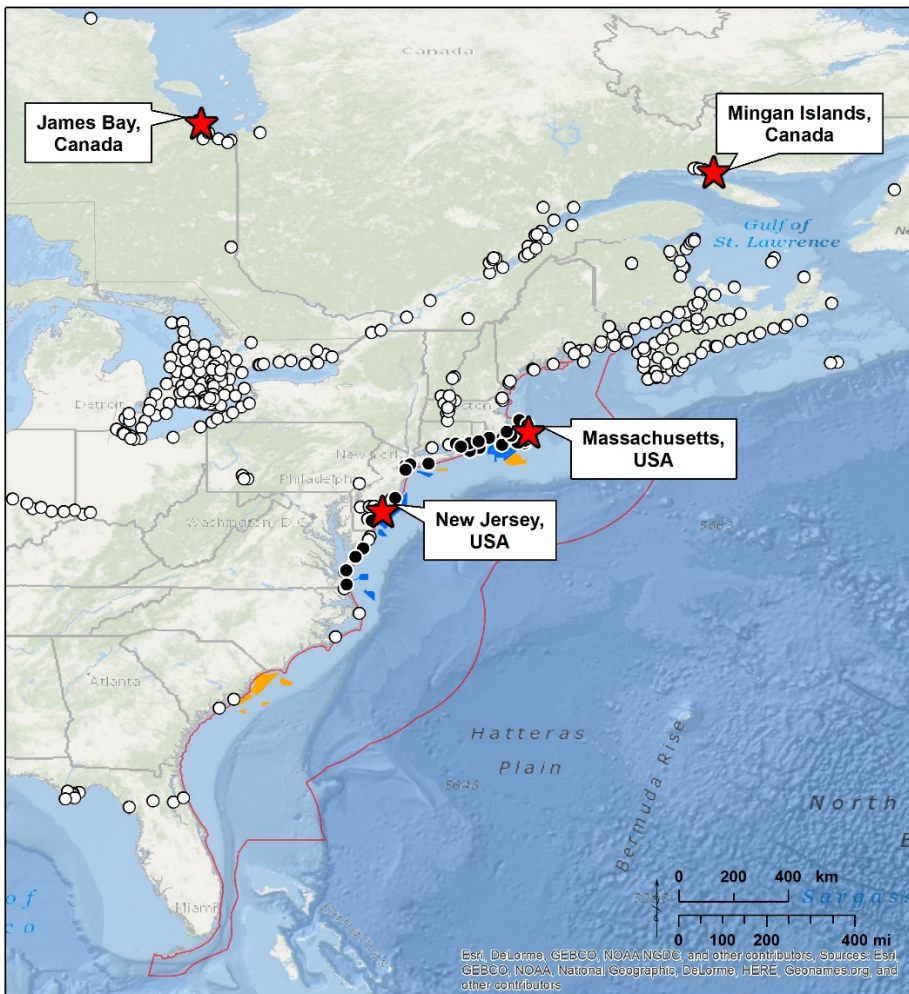
In this study, we tracked the movements of Red Knots during fall migration using digital VHF transmitters (“nanotags”, Lotek Wireless, Ontario, Canada). Study partners deployed two different models of transmitters on Red Knots, Lotek NTQB-4-2 nanotags (1.1 g; 12 x 8 x 8 mm) and Lotek NTQB-3-2 nanotags (0.67 g; 6 x 5 x 12 mm). Each transmitter and attachment materials weighed <2% of the average body mass of tagged Red Knots.

Transmitters in this study were programmed to continuously transmit signals on a shared frequency of 166.380 MHz from activation through the end of battery life. Burst intervals (time between transmissions) were specific to each transmitter and ranged from approximately 4 to 10 seconds. The expected battery life varied by transmitter model and burst rate interval. The expected life of the 1.1 g units ranged from 160 days (5 second burst rate) to 250 days (10 second burst rate), and the expected life of the 0.67 g units ranged from 80 days (5 second burst rate) to 120 days (10 second burst rate).

2.4 Capture and Tag Attachment Summaries by Site

Study co-leads (Paul Smith from Environment and Climate Change Canada, Stephanie Koch from USFWS Eastern MA NWR Complex, and Larry Niles from L.J. Niles & Associates and Conserve Wildlife Foundation of New Jersey) coordinated field efforts to capture and tag Red Knots from major stopover areas in Canada, Massachusetts, and coastal New Jersey (Fig. 2). This study includes data from a total of 388 Red Knots that were tagged during 2016 across the three geographic regions as part of this effort. Metadata from capture and VHF-transmitter deployments for all Red Knots included in this study are provided as supplemental material to this report and described in Appendix A.

Project partners in Canada tagged a total of 253 Red Knots, including nine individuals tagged in James Bay between July 28 and August 13, and 244 individuals tagged in the Mingan Archipelago from August 20 through October 15. In Chatham, Massachusetts, USA field crews tagged a total of 99 Red Knots between July 31 and October 4, including 51 individuals from North Beach Island on July 31; 20 individuals on South Beach on August 3; 14 individuals on North Beach Island on September 1, and 14 individuals on North Beach Island on October 4. Between August 8 and October 21, field crews in New Jersey, USA tagged a total of 35 Red Knots, including one individual captured at Stone Harbor Point on August 8, 28 individuals captured in Brigantine Natural Area on August 9 and 17, and six individuals captured at Avalon Point on Oct 21.



Legend

Automated Radio Telemetry Stations

- BOEM station
- Motus Network partner station

Tagging Sites

- ★ Red Knots

BOEM Wind Energy Areas

- Lease Areas
- Planning Areas

U.S. Federal Waters

- 3 - 200 nautical miles offshore

Figure 2. Map showing locations of Red Knot tagging sites and active automated radio telemetry stations in eastern North America in 2016

All telemetry stations were part of the Motus Wildlife Tracking System. Black points show locations of BOEM telemetry stations, and white points show locations of stations operated by partners on the Motus network. Federal waters of the U.S Atlantic are delineated by the red boundary (3 to 200 nautical miles). Within this boundary, all current (April 2018) BOEM WEAs shown as polygons, with Lease Areas in blue and Planning Areas in orange.

2.5 Capture and Tag Deployment

Red Knots were captured using methods tailored to the sites (e.g., cannon nets, shoulder mounted netguns, or mist nets; Fig. 3a). Once captured, Red Knots were removed immediately from the net and placed in dark, secure boxes until processing (Fig. 3b). Each Red Knot was banded with one standard metal band and a colored leg flag engraved with a unique alpha-numeric combination. Red Knots captured in the US were marked with a dark green flag with white characters and Red Knots captured in Canada were marked with a white flag with black characters. All individuals were measured using standard protocols, and in most cases, bill (± 0.1 mm), head and bill (± 0.1 mm), flattened wing chord (± 1 mm), and mass (± 1 g) were measured; fat condition was scored (at most but not all sites); and feather molt was examined (Fig. 3c). Age class was determined by plumage characteristics and molt, with birds classified as either Hatch Year (HY), Second Year (SY), After Hatch Year (AHY) or After Second Year (ASY). From each bird, three to five contour feathers were collected for molecular-based determination of gender (Avian Biotech, Gainesville, FL). Nanotags were attached by clipping a small area of feathers from the synsacral region and gluing the tags to the feather stubble and skin with a cyanoacrylate gel adhesive (Fig. 3d).

a)



b)



c)



d)



Figure 3. Photos of Red Knot capture and transmitter deployment

a) Field crew sets cannon net at tagging site on Cape Cod, Massachusetts (photo: Meagan Racey/USFWS); b) boxes used to hold Red Knots prior to processing (photo: USFWS); c) wind cord measurement with green leg flag visible (photo: USFWS); d) digital VHF transmitter mounted to synsacral region (photo: Kaiti Titherington/USFWS).

2.6 Automated Radio Telemetry Stations

In 2016, we operated a total of 32 automated radio telemetry stations that ranged from Cape Cod, Massachusetts to Back Bay, Virginia (Fig. 1). These stations were located to maximize reception coverage from coastal vantage points adjacent to BOEM offshore wind planning and lease areas, and within proximity to high-use areas for Red Knots within the Study Area. Ten of these stations were established between May and August of 2016 as part of the present study, and the remaining 22 were already in operation for a BOEM-funded study on Roseate Terns and Piping Plovers (Loring et al. 2017).

The majority of the land-based telemetry stations consisted of a 12.2-m radio antenna mast supporting six, nine-element (3.3 m) Yagi antennas mounted in a radial configuration at 60-degree intervals (Fig.4). The remaining land-based stations consisted of two to four nine-element (3.3 m) Yagi antennas attached to

existing structures. In addition, we deployed a mobile receiving station with a single omnidirectional antenna on a whale watching boat based in Nantucket, MA. A detailed description of the locations, specifications, and installation dates of each receiving station appears in Appendix B.

At each station, the antenna(s) were connected to ports on a receiving unit (Lotek SRX-600, Lotek Wireless, Ontario, Canada) via coaxial cable (TWS 100). The receivers were programmed to automatically log several types of data from each antenna, including: tag ID number, date, time stamp, antenna (defined by monitoring station and bearing), and signal strength (linear scale: 0 to 255). Each receiving station was operated 24 hours per day using one 140-watt solar panel and two 12-volt deep-cycle batteries.

Detection range of each station varies with the height of the station above sea level (asl) and with altitude of the transmitting bird (Appendix C). The maximum estimated detection range of stations 12.2 m asl is approximately 20 km to birds flying at 20 m altitude (lower limit of rotor swept zone of offshore wind turbines), and approximately 40 km to birds 200 m altitude (upper limit of rotor swept zone of offshore wind turbines). Birds flying at migratory altitudes (1,000 m) may be detected at ranges exceeding 80 km.



Figure 4. Automated radio telemetry station on Nantucket NWR (Great Point), Nantucket, MA
Station consisted of a radial Yagi antenna configuration atop a guyed, 12.2 m mast with a solar powered automated receiving unit at the base (photo: Matt Malin).

2.7 Frequency Coordination

We conducted this study in collaboration with the Motus Wildlife Tracking System. The transmitters in our study were programmed to transmit on the Motus Network frequency of 166.380 MHz and were uniquely identifiable by a unique combination of the digital ID code and burst rate interval. In 2016, the Motus Network comprised over 300 automated radio telemetry stations from Arctic Canada to northern South America (Fig. 2) and over 4,000 nano-tagged individuals representing a variety of taxa of birds and bats (Taylor et al. 2017).

Below, we define key terms used to describe different types of data in the Motus database:

- 1) Principal Investigator (PI) stations: automated radio telemetry stations operated by the Principal Investigator of tracking study. Within this report, we refer to automated radio telemetry stations that were funded by BOEM as “BOEM stations”
- 2) Global stations: automated radio telemetry stations operated by cooperators in the Motus network.
- 3) Target transmitters: transmitters deployed by the PI of the tagging study.
- 4) Non-target transmitters: transmitters deployed by cooperators in tagging network.

By participating in the Motus Network, we obtained detailed detection data (including: bird ID, location, time, date, receiving antenna, signal strength value) for target transmitters deployed on Red Knots in this study that are detected by global stations operated by partners within the Motus Network. Access to and use of detection data from non-target transmitters recorded on BOEM stations are pursuant to the Motus Collaboration Policy (Motus Wildlife Tracking System 2016). The Collaboration Policy states that PIs control access and use of detailed detection data from their target transmitters on both their PI stations as well as all global stations. However, basic metadata from tags and receiving stations from all projects (location, deployment dates and species), as well as daily summaries of tag detections at each receiving station will be publicly available. The basic open-access dataset from non-target data collected by BOEM stations is available on the Motus website (www.motus.org) and provided in tabular format as supplementary material to this report (Appendix D).

In addition, participation in the Motus network facilitated use of supplemental data from *rufa* Red Knots that were tagged during spring migration at staging areas in Delaware Bay, USA as part of a study on Red Knot migration ecology funded by Environment and Climate Change Canada in partnership with Conserve Wildlife Foundation of New Jersey. These supplemental data provide additional information on movements of Red Knots tagged in at a major stopover site within our Study Area, Delaware Bay, during spring (northbound) migration, and are summarized in Appendix G.

2.8 Post-processing of Telemetry Data

To post-process detection data collected by the BOEM automated radio telemetry stations, we used a filtering algorithm in the Sensorgnome Package (Brzustowski 2015) within program R (v.3.0.2) to remove false detections from the raw VHF telemetry data. The algorithm was based on the following default parameters applied to each unique transmitter: minimum of three consecutive bursts required to comprise a 'run' (run length), a maximum of 20 consecutive missed bursts allowed within each run, and a maximum deviation of four milliseconds from a tag's unique burst interval between its consecutive bursts (Brzustowski 2015). These parameters were selected according to conservative recommendations from Motus network developers (Taylor et al. 2017).

Data from global automated radio telemetry stations operated by cooperators in the Motus network were processed and disseminated by Bird Studies Canada. We visually inspected the processed global data and identified remaining spurious detection data by quantifying speed and distance of movements between automated radio telemetry stations. We found that some of the global towers showed higher rates of false positive detections than others, which led to our taking a conservative approach in minimizing false detection rate. The source of the false positives was unclear, but was likely attributed to from nearby transmitting VHF or cellular antennas (Taylor et al. 2017), and was more prevalent at sites located in developed areas such as marinas. Due to the high rate of false-positive detections from certain global sites with a high level of interference, we applied a more stringent filter (relative to default) to these data that required a minimum of seven consecutive bursts required to comprise a 'run'. The electromagnetic noise is assumed to be white noise which is uncorrelated in the time domain, so selecting a minimum number of 7 consecutive bursts ensured received signals were from the transmitter and not environmental noise.

2.9 Movement Models

The first main objective of our study was to develop spatially-explicit, three-dimensional models of Red Knot movements along the Atlantic OCS from Massachusetts to Virginia. Our specific aim was to develop movement models that simultaneously: 1) account for observation error; 2) estimate movement parameters (rates, direction); and, 3) estimate behavioral modes (on land, direct flight).

2.9.1 Background and Motivation of Approach

Although automated radio telemetry provides a unique opportunity to estimate detailed 3-dimensional trajectories for many individuals across broad geographic ranges and flight altitudes, the theory behind such estimation and its application remains in development. Automated radio telemetry stations are typically comprised of several directional Yagi-Uda antennas, radially configured to facilitate location estimation, with each antenna designed to receive strong signals along a “main beam” of approximately 35°. However, weaker signals alongside and rear lobes complicate estimation of location. Most studies of avian movement using fixed arrays of VHF towers have involved selecting sequences of detections and analyzing these on a case by case basis, under the assumption that detections are indeed along a main-beam (Taylor et al 2017). Bird trajectories are then inferred either based on locations of towers among sequences of detections (e.g. Duijns et al. 2017, Woodworth et al. 2015), sometimes augmented by manual identification of characteristic signal strength patterns from movement along or across main

beams (Brown et al. 2016), or by inferring flight bearings via the ratio of signal strength between receiving antennas (e.g. Smolinski et al. 2013).

Therefore, previous studies using fixed antennas have not fully accounted for detections away from main antenna beams, nor for variation in signal strength with flight altitude. Given the continental-wide span of the Motus system and complicated nature of signal propagation over heterogeneous terrain, this poses a challenging problem from the location model perspective. In this study, we advanced the development of approaches used to estimate transmitter location and altitude explicitly, based on a two-beam radio propagation model (Janaswamy 2001 and Janaswamy et al. *in review*). This approach allows for completely automated location estimation across many individuals, and accounts explicitly for variation relative to the beam orientation and flight altitudes (Janaswamy 2001, Janaswamy et al. *in review*). This new formulation accounts for how predicted signal strength varies with flight altitude and how this relation differs when received along the main beam, side and back lobes (Fig. 5). For a single given received signal in the absence of near-simultaneous detections, the inherent uncertainty in a bird's location can theoretically be up to 80 km horizontally and several kilometers in altitude.

Given the inherently nonlinear inverse relationship between signal strength and location, simplifying assumptions or constraints are needed to choose between possible solutions (Janaswamy 2001, Janaswamy et al. *in review*). Preliminary results based on a simplified beam equation, which allowed for exact matching between nearly simultaneously detected signals, predicted locations tended to zig-zag between main beams of detecting receivers and additionally, predicted minimum altitudes occasionally exhibited large jumps due to gaps in occurrences of near-simultaneous detections. This implied that constraints were needed to account for ambiguity and unreliability in signal strength (i.e., it can be strongly influenced by other factors, such as meteorological conditions and reflectance effects, as well as any limitations of the two-beam propagation model). In the present study, we accounted more fully for the vertical structure in the Janaswamy et al. method, applied constraints based on known characteristics of shorebird flight, and created a framework that accounted for the uncertainty in signal strength when comparing signal strength among detections. In this way, we estimated the most likely flight path in three dimensions, as well as the uncertainty in this estimate, based on both predicted signal strengths among receiving arrays and known flight characteristics.

Our model workflow proceeds in six steps, outlined in detail below and in Table 1. In the first two model steps, we derived the most consistent estimated locations among plausible detections, based on their signal strength (Sections 2.9.2-2.9.4) and on behavior-based constraints (Sections 2.9.5-2.9.6). Specifically, the location was determined to be the weighted mean among locations resulting in the lowest discrepancy between measured and predicted signal strength, weighted by the inverse-square discrepancy in signal strength among all near-simultaneous detections. The constraints involved differentiating between movement during staging (stopover) and non-stop flight according to (i) limits to a bird's possible flight speeds in the horizontal and vertical and (ii) the assumption that a bird limits variation in its horizontal and vertical speed (Section 2.9.1). Because these detections occurred at irregular intervals, the third step interpolated the estimated locations to one-minute time steps, using a Brownian Bridge movement model (Horne et al. 2007). Choosing a time window represents a trade-off between the advantage of adding more information (detections) to co-locate position, and the disadvantage of the bird's actual position changing within the time window. The 1-minute time step was selected to estimate

location estimates at approximately a 1-km scale (assuming 20 m/s flight speed), which we felt was an appropriate resolution for assessment of macro-exposure to WEAs throughout the Study Area.

In the fourth model step, meteorological data (approximately 32-km spatial resolution and 3-hour temporal resolution) were spatiotemporally-interpolated to each one-minute record, and orientation and airspeed derived from flight speed and wind data (Kemp et al. 2012). Meteorological data were downloaded from the National Centers for Environmental Prediction North American Regional Reanalysis (NARR; National Oceanic and Atmospheric Administration 2017). In the fifth model step, occurrence in WEAs and in Federal waters was quantified using the output from the Brownian Bridge model and the standard deviation of location estimates in the horizontal plane, as described in Section 2.9.7. Finally, in the sixth model step, we extracted the magnitude of all meteorological and flight speed related covariates to assess incidence in offshore waters, including flight direction and heading, wind support, and crosswinds.

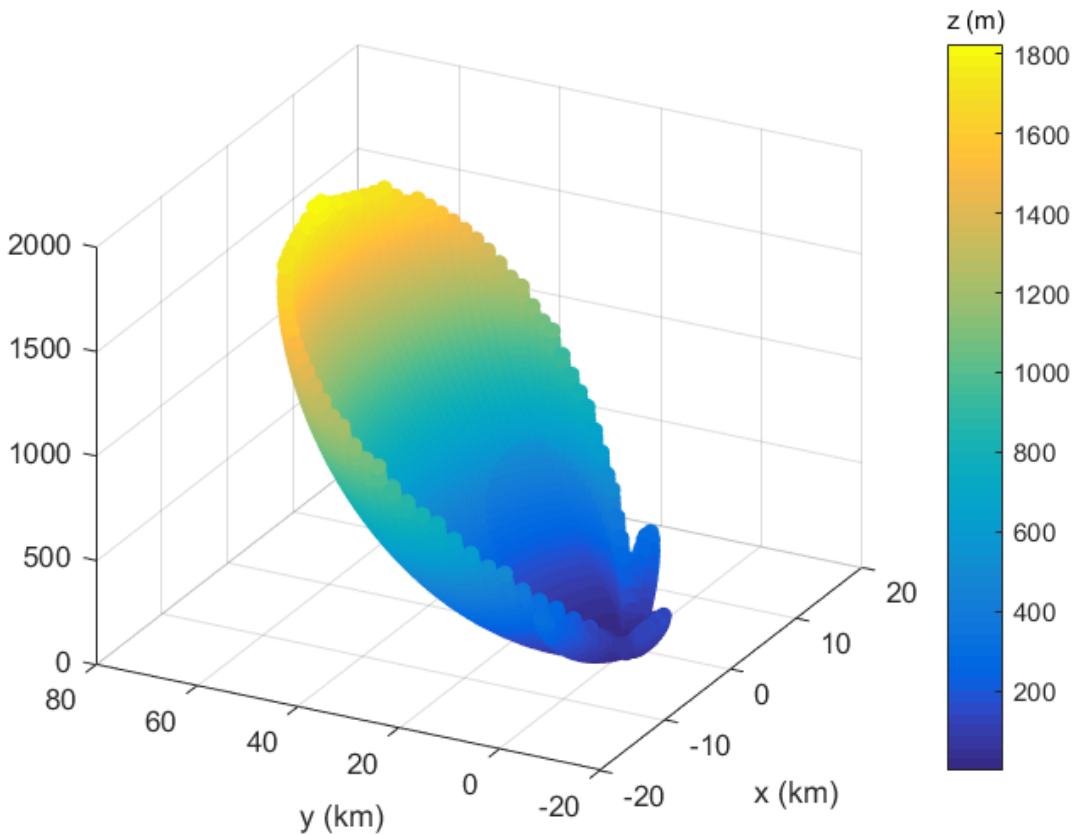


Figure 5. Radiation pattern of antenna beam

Possible locations, measured in distance from an automated radio telemetry tower with a Lotek SRX-600 receiver (set to standard gain of 80) to a source (i.e., target bird) are depicted for a relatively strong received signal (~250 on a scale of 0-255). The main beam is oriented along the x -axis at $x=0$, with the tower mast located $x=0$ and $y=0$ with crossbeam distance x , along-beam distance y (km) and vertical receiver height (z) in m).

Table 1: Model workflow: steps 1-3 govern localization estimation, step 4 interpolates covariate data, and step 5 estimates exposure to Federal waters and WEAs

Step	Action	Section	Method
1a	Determine periods non-stop flight	2.9.5	Based on thresholds for inter-tower distance (default minimum, 50 km) and inferred flight speed (default for rufa knots, 4-40 m/s)
1b	Determine locations with near-simultaneous detection (default time window <1 minute)	2.9.3	Consistency of signal strength for each location and detecting beam (see Fig. 5) within altitude bounds (1-200 m for stopover flight bouts and 10-2500m during non-stop flight)
1c	Re-determine periods non-stop flight based on output 1b	2.9.5	Minimum 4 m/s, excluding interim periods >2 hrs with speeds below 2 m/s
2a	Determine locations from other ('single') detections	2.9.4	Height range interpolated from step 1b, (maximal vertical speed 2 m/s) locations based on main beam and tower locations
2b	Refine periods non-stop flight based on output 2a	2.9.5	Minimum 4 m/s, excluding interim periods >2 hrs with speeds below 2 m/s
2c	Refine non-stop flight locations from step 2b in accordance with behavioral-based constraints	2.9.5	Constrained by flight speed (range horizontal speed 4-30 m/s, max vertical speed 2 m/s) and minimizing discrepancy in location estimates and in accelerations (default: minimizing 50% sum of square location discrepancy and acceleration)
3	Interpolate to one-minute time step	2.9.7	Brownian Bridge model based on standard deviation in horizontal position
4	Add dynamic weather covariates	2.11	Spatiotemporally interpolated NARR data
5a	Determine incidence in Federal waters	2.10	Categorical (binary 0-1), based on estimated location (minimum 10 m/s ground speed)
5b	Determine incidence in WEAs	2.10	Categorical (binary 0-1), based on standard errors from step 2b (minimum 10 m/s ground speed and 10% overlap with WEA)

2.9.2 Formulation

In the two-beam model, derived in Janaswamy et al. (*in review*), the resultant signal strength (in dBm, normalized to a transmitter and receiver specific gain factor) varies with the two-dimensional and three-dimensional ranges (i.e. distance to receiver; r and R , respectively), radial angle ψ between receiver and transmitter, and the heights z of the (bird) transmitter and H of the receiving tower:

Equation 1

$$\xi^2 = \frac{g^2(\psi)}{k_0^2 \cdot R^2} \sin^2(k_0 H z / r),$$

where $g(\psi)$ governs the shape of the directional beam and k_0 (m^{-1}) represents the wavenumber in free-space (Janaswamy 2001). The sinusoidal dependence of flight altitude z on signal strength in Equation 1, and Fig. 5, together illustrate how significant signal gain with height is possible, resulting in possible detection of high-flying open-ocean migrants such as Red Knots.

For horizontal ranges much larger than the vertical range ($z \ll r$), Equation 1 can be simplified and inverted to determine the transmitter (bird) height (z) above the ground as a function of horizontal range, r :

Equation 2

$$z = \frac{r}{k_0 H} \sin^{-1}(k_0 r \cdot \xi / g(\psi)).$$

2.9.3 Near-simultaneous Detections

In the first model step, we derived estimated locations, and uncertainty in location, for all detections from separate towers or antennas within a time window of 60 seconds (hereafter, near-simultaneous detections). Near-simultaneous detections help reduce the inherent ambiguity in signal strength (Fig. 5). A one-minute time window ensured that exposure to the WEAs could be adequately assessed without compromising the accuracy of estimated locations since Red Knots are predicted to cover only about 1-km in one minute, and shorter time windows reduce the number of near-simultaneous detections and thereby the accuracy of location estimates.

Using Equation 2, rather than searching for an exact match in location between signals, we evaluated the degree of correspondence among all received signals within the time window, considering all plausible horizontal ranges r and axial angles ψ : for each detection within the 1-minute time window, we searched through 2,880 candidate horizontal locations (radial distances between 100 m and 50 km, and every 0.5° radially) to determine the consistency of each location given the other detections. For each detected signal and candidate horizontal location (and corresponding vertical location, via Equation 2), the mean discrepancy in signal strength from all other detections was calculated (based on what their signal strength would be at this location using Equation 1). Estimated locations that fell outside of the possible bounds on vertical location were excluded. Among the remaining locations (typically 500-100 for each

detection), we then chose the median location among those having the lowest 10% discrepancy in signal strength, and the mean of these best location estimates among all detections as the best ('mean') estimated location within the time window. Selecting the most representative value in the 10% most probable set of points was found to improve both the kite validation (Section 2.9.8) and the smoothness of non-stop flight trajectories, especially once these were constrained to conform to non-stop flight (see 2.9.5-2.9.6). To assess exposure to Federal waters and WEAs, uncertainty around this 'mean' location was quantified by the standard deviation in horizontal coordinates and the upper and lower quartile in vertical height. For updating locations to conform with dynamic flight constraints (Section 2.9.5), 5-95% confidence intervals in both the horizontal and vertical were also retained.

2.9.4 Single Detections

Estimation of locations for other, i.e. non near-simultaneous detections (hereafter, single detections) was conducted following one of two procedures: (1) numerical estimation of straight-line trajectories from a sequence of single-antenna detections (i.e. a computational version of that employed by e.g. Brown et al. 2017), or (2) estimation of the most likely location of a single detection based on received signal strength and interpolated near-simultaneous location estimates. Specifically, (1) when three or more consecutive detections from (only) a single antenna 'beam' occurred within a span of 30 minutes, a straight-line trajectory was fit among candidate locations to minimize the discrepancy in single strength (log-transformed ξ squared) within the bounds for horizontal speed (4 to 40 m/s), using MATLAB routine `fmincon`. An initial trajectory was used in the optimization procedure according to a linearized version of equation 2 (or, equivalently, assuming, $z \ll r$). Additionally, among these 'sequential' single-beam detections, a constant vertical (climb speed) between 0 and 2 m/s was also fit whenever initiation of non-stop flight was inferred (see Section 2.9.5) or if such a sequence occurred as final detections. Finally, horizontal uncertainty was quantified in these cases by an interpolation of the horizontal uncertainty between the closest simultaneous detections, or of the closest simultaneous detection if only one occurred. Alternatively, (2) when fewer than 3 consecutive single detections occurred within 30 minutes, birds were presumed to be located along the main-beam (within 30 degrees of the main axis) and on the same side of the beam as the horizontally interpolated location from previous or following near-simultaneous detection. As with near-simultaneous location estimation, 2880 candidate horizontal locations were tested for consistency with measured signal strength, being within the visible horizon and vertical bounds, and proximity to the interpolated location between any previous or subsequent location estimates derived from near-simultaneous detections.

2.9.5 Determination of Non-stop Flight

Refining the movement trajectory of birds through time and space required differentiation between stopover behavior and non-stop flight. The reasons for this are two-fold: (1) previous or subsequent location estimates should be used to facilitate current locations only if they are consistent with non-stop flight, and (2) given the potentially large range in flight altitudes and associated horizontal locations for any given signal strength (Fig. 1), using biologically reasonable bounds in altitude greatly improved model performance (see also Poessel et al. 2018). During non-stop flight, modeled flight altitudes were bounded by a minimum of 10 m and maximum 2500 m (Williams and Williams 1990). During flight in other ('staging') periods, a minimum of 1 m and 200 m were assumed (Dirksen et al. 2000). Non-stop flight periods were determined iteratively in the model, beginning by deriving proxy flight speeds based

on inter-tower distances and the timing of subsequent detections. In level flight, Red Knots fly at airspeeds of approximately 20 m/s (excluding wind effects; Alerstam et al 2007), but estimated this way, ground speeds vary with proximity to detecting towers, wind effects and measurement imprecision. Therefore, at the beginning of the first model step, non-stop flight was inferred when detections occurred at towers separated by at least 50 km (to minimize including simultaneous detections during stopover), implying flight speeds between 4 m/s and 40 m/s (Table 1; even when climbing, knots rarely fly slower than 10 m/s; Hedenström and Alerstam 1994). Non-stop flight periods were subsequently updated and refined using the improved location estimates derived for multiple detections (step one) and single detections (step two). In general, non-stop flight was assumed for all detections occurring in the time interval between two detections inferring a minimum ground speed of 4 m/s. However, to prevent misclassification of brief stopovers between two non-stop flight bouts, any interim period implying less than 2 m/s for longer than two hours was considered as a stopover as opposed to non-stop flight. We further categorized migratory movements as either long-distance linear non-stop flights (e.g. from Massachusetts to the mid-Atlantic) or final non-stop departure flights with final locations within the Study Area intersecting Federal waters and heading offshore.

2.9.6 Behavioral Flight Constraints

Location estimates during non-stop flight sequences were further refined, based on known characteristics of flight of migrating shorebirds, to ensure that flight trajectories were feasible, smooth and behaviorally reasonable. Specifically, following initial location estimation of both near-simultaneous and single detections, location estimates were adjusted, within the 5% and 95% bounds of the candidate locations, to ensure that (i) vertical speeds, i.e. as implied by estimated changes in flight altitude between detections, were less than 2 m/s in magnitude, (ii) horizontal speeds remained within 4 to 40 m/s (Table 1; airspeeds of migrating knots could approach 20 m/s but inferred flight speeds would vary with straightness of flight paths, wind conditions and proximity to towers) and (iii) the total horizontal and vertical acceleration were minimized given constraints (i) and (ii). The uncertainty in each dimension was retained according to the standard deviations in the x and y components, and the 5 to 95% quantiles in the vertical dimension among candidate locations within the interquartile range of candidate vertical locations.

2.9.7 Temporal Interpolation Using Brownian Bridge Movement Model

To estimate occurrence within both WEAs and initiation of migratory flights across Federal waters, we spatiotemporally interpolated the irregular location estimates into one-time steps using a Brownian Bridge model (Horne et al. 2007). Spatial locations were interpolated in three dimensions between all near-simultaneous and single detections. Uncertainty of one-minute horizontal location estimates was quantified as the root-mean square of estimated variance in location from detections and due to time gaps between detections (via a horizontal flight speed of 20 m/s; see Horne et al. 2007). Vertical uncertainty in one-minute time steps was linearly interpolated between all near-simultaneous and single location estimates.

2.9.8 Calibration and Validation

Since Equation 1 is dependent on the transmitter and receiver properties, signal strength of the SRX-600 receiver (on a scale of 0-255) needed to be calibrated using data from a known location:

Equation 3

$$\tanh^{-1}\left(\frac{Z}{255-Z}\right) = b \cdot \ln\left(\frac{\xi^2}{P_0} + 1\right),$$

where Z represents the SRX-600 receiver signal (0-255), b represents a rate of signal saturation and P_0 is a noise threshold (see Bai 2016 and Janaswamy et al. *in review*).

To estimate these two coefficients, two 1.0 g nanotags were attached to a kite that was flown from the back of a motorboat. The motorboat was driven in transects within range of two land-based 12.2 m automated radio telemetry stations, each supporting six, 9-element Yagi antennas arranged in a radial configuration.

The first (calibration) dataset comprised detections from flying the kite along the main beam of two automated radio telemetry stations, located 6.7 km apart on Monomoy NWR in Massachusetts. We flew the kite at two heights, 30 and 60 m above sea level (asl), to optimize our calibration estimates within rotor height, within limitations of FAA regulations. We aligned the transmitting antennas of two nanotags horizontally and vertically (i.e. parallel and perpendicular to the water surface, respectively). This resulted in horizontal ranges from two detecting towers up to 10 km (maximum distance of transect length), and, between the six antennas on each, all possible bearings between the transmitter and receiver. All detections were pooled and the data calibrated by fitting the coefficients p_0 and b in equation 3 using non-least squares based on GPS location of the boat, the measured signal strength Z , and predicted signal strength (Equation 2). To validate the location model and coefficients, we used a second set of surveys for our calibration dataset, which involved a VHF-tagged kite flown at altitudes ranging from 10 to 30 m asl in a zig-zag pattern between the two receiving arrays. To facilitate the kite's erratic movement, we used a shorter time window (20 seconds) and constrained modeled flight to altitudes to fall within 10 to 40 m.

The mean pairwise distance between each tag location (Fig 6, red points) and corresponding model estimate location (Fig 6, green points) was 1,351 m (SD 690 m, range 134 to 3,600 m). The mean pairwise difference in the East-West (x) coordinates was 777 m (SD 638 m, range 20 to 3,313 m) and the mean pairwise difference in the North-South (y) coordinates was 909 m (SD 688 m, range 1 to 3,246 m).

The model-estimated location error (shown as green polygon in Fig 6) was considerably higher than the actual error, with a mean in East-West (x) coordinates of 1,316 m (SD 1,433 m, range 585 to 12,377 m) and in North-South (y) coordinates of 1,260 m (SD 392 m, range 761 to 4,270 m).

During the calibration survey, the altitude of the kite/transmitter was not accurately recorded because it varied with the wind, ranging between 10 and 30 m. The mean model estimated kite altitude was 20 m (SD 0.6 m, range 20 to 24 m; Fig. 7).

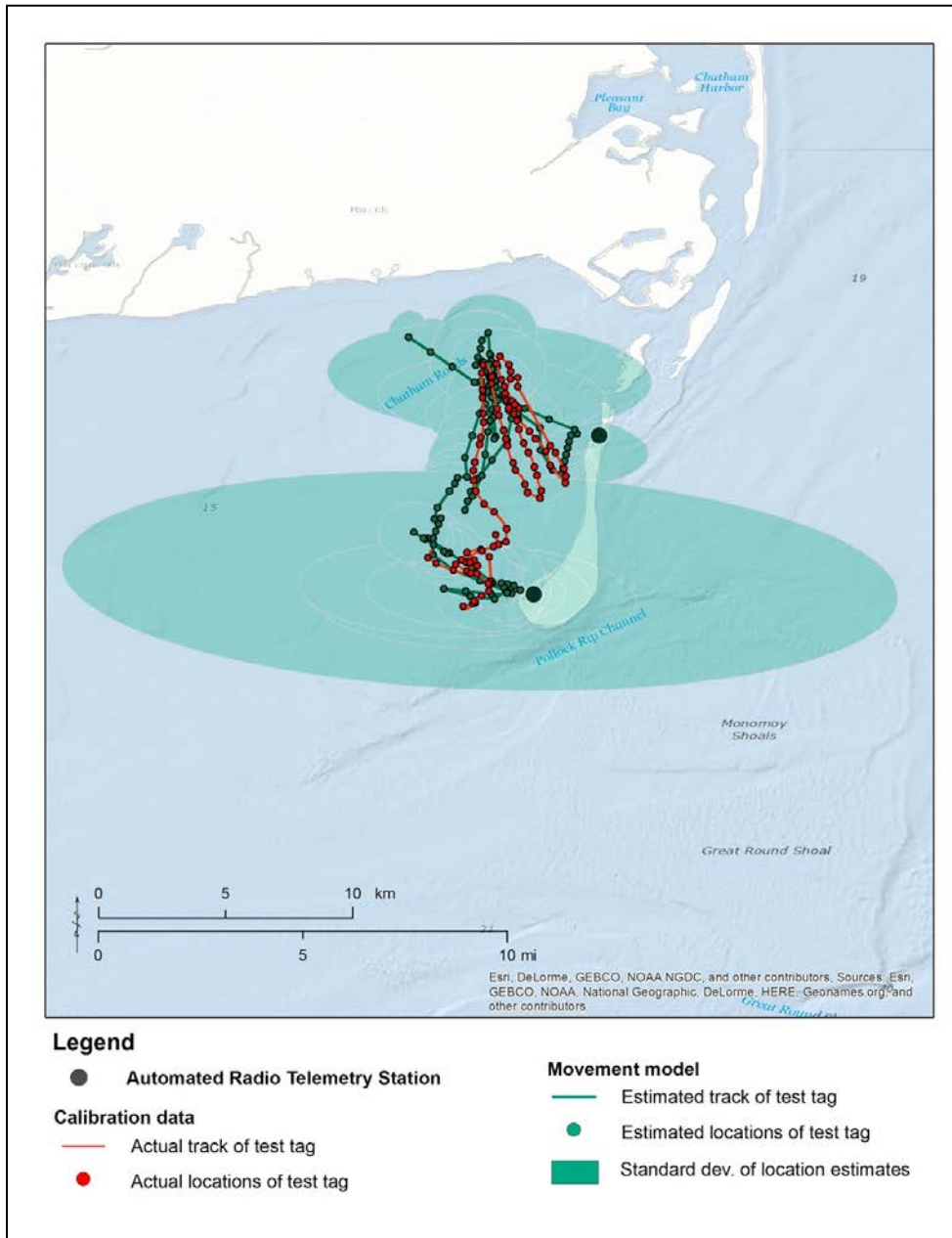


Figure 6. Results of model calibration survey conducted during September 2014 adjacent to two automated radio telemetry towers on Monomoy NWR, MA, USA

Red line shows GPS track of boat towing a kite with a VHF transmitter attached to it flying at approximately 10 to 30 m above sea level (ASL). Red points show GPS locations collected every minute. The green track shows corresponding locations and track estimated by the movement model. Green ellipses show model-estimated error (SD) corresponding to each location estimate.

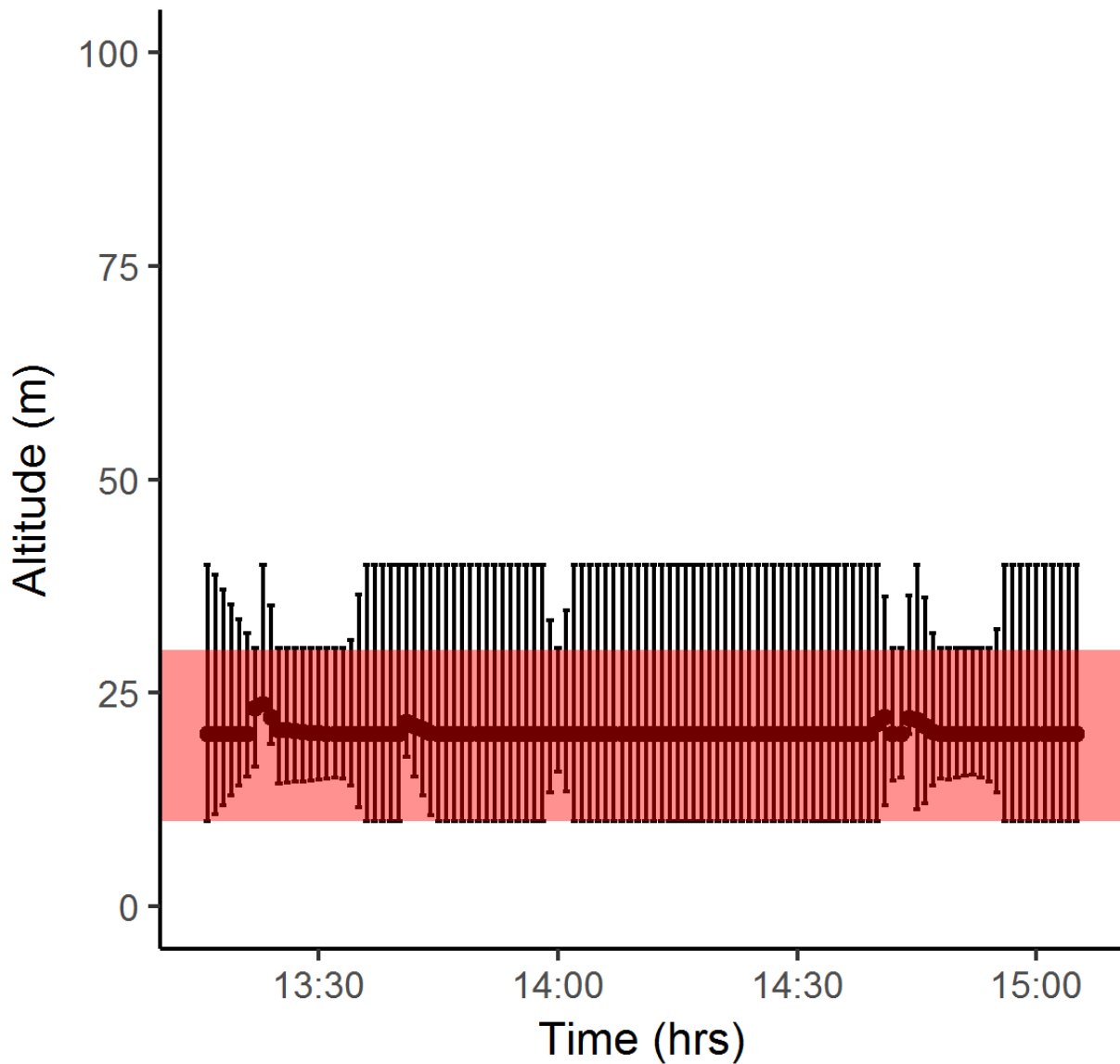


Figure 7. Model estimated mean and standard deviation of altitude (m, ASL) over time (min) of VHF-tagged kite during September 2014 calibration survey

The black error bars represent the predicted interquartile range of plausible altitudes, which depended on the consistency of received signal strength among all detections (modeled altitude was constrained from 10 to 40 m). The dark line represents the most plausible vertical trajectory as solved by the dynamic smoothing. During survey, actual height of the VHF-tagged kite fluctuated between 10 and 30 m (red shading).

2.9.9 Including Sensorgnome Receiving Stations

Most of the towers in the Study Area were equipped with SRX-600 receivers and gain set to 80, but some (e.g. New Jersey) in the region and many outside the region (especially in Canada) used Sensorgnome equipment (Taylor et al. 2017). Sensorgnome measurements are converted from received power to and reported in raw dBm units, which will vary with gain and other settings. To standardize Sensorgnome and SRX-600 signal strength data for this study, a gain of 80 was assumed and dBm units transformed to SRX-600 receiver Z units using a simple linear relationship (J. Brzustowski, personal communication):

Equation 4

$$Z = (40G_0 + 44 \cdot dBm + 4565)/11$$

2.10 Assessment of Occurrence in Federal Waters and WEAs

Primary objectives of this study were to estimate the occurrence of Red Knots in Federal waters, within each BOEM Lease Area, and BOEM Planning Area from Massachusetts to Virginia.

For the BOEM Atlantic Region, we obtained GIS shapefiles of the Submerged Lands Act boundary line, delineating the boundary between state waters (landward) and Federal waters (seaward), and Atlantic OCS WEAs (v. Apr 10, 2017, BOEM 2017c). We clipped these shapefiles to the boundaries of the Study Area (Cape Cod, MA to Back Bay, VA), retaining a total of thirteen renewable energy lease areas and two wind planning areas in the Study Area bounds (Fig. 1). We also include the boundary of the Renewable Energy Zone in state waters of Rhode Island to evaluate exposure to the Block Island Wind Farm, which is currently the only operating wind energy facility in the US (Northeast Regional Ocean Council 2017).

For the analysis of exposure to WEAs, we combined adjacent lease areas within each state to better match the spatial resolution of model output (Table 2). The number of VHF-tagged Red Knots). We assessed occurrence in WEAs and Federal waters of the Study Area using the mean and standard deviations in locations estimates (X and Y, in UTM coordinates) interpolated to a one-minute time step. Interpolations generated from tracking tower detections on long distance offshore flights were sometimes widely separated in time and space, and as a result subjected to artificially low flight speed estimates and large locational error. To address uncertainty in model output, we considered locations as occurring within Federal waters or WEAs when at least 10% of the location's X-Y error distribution intersected a WEA and/or Federal water polygon, and when the estimated ground speed was at least 10 m/s.

2.11 Meteorological Conditions

To examine movements relative to meteorological covariates, we obtained satellite-derived North American Regional Reanalysis environmental data for the Study Area (Atlantic OCS from Cape Cod, Massachusetts to Back Bay, VA) in 3-hr time steps and approximately 32-km spatial resolution (National

Oceanic and Atmospheric Administration 2017). The specific meteorological covariates that we included were: wind at a pressure level of 1000 mb (about 100 m above sea level), quantified as wind speed (m/s), Zonal (Eastward) and Meridional (northward) wind components (m/s), and wind direction (the direction wind blows toward, measured clockwise from geographic north); and additionally four other weather covariates at surface level values: barometric pressure (Pascal [Pa]), precipitation accumulation (kg/m²), air temperature (Kelvin [K]) and visibility (m).

These data were interpolated from their native Lambert conic grid to each location along the predicted trajectory (stored in the model in NAD83 UTM 18N coordinates), using a cubic spline based on the nearest 8 spatial locations, and linearly interpolated in time (MATLAB routines `lambert1` and `latln2val`, respectively). This facilitated more precise estimates of covariates and for the predicted trajectories when simulating in between and beyond detections.

We also estimated wind support (i.e., tailwind) and crosswind components for each individual at each 1-minute time step, based on equations described in Kemp et al. (2012). These quantities inherently depend on a bird's heading, i.e. how it orients its horizontal body axis relative to the ground, and how they might compensate for any wind drift, i.e. adjust their heading to incident wind to maintain a preferred or intended direction (see Kemp et al. 2012 and McLaren et al. 2012). For simplicity, and because many of the 1-minute interpolations reflected time spent on the ground, we used measures for wind support and crosswind reflecting full compensation for any wind drift relative to track directions.

Geospatially referenced detection data and corresponding covariates for all Red Knots in this study were submitted to BOEM as a supplement to this report (Appendix E).

2.12 Covariate Analysis of Exposure to WEAs

We fit logistic regression models for each tag site to examine at demographic variation (age, sex, and their interaction term) in exposure to WEAs. Models were fit using function `glm` with a binomial family and logit link, in base R (version 3.4.1, R Core Development Team 2017).

For analysis of timing, meteorological conditions, and altitude of flights across WEAs, we used model location estimates (1-minute time step) for each location that intersected a WEA and met the criteria for exposure described in Section 2.10 (10% of the location's horizontal error distribution intersected a WEA and estimated ground speed at least 10 m/s). We then calculated the mean of each covariate, per WEA exposure event by individual, to generate summary statistics. For circular variables (time of day, in hours Eastern Standard Time [EST] and wind direction, in degrees relative to true north) we calculated the mean and ρ , a measure of dispersion of a sample of directional measurements, based on the circular distribution (R package 'Circular', Agostinelli and Lund 2017). To examine movements relative to daylight, we used the R package 'maptools' (Bivand and Lewin-Koh 2016) to calculate local sunrise and sunset times for each WEA crossing event. WEA crossing events that occurred entirely between the time of local sunrise and the time of local sunset were considered to have occurred during daytime hours. Conversely, WEA crossing events that occurred entirely between the time of local sunset and the time of local sunrise were considered to have occurred during nighttime hours. WEA crossing events that

spanned the timing of local sunrise or sunset were considered to have occurred at dawn or dusk, respectively.

For each remaining covariate (wind speed, wind support, crosswind, barometric pressure, precipitation accumulation, temperature, visibility) we report summary statistics (mean, SD, range). We also report summary statistics of flight altitudes (relative to rotor swept altitudes) for each WEA exposure event.

2.13 Covariate Analysis of Migratory Departures into Federal Waters

For each of these weather covariates, standard statistics (medians, quartiles and range) were derived to compare occurrence offshore in Federal Waters to staging movements within the Study Area. Based on the location model output (Appendix E), we compared migratory departures into Federal Waters to non-departures in the study region (hereafter, staging movements). Given the importance of and relation between flight and wind direction on long-distance migratory movements, we included Zonal (Eastward) and Meridional (Northward) components of wind separately for this analysis (we expected selectivity for winds blowing to the South and to the East for open-ocean migratory movements).

Preliminary analysis revealed that departure hours were typically clustered before civil dusk or else after civil dawn; therefore, meteorological covariates for staging movements were included in the analysis from all 1-minute time intervals at the beginning of nautical dawn and end of nautical dusk for each 12-hour period without a departure. We used the R package 'maptools' (function 'crepuscule') to identify model estimated locations corresponding to the time of dawn and dusk (civil twilight, when the sun is 6 degrees below the horizon; Bivand and Lewin-Koh 2016)

We next assessed whether the life history covariates (age and sex) differed regarding the relation of the above meteorological covariates to offshore movement, and additionally date (day of year, hour of day in EST) and location (Latitude and Longitude). We used a Chi-squared test to assess if meteorological covariates differed between staging movements and migratory departure, and a nonparametric Kruskal-Wallis test (MATLAB function `kruskalwallis`, The Mathworks 2016) to test for differences in the covariates in offshore movements amongst the age and sex related groups (HYs, AHY males, and AHY females).

We then performed an integrated analysis of all covariates, i.e. the meteorological, flight orientation-related and life history covariates, to predict migratory departure into Federal waters using a regression-based method, boosted GAMs (MATLAB package BGAM). We included covariates from the 1-minute interval when departing migrants first crossed Federal waters as 'migration' events, and covariates twice-daily (at dusk and dawn) while individuals remained in the Study Area as staging events.

The boosted approach allows estimation of both the relative 'influence' of covariates to exposure to water areas (i.e., the percentage reduction in deviance attributable to each predictor), and of the 'relative' response to these covariates (Hastie et al. 2009). To reduce possible bias and overfitting, the method employs stochastic gradient boosting, a machine learning technique by using small 'gains' (0.075) when adding iterative 'learner' models (based on step functions) to reduce model deviance (a generalization of sum of squared errors). The model is fit by averaging a number (here, $n=7$) of independently sampled fits ('folds'), and by adjusting each fold by small learning rates ('gains') and randomly sampling a fraction

(10%) of the data, together with early stoppage ('shrinkage') can help avoid overfitting and bias associated with sparsely sampled and highly varying spatially explicit data (e.g. Maloney et al. 2012). Note also that modeled responses should act independently of the underlying frequency of each covariate (given sufficient information to identify relevant responses); we verified this by testing whether predicted responses were robust to bias.

We used a Binomial logistic regression formulation (i.e. based on migratory departure into Federal waters as a 'success') as the basis of the BGAM to fit the covariates. In this formulation probability of migratory departure into Federal waters is incorporated as an 'inverse log-link', with positive values indicating heightened likelihood and negative values a diminished likelihood. An additional advantage of this method is that it allows highly nonlinear responses to covariates, and being additive is readily predictable, i.e., responses are independent, though at the expense of not being able to resolve interaction effects, e.g. between life history stage, date and weather conditions. Therefore, separate models were run for HY birds, as well as for AHY females and for AHY males.

3 Results

3.1 Movement Model

We developed a spatially-explicit modeling framework to estimate 3-dimensional locations of *rufa* Red Knot movements along the Atlantic OCS from Massachusetts to Virginia. This model provides a framework to quantify likely paths taken and uncertainty in location in continuous time.

The model validation using the kite data (Figs. 6 and 7) revealed that the model was capable of tracking fine-scale movements (on the order of several kilometers), in an area that had two receiving stations separated by approximately 10 km. The calibration data also revealed that the model's predicted uncertainty was much greater than its precision. This indicates that the uncertainty reflects the range of plausible locations rather than the error in the median location.

Given the results from the calibration surveys, the Red Knot simulations presumably also produced more accurate predicted trajectories than indicated by the estimated model uncertainty, where the estimated trajectory was highly consistent with goal-directed flight. The high uncertainty in horizontal location estimates derived by the model also stem from uncertainty in altitudes. We chose an upper bound for possible flight altitudes of 2,500 m, since shorebirds including knots can attain altitudes above 1,000 m (Richardson 1976). However, median flight altitudes were nonetheless consistently low (Fig. 8) with a median 60 m among all detections within the Study Area, reaching a maximum of 1,035 m. Despite the model uncertainty, altitudes were frequently expected to fall largely within rotor swept altitudes (20 to 200 m; Fig. 8).

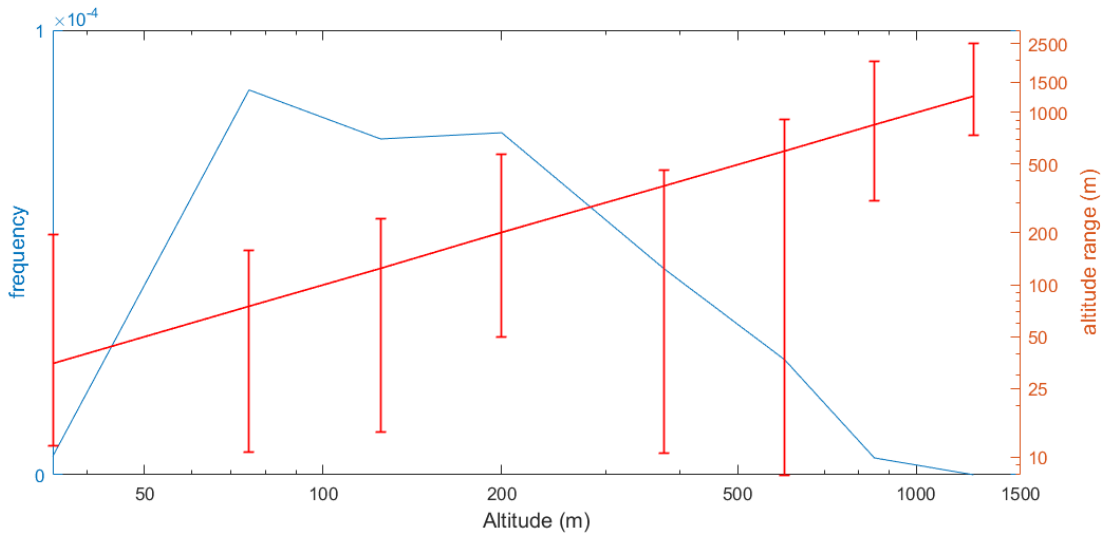


Figure 8. Frequency distribution of estimated flight altitudes

Flight altitudes (blue curve) are from all 1-minute location model outputs, with red bars representing lower and upper quartiles (reflecting model uncertainty) within altitudinal ranges.

3.2 Probability of Detection

Based on the radiation pattern of a single antenna (Fig. C-1), the higher a bird is flying, the farther away it can be detected by a tower. Using this relationship, we calculated the overall detection rate from the calibration surveys (p), as the proportion of kite locations that were accurately detected by the towers, given the kite's signal strength, GPS location, speed and trajectory. Detection rate per antenna within 40 second total scan time was calculated at approximately $p = 0.5$ (Appendix C). This can be seen from Figure 11, which depicts within-cycle detection rate as a function of bearing to the receiver and the angle of transmitter to receiver. Across the calibration surveys, the overall detection rate was highest along the main beam axis, i.e., bearing to receiving beam close to zero degrees (Fig. 9a), and varied marginally with the angle of transmitter to receiver (Fig. 9b). The relationship between signal gain and altitude z given in Equation 2 indicates that detection rate increases with increasing altitude, if z remains smaller than the horizontal range. Based on this overall detection rate for each antenna ($p = 0.5$), we developed a coverage map to identify areas of low-to-high overall detection probability (P) within our study region (Fig. C-2). For this, we estimated the probability of detection (P) by all antennas on a tower at any point in the radiation pattern, considering overlapping antenna beams (Appendix C). The detection summaries in Massachusetts and New Jersey indicate that although detection probability is relatively high within our Study Area, it is not complete, particularly along the New Jersey to Virginia coast where tower coverage is less dense. Lack of detections from individuals tagged within the Study Area could be due to gaps in coverage of the telemetry array, particularly for tracking low altitude flights (see Appendix C). Additional data loss occurs when transmitters malfunction or fall off prematurely, but these issues can be challenging to quantify and were not addressed in the present study. However, due to the large numbers of birds

tagged at Canadian stopover sites, and the assumed high detection probability that occurs during high-altitude, long distance migratory flights, there is a strong indication that birds tagged within the Mingan Islands and Hudson Bay regions largely did not fly through the Study Area during migration.

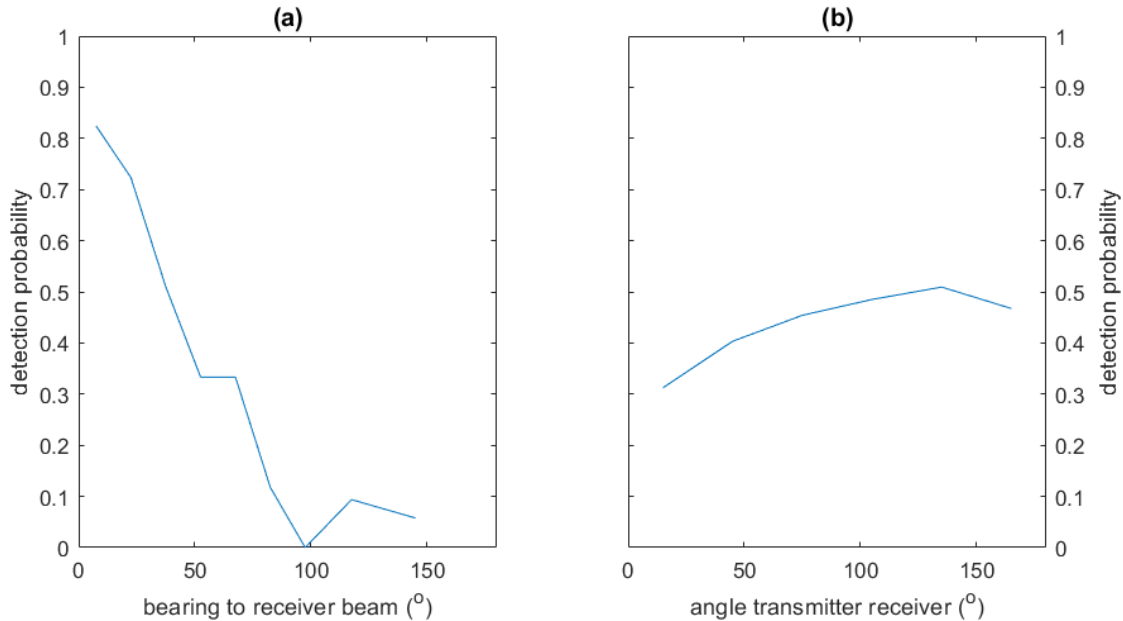


Figure 9. Detection probability of kite in relation to receiver location and transmitter alignment

Detection probability was calculated as proportion of received signals within each 40 second duty cycle, based on (a) the kite's GPS location and the angles of kite to the main axis of the receiver antenna and (b) the angle of the transmitter antenna to the main receiver axis. Across the calibration surveys, the overall detection rate was highest along the main beam axis, i.e., bearing close to zero degrees (a), and varied marginally with the angle of transmitter to receiver (b).

3.3 Demographic Variation in Movements and WEA Exposure Summary

During fall migration, a total of 388 Red Knots were tagged by partners in this study across four different tagging sites (Table 2). Of the 388 Red Knots tagged, 80 were tracked within Federal waters of the Study Area and 16 individuals were exposed to one or more WEAs within the Study Area, with a total of 30 exposure events across individuals (Table 2). Below, we describe demographic variation in movements and WEA exposure during staging and migration by Red Knots from each tagging site.

3.3.1 James Bay, Canada

In James Bay, Canada (Project 38), we tagged 9 Red Knots (3 AHY females, 4 AHY males, 1 AHY unknown sex, and 1 HY male) between July 28 and August 13. Two (AHY female and HY male) were

detected in the US, each for less than one day, on August 7 and September 1, respectively. Both passed through Federal waters of Nantucket Sound, Massachusetts.

3.3.2 Mingan Islands, Canada

In the Mingan Islands, Canada (Projects 15 and 38), we tagged 245 Red Knots (8 AHY females, 28 AHY males, 12 AHY unknown sex, 92 HY females, 104 HY males, and 1 HY unknown sex) between August 20 and October 15. Six Mingan Islands Red Knots (2 AHY males and 4 HY males) were detected in the Study Area between November 12 to November 27. All six intersected Federal waters of the Study Area, primarily between Rhode Island Sound and Delaware Bay. Five occurred in the Study Area for one day or less, and one HY male (id 316) remained for a total of 22 days, departing on December 11. This HY male, as well as an AHY male (id 328), were exposed to WEAs in New York (NY OCS-A 0512; Fig F-1) and Delaware (DE OCS-A 0482; Fig. F-2), respectively, on Nov 19, 2016.

3.3.3 Massachusetts, USA

In Massachusetts, USA (Project 88), we tagged 99 Red Knots (38 ASY females, 31 ASY males, 7 SY females, 13 SY males, 7 HY females, and 3 HY males) between July 31 and October 4. Of these, a total of 88 Red Knots (33 ASY females, 26 ASY males, 7 SY females, 13 SY males, 7 HY females, and 2 HY males) were detected in the Study Area (detection rate = 93%) and remained for an average of 30 days (SD 28 days, range: <1 to 105 days).

Of the 99 Massachusetts Red Knots tagged, 17 (17%) were tracked moving through Federal waters during staging, and of these, three were exposed to WEAs during flights on the staging grounds. Two female Red Knots (HY id 471 and SY id 464) crossed MA OCS-A 0478 on Sep 5 (Fig. F-3) and Nov 4 (Fig. F-4), respectively, while moving throughout Nantucket Sound. An additional SY female (id 453) had a total of 4 WEA exposure events during staging while moving between Nantucket Sound and southern Long Island, New York (Figs. F-5 to F-8). This individual crossed MA OCS-A 0478 on Oct 7 while departing from Cape Cod, Massachusetts towards Rhode Island Sound, and returned to Cape Cod, Massachusetts Nov 1, crossing the Block Island Wind Farm in state waters of Rhode Island, RI / MA OCS-A 0486 in Rhode Island Sound, and MA OCS-A 0478 in Nantucket Sound.

Final dates of detection in the Study Area ranged from August 1 and December 29. Migratory departure flights from 50 Massachusetts tagged Red Knots intersected Federal waters. Seven Massachusetts-tagged Red Knots were exposed to WEAs during migratory departure flights through Federal waters, with number of exposure events ranging from one to six events per individual.

Two Red Knots (id 434, a SY female and id 454, a SY male) crossed MA OCS-A 0478 in Nantucket Sound on September 9 (Fig. F-9) and November 7 (Fig. F-10), respectively. The SY female followed a western trajectory through Rhode Island Sound and then along the southern coast of Long Island. The SY male was last detected departing to the southwest of Nantucket, Massachusetts.

Id 437, a SY male, departed from Cape Cod, Massachusetts in mid-September and intersected two WEAs in Rhode Island Sound (RI / MA OCS-A 0486 and the Block Island Wind Farm), then followed a coastal route south to Virginia (Fig. F-11). Migratory departure flights of id 449 (SY female; Figs. F-12 to F-13) and id 470 (HY female; Figs. F-14 to F-15) each intersected WEAs in Nantucket Sound (MA OCS-A

0478) and Rhode Island Sound (RI / MA OCS-A and Block Island Wind Farm) in early November. The SY female departed offshore heading southeast of Block Island, and the HY female continued along the coast to Delaware Bay.

Id 458 (HY female) intersected WEAs in Federal waters off the coasts of Massachusetts (MA OCS-A 0478, MA OCS-A 0500 and 501, RI / MA OCS-A 0486), New Jersey (New Jersey OCS-A 0498 and 0499), Delaware (DE OCS-A 0482), and Maryland (MD OCS-A 0489 and 0490) during an overnight flight initiated on Nov 17 (Figs. F-16 to F-18). Id 451 (SY male) departed from Massachusetts on the evening of Nov 23 and followed a similar route to the mid-Atlantic, intersecting WEAs offshore of Massachusetts (MA OCS-A 0500 and 501), Delaware (DE OCS-A 0482), and Maryland (MD OCS-A 0489 and 0490; Figs F-19 to F-20). Two additional Red Knots, id 397 (ASY M) and ID 459 (SY F), flew from Massachusetts to the mid-Atlantic during migration but the tracking data collected within the Study Area is insufficient to determine WEA exposure (model derived ground speed <10 m/s).

Analyses of demographic variation in WEA exposure by age and sex for Red Knots tagged in Massachusetts indicated that HY birds had a significantly ($p=0.03$) higher probability of occurrence in WEAs relative to AHYs. There was no evidence of a significant effect of sex ($p=0.71$), or of an interaction between age and sex ($p=0.99$). By age and sex categories, percentages of Massachusetts tagged birds exposed to WEAs were: 30% of HYs (of $n=10$ tagged), 7% of AHYs (of $n=89$ tagged), 6% of males (of $n=47$ tagged) and 13% of females (of $n=52$ tagged).

3.3.4 New Jersey, USA

In New Jersey, USA (Project 14), we tagged 35 Red Knots (5 AHY females, 21 AHY males, 1 AHY unknown sex, 2 HY females, 2 HY males, 1 unknown age female, 2 unknown age males, 2 unknown age and sex) between August 8 and October 21. Of these, 27 Red Knots (3 AHY females, 17 AHY males, 1 AHY unknown sex, 2 HY females, 1 female unknown age, 2 males unknown age, 2 unknown age and sex) were detected in the Study Area (detection rate = 77%) and remained for an average of 17 days (SD 21 days, range <1 to 93 days).

Seven New Jersey tagged Red Knots were tracked crossing Federal waters within the Study Area during the staging period, as they moved between sites along the Atlantic coast ranging from Long Island, New York to southern Virginia. Of these, one individual (id, 47, age and sex unknown) crossed DE OCS-A 0482 and MD OCS-A 0489 and 0490 during a staging movement that occurred on Nov 9 (Fig. F-21).

Final dates of detection in the Study Area ranged from Aug 18 through November 26. Migratory departure flights from nine New Jersey tagged Red Knots intersected Federal waters. Four New Jersey-tagged Red Knots were exposed to WEAs during migratory departure flights through Federal waters, with number of exposure events ranging from one to three events per individual. In late August, AHY male (id 101; Fig. F-22) and AHY female (id 478; Fig. F-23) departed from the New Jersey coast heading offshore and intersected NJ OCS-A 0498 and 0499. Three additional AHY males (ids 97, 449, and 451) departed offshore on migration directly toward NJ OCS-A 0498 and 0499 in late Aug, but their final estimated locations did not reach far enough offshore to intersect the lease areas.

In mid-November, Id 48 (HY female; Figs. F-24 to F-25) departed from coastal New Jersey along a southern trajectory, intersecting WEAs off the coast of Delaware (DE OCS-A 0482), Maryland (MD

OCS-A 0489 and 0490) and Virginia (VA OCS-A 0483 and 0497). Id 47 (age and sex unknown), departed offshore to the east from staging grounds in Virginia on Nov 18, and intersected VA OCS-A 0483 and 0497 (Fig. F-26).

Analyses of demographic variation in WEA exposure by age and sex for Red Knots tagged in New Jersey did not indicate a significant effect of age ($p=0.442$), sex (0.961), or the interaction of age and sex (0.995). By age and sex categories, percentages of New Jersey tagged birds exposed to WEAs were: 33% of HYs (of $n=3$ tagged), 20% of AHYs (of $n=26$ tagged), 20% of males (of $n=22$ tagged) and 28% of females (of $n=7$ tagged).

Table 2. The number of VHF-tagged Red Knots that were detected crossing each BOEM Lease Area and BOEM Planning Area by tagging site during fall migration 2016. Sample size (N) of birds tagged at each site appears in top row.

BOEM Lease Areas¹ and Planning Areas (area in km²)	James Bay, Canada (N=9)	Mingan Is., Canada (N=245)	Massachusetts, USA (N=99)	New Jersey, USA (N=35)	Total (N=388)
Cape Wind Lease Area: MA OCS-A 0478 (119.5)	0	0	8	0	8
MA Lease Areas: MA OCS-A 0500 (759.0) and 501 (675.4)	0	0	2	0	2
RI/MA Lease Areas: RI / MA OCS-A 0486 (394.6) and 0487 (272.2)	0	0	5	0	5
NY Lease Area: NY OCS-A 0512 (321.1)	0	1	0	0	1
NJ Lease Areas: NJ OCS-A 0498 (649.4) and 0499 (742.0)	0	0	1	2	3
DE Lease Area: DE OCS-A 0482 (390.2)	0	1	2	2	5
MD Lease Areas: MD OCS-A 0489 (132.5) and 0490 (190.1)	0	0	2	2	4
VA Lease Areas: VA OCS-A 0483 (456.5) and 0497 (8.6)	0	0	0	2	2
MA Wind Energy Area (1,572.5)	0	0	0	0	0
NY Proposed Commercial Lease – Unsolicited (166.0)	0	0	0	0	0

Total	0	2	20	8	30
--------------	---	---	----	---	----

¹ Adjacent BOEM Lease Areas in MA, RI/MA, NJ, MD, and VA were pooled for exposure analysis

3.4 Timing, Meteorological Conditions, Altitude of Flights Across Offshore WEAs

We tracked a total of 30 flights across WEAs by 16 different Red Knots (N=2 from Mingan Islands, N=10 from Massachusetts, N=4 from New Jersey). For summaries of timing, meteorological conditions, and altitude of WEA exposure events, we pooled continuous flights across adjacent WEAs by individual, resulting in a total of 26 events (Appendix F).

3.4.1 Temporal Variation

Dates of WEA exposure events for Red Knots tagged in the US ranged from Aug 22 to Nov 24, with peak occurrence during November (Fig. 10). Two Red Knots tagged in the Mingan Islands, Canada were exposed to WEAs on Nov 19. Number of WEA exposure events that occurred per date ranged from 0 to 5, with the maximum occurring on Nov 5.

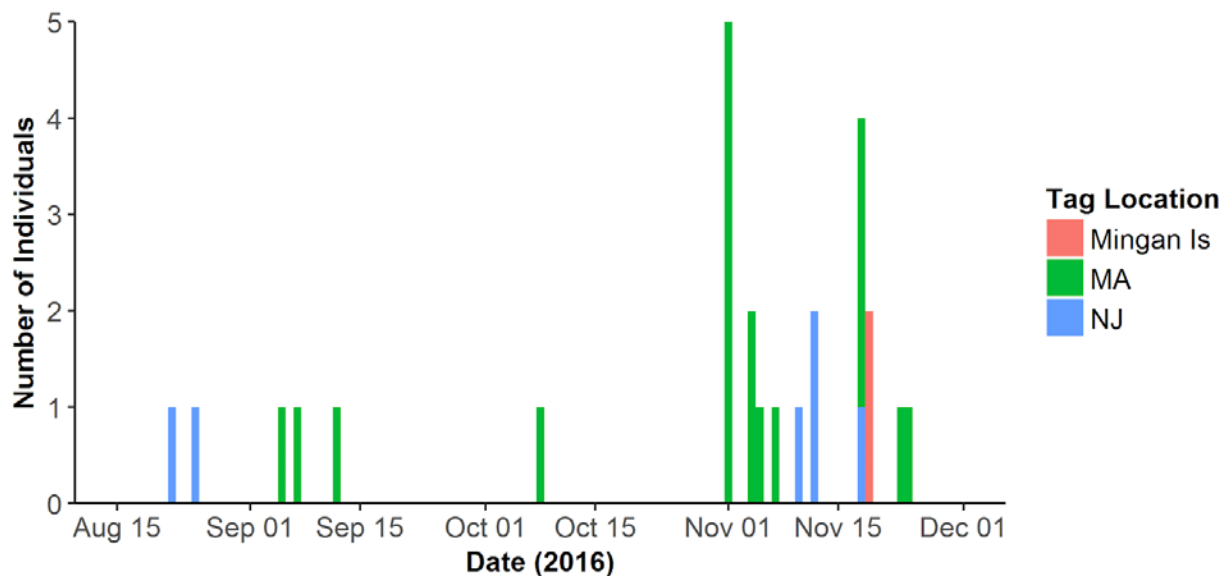


Figure 10. Frequency distribution in calendar of WEA exposure events (n=26) in 2016 by location of tag deployment

WEA exposure events primarily occurred at night (80%), between 15:00 hrs EST (3 hours prior to local time of local sunset) to 8:00 hrs EST (1 hour following time of local sunrise; Fig. 11). Peak timing of WEA exposure events occurred between midnight and 02:00 hrs EST ($\rho = 0.57$).

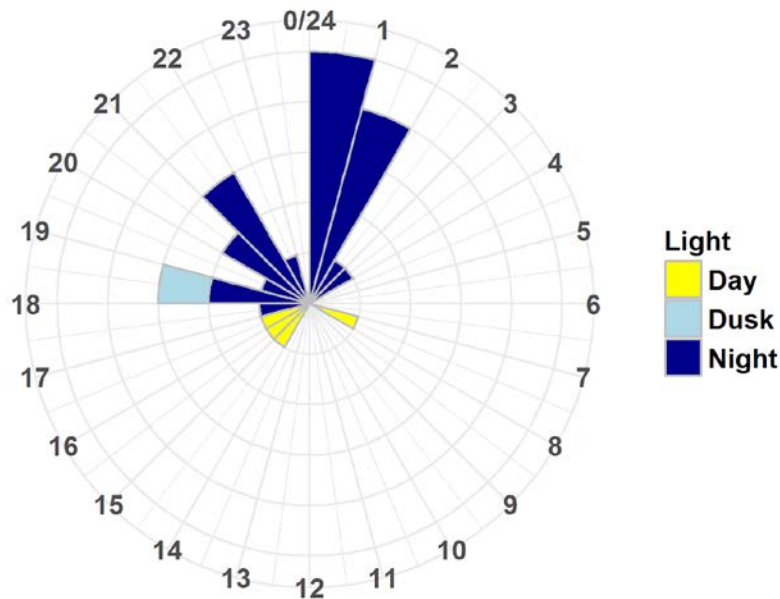


Figure 11. Diel variation (hrs, in EST) in timing of WEA exposure events (n=26), categorized by daylight using timing of local sunrise and sunset

3.4.2 Meteorological Conditions

Flights across WEAs occurred during periods of moderate wind speed (mean 6.9 m/s; range 1 to 12.3 m/s; Fig. 12), with winds primarily blowing to the southeast (circular median wind direction 165 degrees, $\rho=0.5$; Fig. 13). There was some indication of variation in wind direction during WEA exposure event by tagging location. Red Knots from Massachusetts crossed WEAs during southern winds (median=176 degrees), but with higher variability ($\rho=0.42$), whereas Red Knots from New Jersey primarily crossed WEAs during southeast winds (median=164 degrees) with lower variability ($\rho=0.71$). On average, Red Knots crossed WEAs with variable wind support (mean wind support = 1.76 m/s, range -7.36 m/s to 11.06 m/s; Fig. 14) and crosswind conditions (mean crosswind 2.94 m/s, range -6.30 m/s to 10.04 m/s; Fig. 15).

Flights across WEAs occurred during fair weather, under clear skies (mean visibility 19,634 m; range 15,116 to 20,035 m; Fig. 16) with above-average barometric pressure (mean 102101 Pa, range 101309 to

102847 Pa; Fig. 17), mild temperatures (mean 285 K, range 278 to 298 K; Fig. 18), and little to no precipitation (mean accumulation 0.0053 kg/m², range 0 to 0.0653 kg/m²; Fig. 19 and Table 3).

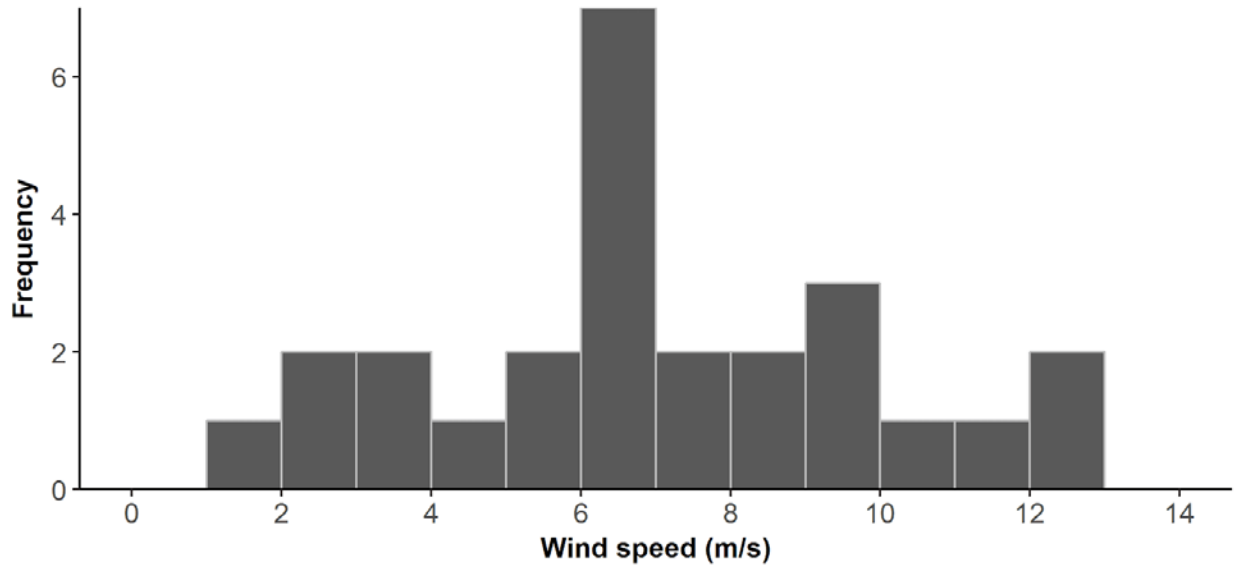


Figure 12. Frequency distribution of wind speed (m/s) during WEA exposure events (n=26)

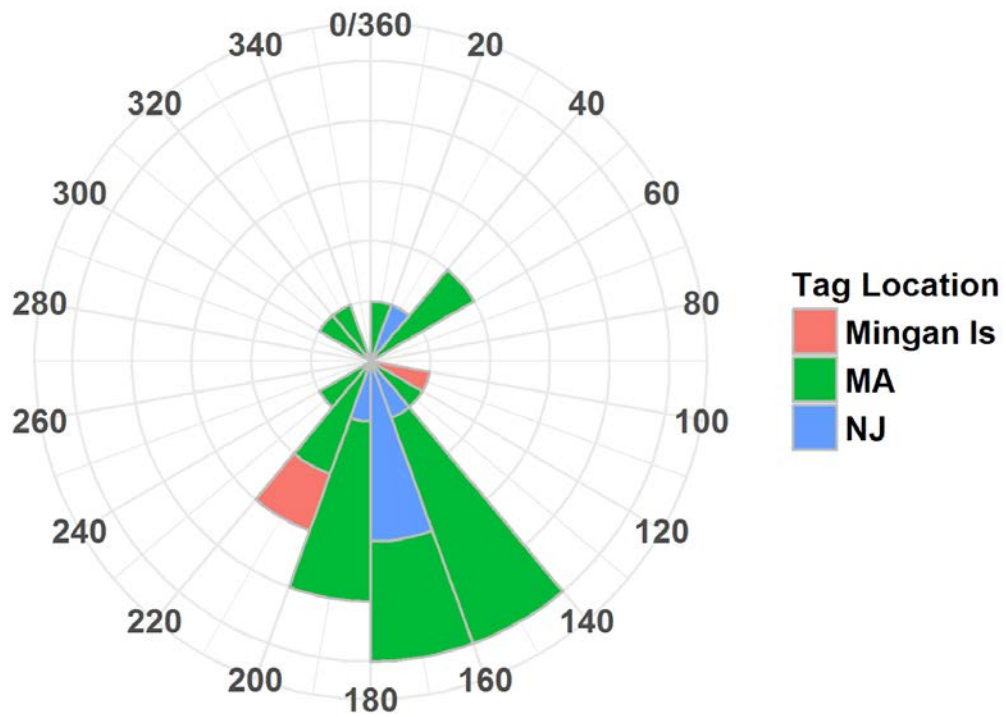


Figure 13. Circular histogram of wind direction (degrees clockwise from N) during WEA exposure events (n=26), by location of tag deployment

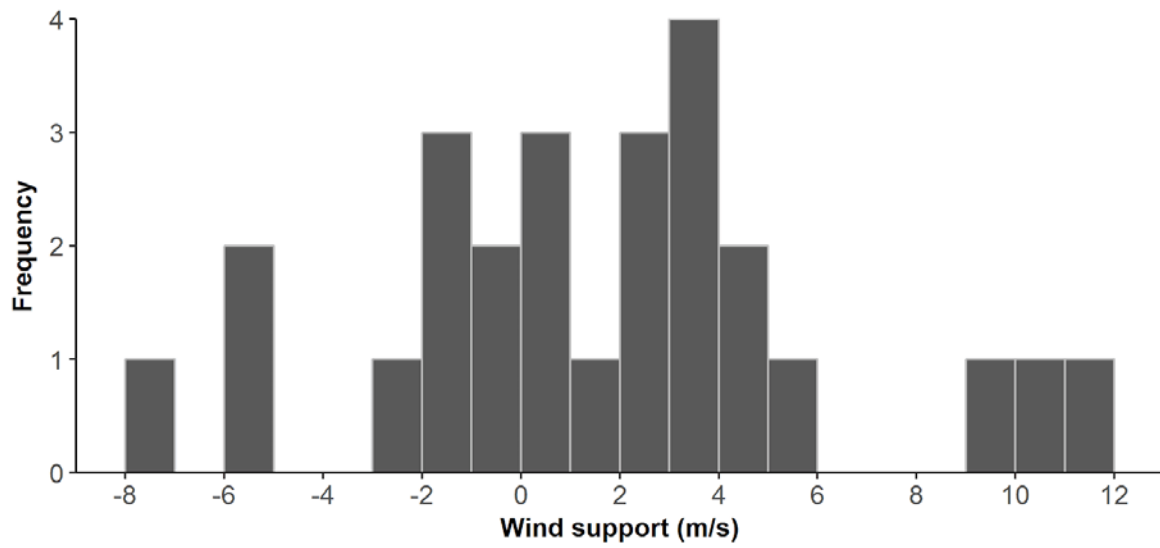


Figure 14. Frequency distribution of wind support (m/s) during WEA exposure events (n=26)

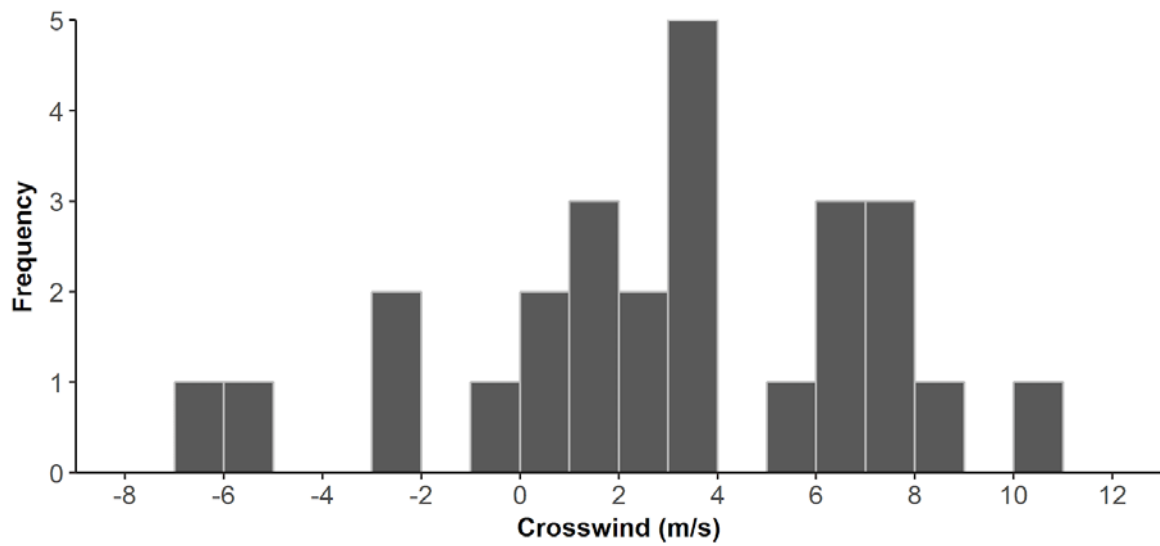


Figure 15. Frequency distribution of crosswind (m/s) during WEA exposure events (n=26)

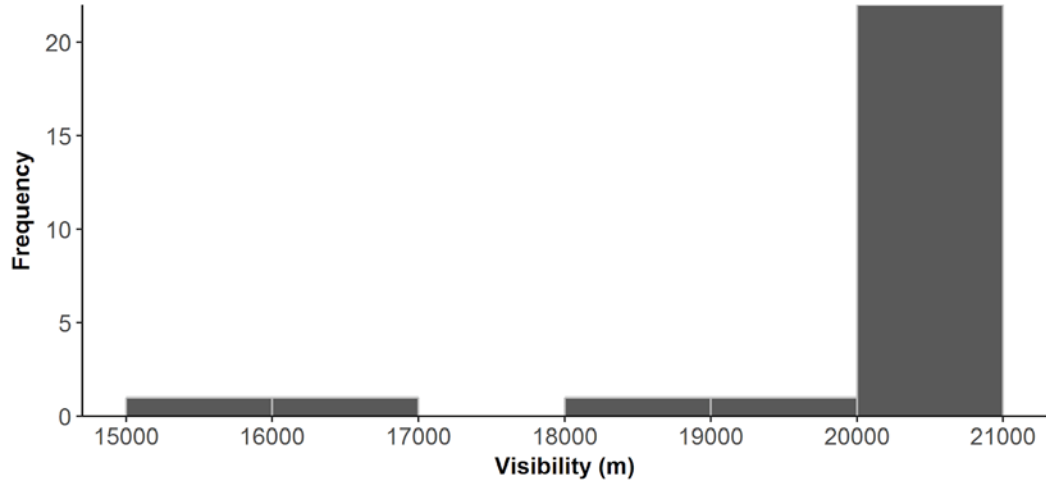


Figure 16. Frequency distribution of visibility (m) during WEA exposure events (n=26)

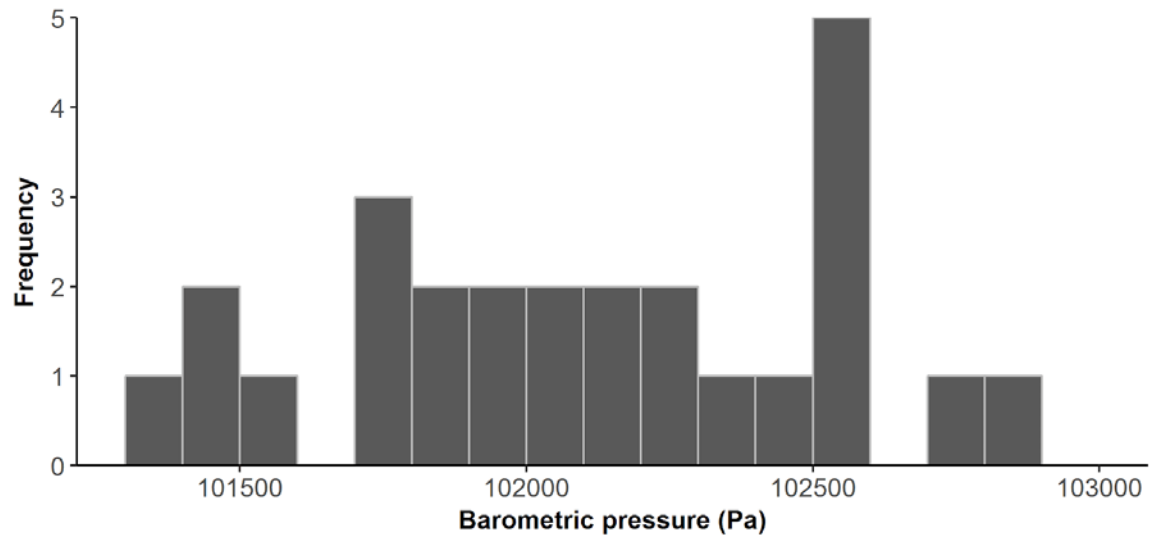


Figure 17. Frequency distribution of barometric pressure (Pa) during of WEA exposure events (n=26)

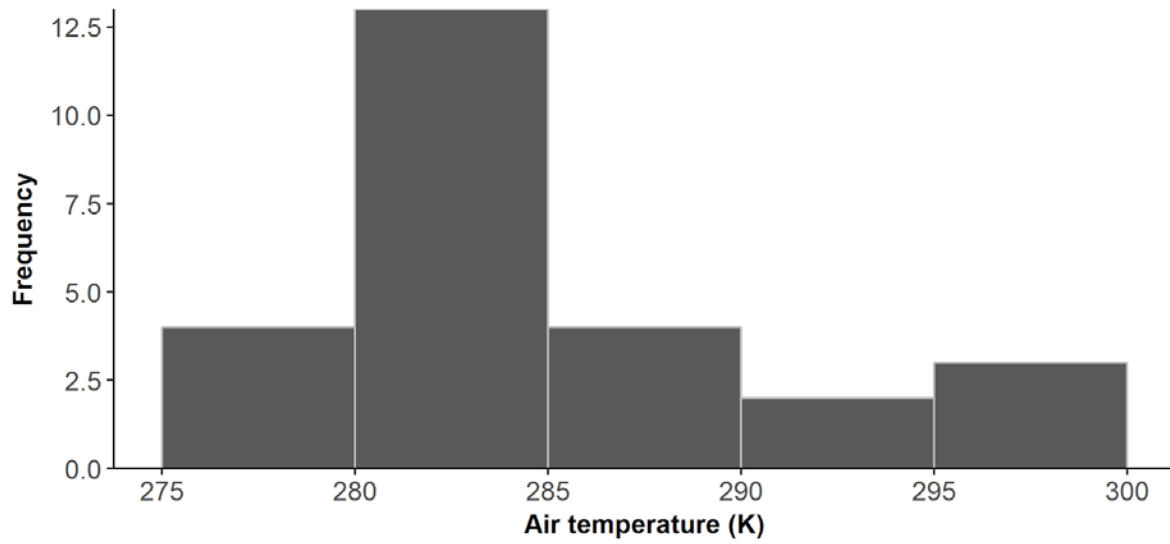


Figure 18. Frequency distribution of precipitation air temperature (K) during of WEA exposure events (n=26)

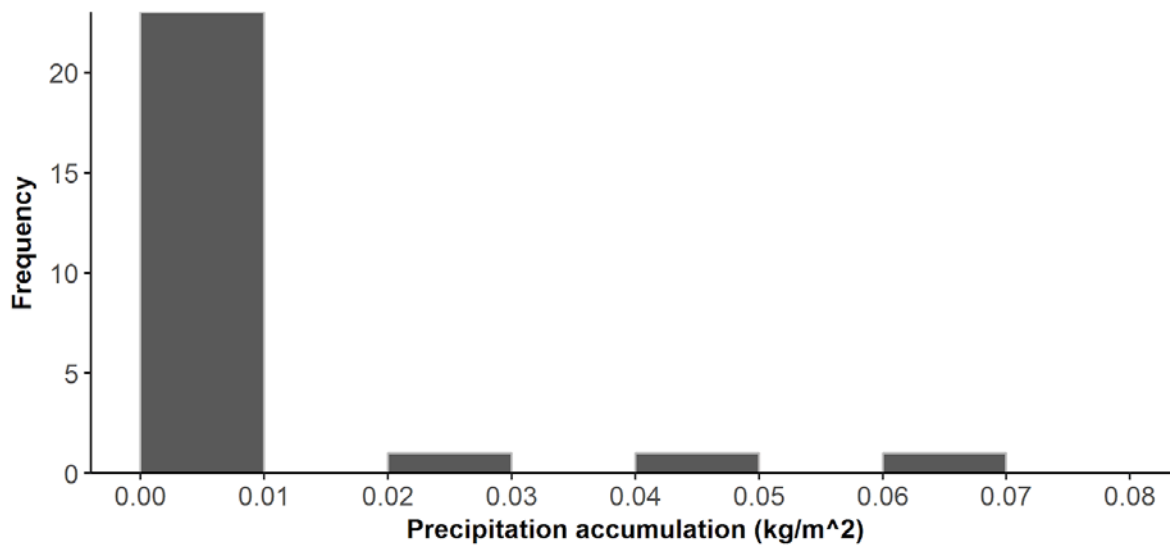


Figure 19. Frequency distribution of precipitation accumulation (kg/m²) during of WEA exposure events (n=26)

Table 3. Summary statistics of meteorological conditions during WEA exposure events (n=26) for Red Knots tracked during fall migration 2016.

Meteorological Condition	Mean (SD)	Range
Wind speed (m/s)	6.96 (2.89)	1.32 - 12.31
Wind support (m/s)	1.76 (4.53)	-7.36 - 11.06
Crosswind (m/s)	2.94 (4.20)	-6.30 - 10.04
Barometric pressure (Pa)	102,101 (429)	101,310 - 102,847
Precipitation accumulation (kg/m ²)	0.005 (0.016)	0.00 - 0.065
Temperature (K)	285.28 (5.53)	278.06 - 298.06
Visibility (m)	19,633 (1,141)	15,115 - 20,035

3.4.3 Altitude of Flights Across WEAs

The estimated mean altitude of flights across WEAs was 106 m (range 22 m to 882 m; Fig. 20 and Appendix F). The majority (77%) of flights across WEAs were estimated to occur in the rotor swept zone of offshore wind turbines (20 to 200 m). For all flights across WEAs, the maximum distance between two towers receiving detections simultaneously from the same bird was 50 km. The lack of long-distance simultaneous detections provides evidence that Red Knots were crossing WEAs at low altitudes (< 200 m; Appendix C). However, given the theoretical uncertainty in predicted altitudes (>100 m; Fig. 21), estimates of occurrence within the rotor swept zone are coarse relative to the size of the rotor swept zone (20 to 200 m).

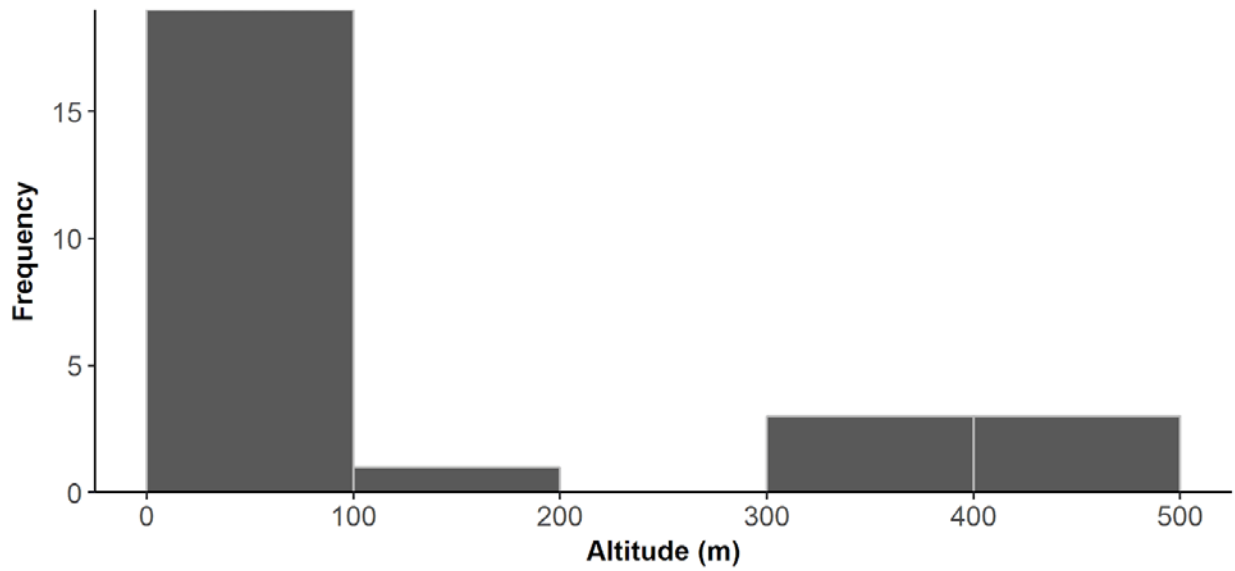


Figure 20. Frequency distribution of model-estimated altitude (m) during WEA exposure events (n=26).

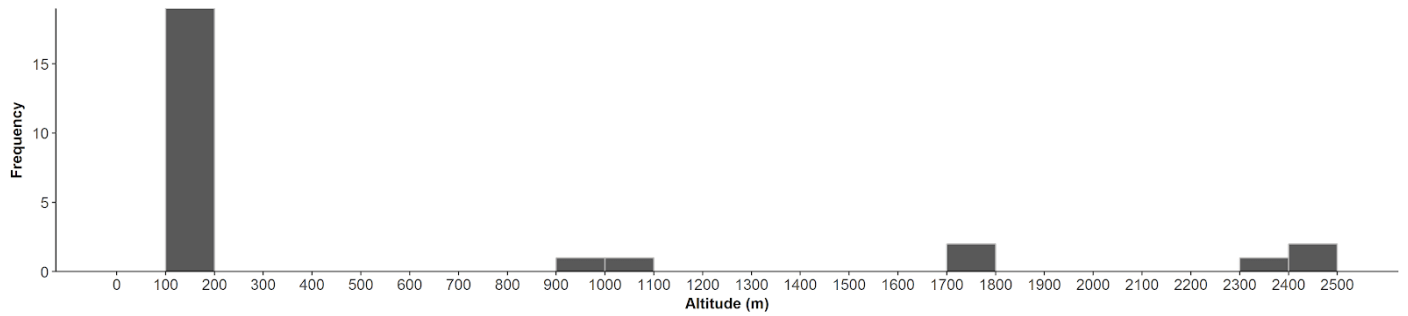


Figure 21. Frequency distribution of uncertainty (interquartile range) of altitude estimates (m) during WEA exposure events (n=26).

3.5 Covariate Analysis of Migratory Movements in Federal Waters

3.5.1 Temporal, Demographic, and Meteorological Variation

We assessed migratory departure into Federal waters relative to local movements on the staging grounds using data from 107 Red Knots that were tagged at staging sites in Massachusetts and New Jersey and remained in the Study Area for at least two days. This sample comprised 39 AHY females, 51 AHY males, 11 HYs (9 females and 2 males), and 6 individuals of unknown age and sex. Overall, 58 individuals initiated migratory flights into Federal waters, with similar proportions from each demographic cohort: 64% (n=25) of the adult females, including one female (project 88, id 434) that undertook two offshore departure flights (from Cape Cod, Massachusetts across the mid-Atlantic Bight to stage in New Jersey, and subsequently from New Jersey heading offshore), 53% (n=27) of the adult males, 36% (n=4) of the HY individuals (all females), and two individuals of unknown age and sex.

Timing during the day revealed that birds typically initiated migratory flights into Federal waters within several hours of civil dusk, but also sometimes during dusk, night or close to dawn (Fig. 22). Within the season, timing of migratory departure into Federal waters varied by age class (Figs. 23 and 24, Table 4). Among the individuals that departed into Federal waters, adult male and females initiated migration earlier (median departure 16 to 17 August) relative to HYs (median departure November 14; Kruskal-Wallis test $p=0.01$). Birds that initiated migration earlier (August through late September) departed in a southeast direction but with higher variability (median 113 degrees, $\rho = 0.42$; Fig. 25). Red Knots that initiated migration later into fall (mid-October through late November), departed in a more southern direction (median 189 degrees) with less variability ($\rho = 0.76$; Fig. 26).

To assess the conditions during which Red Knots depart on migration over Federal waters within the Study Area, we compared the covariate distributions between staging locations (daily, at dawn and dusk) of all individuals tagged in the Study Area (n=123), with the covariate distributions at migratory initiation for 58 individuals that departed into Federal waters (Fig. 27 and Table 5). Departure tracks from the remaining 64 individuals either followed the coast or were not resolved by the movement model due to unknown factors (e.g. tag loss, tag malfunction, movements outside detection coverage of telemetry array prior to migration). Overall, individuals with clear migration tracks into Federal waters departed earlier in the season versus the overall distribution of staging movements ($p = 0.01$).

Among meteorological covariates, wind conditions were also strongly associated with migratory departures into Federal waters. Departures into Federal waters were associated with stronger winds blowing towards the south (median 3.4 m/s vs. 0.8 m/s; Kruskal-Wallis test, $p < 0.0001$) as well as stronger wind support (median 2.1 m/s vs. 0 m/s; Kruskal-Wallis test, $p < 0.0001$). This can also be seen by comparing the distributions of wind direction and track direction on departures, with a strong selectivity of winds blowing to the southeast. Wind speeds did not differ significantly between staging and migratory movements ($p = 0.52$).

Few differences between wind-related factors among life history classes were evident in the univariate analysis, although crosswind differed between HY and AHY birds (Fig. 24, Kruskal-Wallis test, $p = 0.02$). This could be related to differences in wind selectivity and reaction to wind; however, the sample size of HY birds was small (n=4 among 11 individuals staging in the area).

As with WEA exposure events, migratory departures into Federal waters occurred during favorable weather conditions, including clear skies, and little to no precipitation (Table 4).

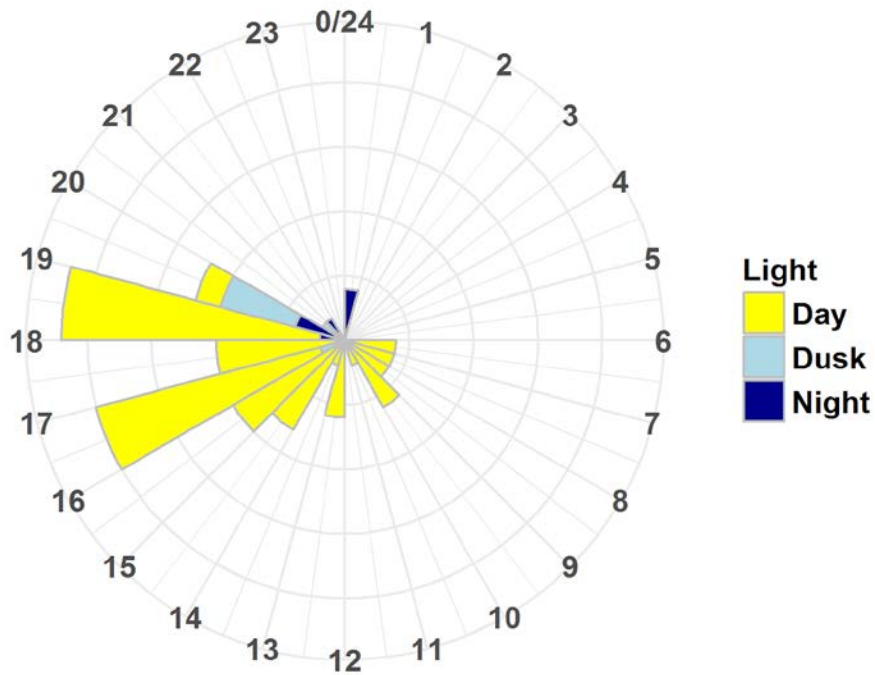


Figure 22. Diel variation (hrs, in EST) in timing of migratory initiation for flights (n=59) into Federal waters of the Study Area

Migratory initiation times are categorized by daylight using timing of local sunrise and sunset.

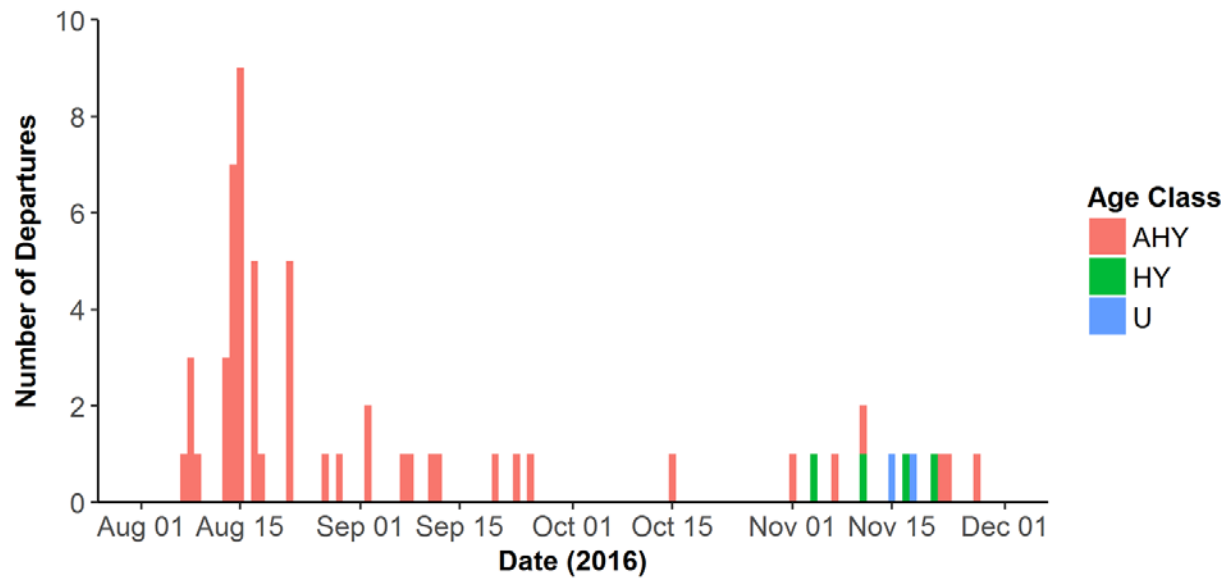


Figure 23. Demographic variation in dates of migratory initiation for flights (n=59) into Federal waters of the Study Area

Migratory initiation dates are categorized by age class: After Hatch Year (AHY), Hatch Year (HY), and Unknown (U).

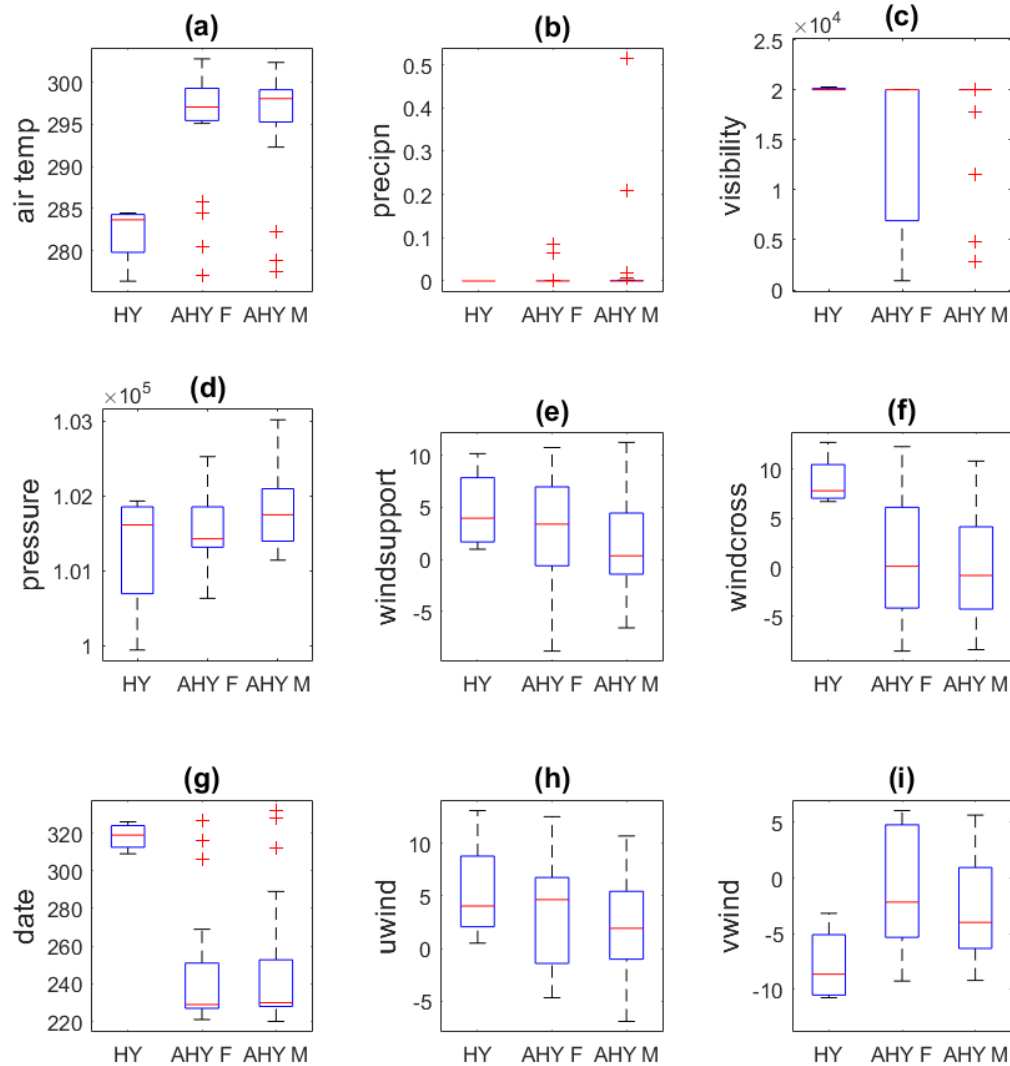


Figure 24. Distributions of meteorological and temporal covariates

Among age and sex classes (HY, and AHY females and males) associated with migratory departures into Federal waters (n=59): (A) surface air temperature ([K]), (B) accumulated 3-hourly precipitation (kg/ m²), (C) visibility (m), (D) barometric pressure (Pa), (E) wind support (m/s), (F) crosswind (m/s), (G) day of year, (H) zonal (Eastward) wind (m/s) and (I) meridional (Northward) wind (m/s). The blue lines indicate the quantiles, the red line indicates the mean, the dashed lines indicate the interquartile (25-75%) range, with red crosses indicating outliers (beyond twice the interquartile range).

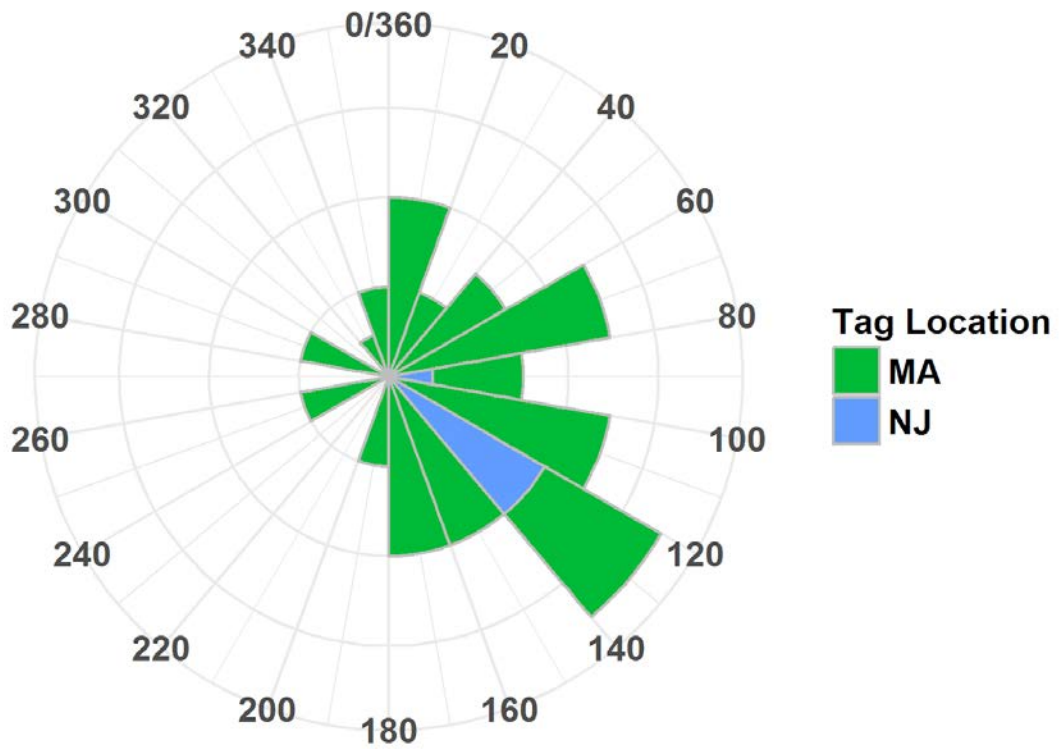


Figure 25. Angular distribution of track directions (degrees clockwise from N)
 Of migratory departure flights into Federal waters of the Study Area that were initiated from mid-August to late September (n=46).

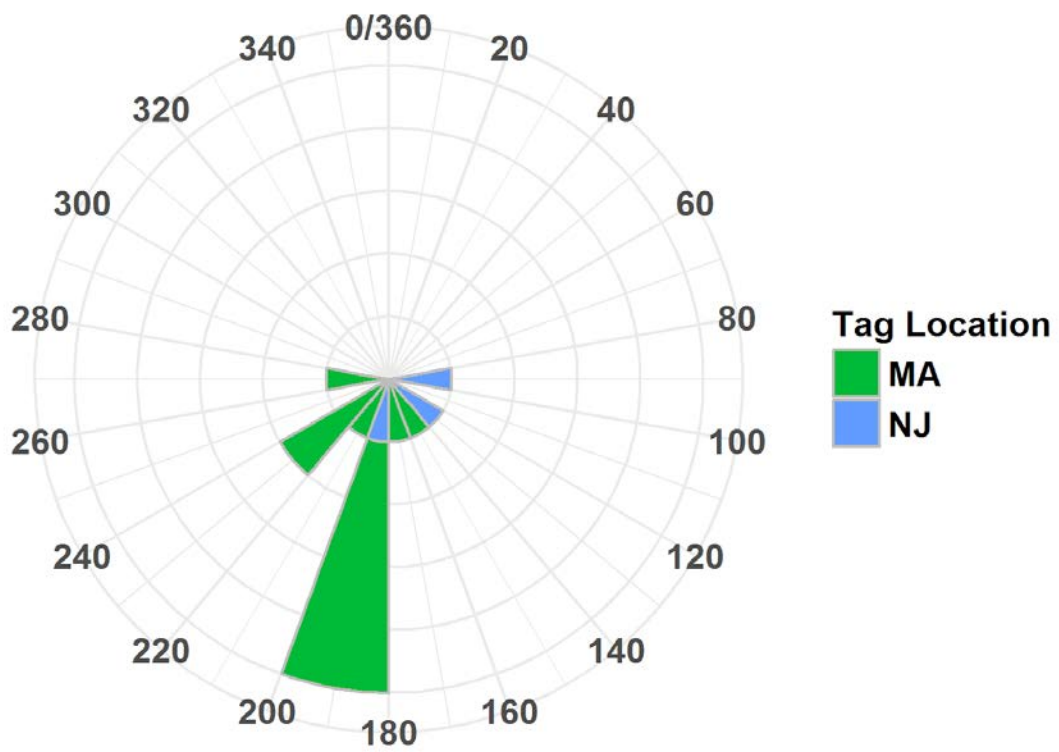


Figure 26. Angular distribution of track directions (degrees clockwise from N)

Of migratory departure flights into Federal waters of the Study Area that were initiated from mid-October to late November (n=13).

Table 4. Summary of meteorological covariates by demographic cohort among migratory departures into Federal waters.

Covariate	Median All (n= 9)	Median HY (n=4)	Median AHY Female (n=26)	Median AHY Male (n=27)	p(HY ≠ AHY Female, Male)
Air temperature at 1000 mb (°K)	297.3	283.7	297.1	298.1	0.02
Accumulated precipitation (kg/m ²)	0	0	0	0	0.23
Visibility (m)	20010	20006	20009	20010	0.65
Surface barometric pressure (Pa)	101535	101611	101425	101747	0.13
Wind support (m/s)	2.07	3.96	3.38	0.33	0.34
Crosswind (m/s)	0	7.8	0.12	-0.81	0.02
Date	230	319	229	230	0.01
Zonal (Eastward) wind (m/s)	3.41	4.05	4.65	1.93	0.37
Meridional (Northward) wind (m/s)	-3.4	-8.62	-2.16	-3.98	0.07
Wind speed (m/s)	7.4	10.8	7.8	6.8	0.02

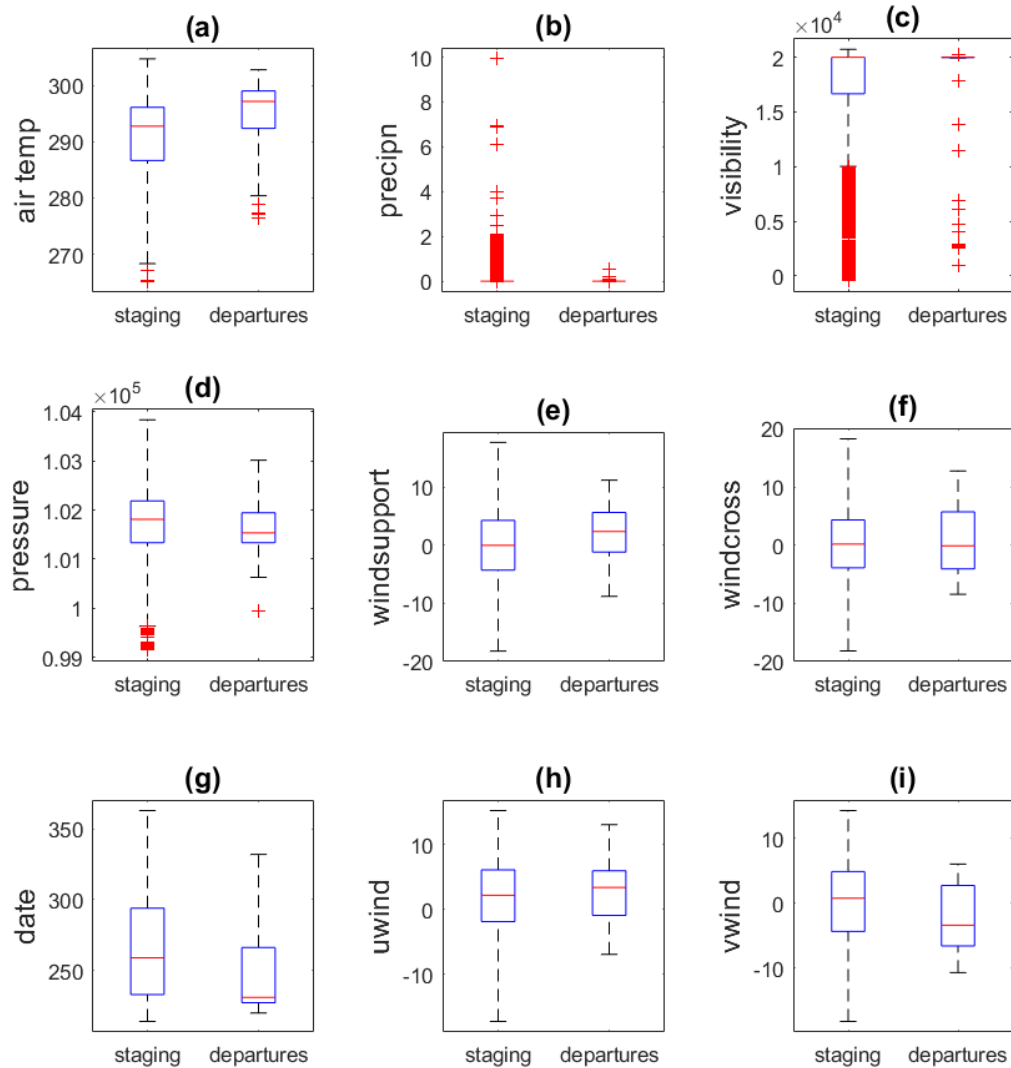


Figure 27. Distributions of meteorological conditions and day of year among staging locations (at civil dusk and dawn) versus initiation of migratory departure flights into Federal waters

(A) surface air temperature ([K]), (B) accumulated 3-hourly precipitation (kg/m^2), (C) visibility (m), (D) barometric pressure (Pa), (E) wind support (m/s), (F) crosswind (m/s), (G) day of year, (H) zonal (Eastward) wind (m/s) and (I) meridional (Northward) wind (m/s). The blue lines indicate the quantiles, the red line indicates the mean, the dashed lines indicate the interquartile (25-75%) range, with red crosses indicating outliers (beyond twice the interquartile range).

Table 5. Summary of meteorological covariates among migratory departures into Federal waters versus staging locations (twice-daily) at civil dawn and dusk

Covariate	Median all events (n=6,250)	Median departures (n=59)	Median staging (n=6,191)	p(departures ≠ staging)
Air temperature at 1000 mb (°K)	293	297	293	< 0.0001
Accumulated precipitation (kg/m ²)	0	0	0	0.27
Visibility (m)	20006	20010	20006	0.01
Surface barometric pressure (Pa)	101809	101535	101812	0.09
Wind support (m/s)	0.01	2.07	0	< 0.0001
Crosswind (m/s)	0.14	0	0.14	0.56
Date	259	230	259	0.01
Zonal (Eastward) wind (m/s)	2.21	3.41	2.2	0.13
Meridional (Northward) wind (m/s)	0.75	-3.4	0.77	< 0.0001
Wind speed (m/s)	7.4	7.3	7.4	0.52

3.5.2 Multivariate Boosted GAM Analysis

The covariate distributions and the boosted GAM model selection procedure revealed that Red Knots departed into Federal waters during migration in association with certain meteorological and temporal covariates. The boosted GAM provided a quantitative multi-covariate assessment of both covariate influence (related to the frequency with which a covariate affected occurrence across the region and season) and the response to each covariate, related to the size (increased likelihood of departure into Federal waters) of any such effect. Together, these help to quantify the overall likelihood of departure into Federal waters (through the covariate distributions) and the relative likelihood of migratory departure into Federal waters for any given covariate distribution, through the boosted GAM prediction for a given meteorological and demographic covariate. Below, we discuss the most significant of these associations.

The relation between covariates and initiation of migratory flights into Federal waters was quantified using the boosted GAM fits by two measures: (1) model “influence”, representing the overall frequency (%) a covariate was chosen among the boosted iterations and (2) predicted covariate “responses”, indicating the relative likelihood of departure into Federal waters for a given covariate value; positive responses indicate increased likelihood and negative values decreased likelihood. Since the model is additive, the probability of departure into Federal waters is proportional to the sum of all responses through an inverse binomial logistic link.

The boosted regression analysis supported the univariate covariate analysis, with seasonal (temperature and day of year), and wind-related covariates (Meridional wind and wind support) being the most influential in predicting migratory departures into Federal waters. The model incorporating all staging and departure flights reduced 23% of total deviance, that incorporating AHY females 27%, AHY males 28% and HY individuals 11%. Deviance is analogous to but not directly comparable with reduction of variance in maximum likelihood-based models.

Considering all individuals, air temperature, Meridional (northward) wind and visibility were most influential among iterative boosts (together ~75%) in the model (Fig. 28; covariates are selected according to maximum likelihood in reducing remaining model deviance). Day of year, wind support and Zonal (eastward) wind component accounted for approximately 5% more reduction in deviance each.

Figures 29 to 32 depict predicted responses (left-hand y-axis values in Fig. 29, i.e. blue curves, indicating relative increase in likelihood of departure) among all individuals (n=123, Fig. 29), AHY females (n=25, Fig. 30), AHY males (Fig. 31) and HY individuals (Fig. 32). The magnitude of responses among covariates in predicting occurrence of migratory departure flights into Federal waters matched their influences. Note that these responses reflect probability of migratory departure into Federal waters, given individual staging and given covariate value. The red curves in Figures 29 to 32 represent frequency distribution of covariate values within the Study Area, which will also affect the overall occurrence in the Area.

Considering all individuals, likelihood of departure increased when temperatures were seasonally cool (below 280 K) or, especially, seasonally warm (300 K, Fig. 29 a); correspondingly, we observe two departure peaks early and late in the season (Fig. 29 d). Departure was also associated with supportive

winds blowing to the south (Fig. 29 b, e, f), relatively high visibility (Fig. 29 c). Barometric pressure, precipitation, and crosswind (Fig. 29 g, h, i) were predicted to be of little influence.

Boosted GAM predictions for each AHY females (Fig. 30) and AHY males (Fig. 31) were overall very similar to the overall model, with the exception that both tended to depart earlier in the season (Fig. 30 g and Fig. 31 f) and that AHY males tended to select winds blowing to the east less strongly (Fig. 30 e and Fig. 31 h). Responses among HY individuals to covariates (Fig. 32) revealed only a clear association with positive crosswinds; in all four cases this occurred while flying towards the southwest under winds blowing towards the southeast.

3.5.3 Effects of Temperature, Pressure, Visibility and Precipitation

Temperature and barometric pressure and, to a lesser extent, visibility and precipitation were also influential in predicting migratory departure into Federal waters. Temperature was considered more significant (Table 4) and influential (Fig. 28) than date of year, both in distinguishing among sex and demographic cohorts and in likelihood of migratory departure into Federal waters (Table 5 and Fig. 28). However, this may reflect seasonal phenology more so than a direct response to synoptic weather (although the boosted GAM framework can potentially distinguish between effects among closely correlated variables, e.g. McLaren and Buler 2018). Otherwise, covariate distributions among all locations at dawn and dusk in staging areas (Fig. 29) revealed a general moderate increase in departure likelihood in high (close to 20 km) visibility among all cohorts, but no clear response to precipitation or pressure, except for a weak increased likelihood in precipitation among AHY males.

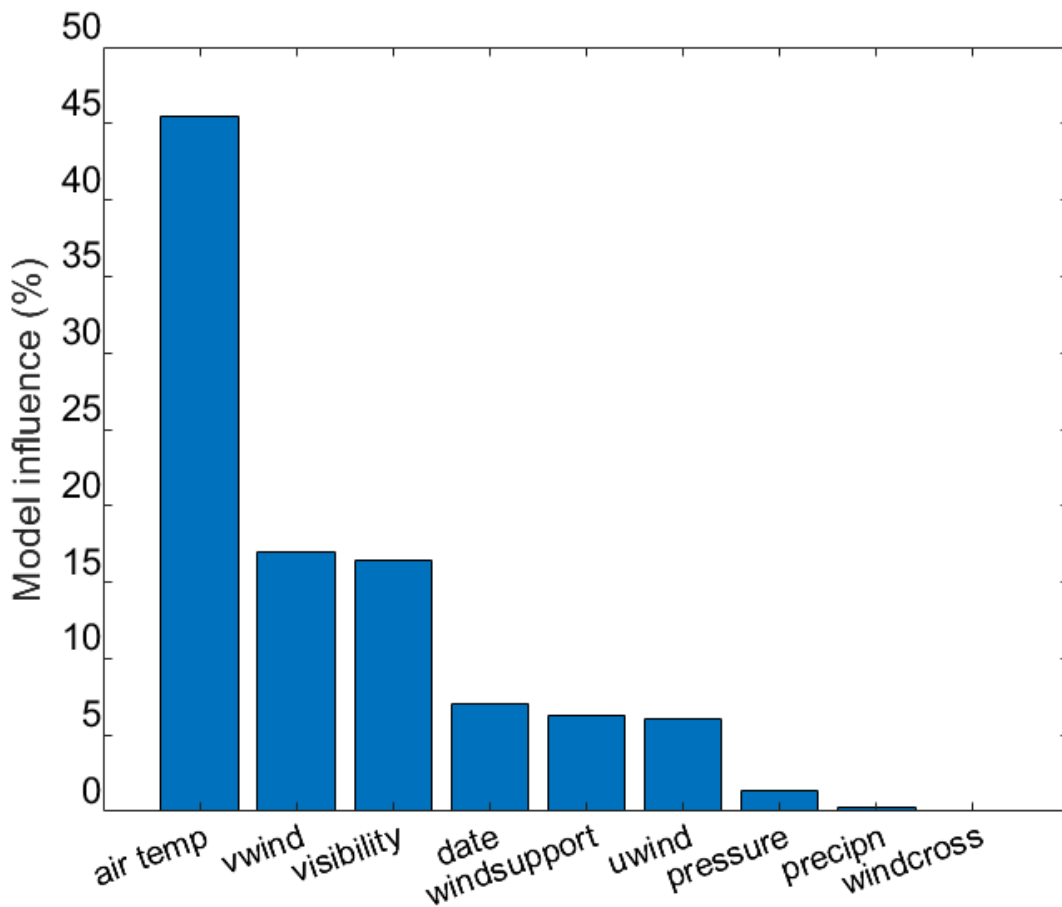


Figure 28. Predicted influence of covariates on relative likelihood of initiating migratory flights into Federal waters

In terms of minimizing model deviance, with predicted covariates during departing (n=59) flights and while staging within the Study Area (sampled at dawn and dusk, n=6,523).

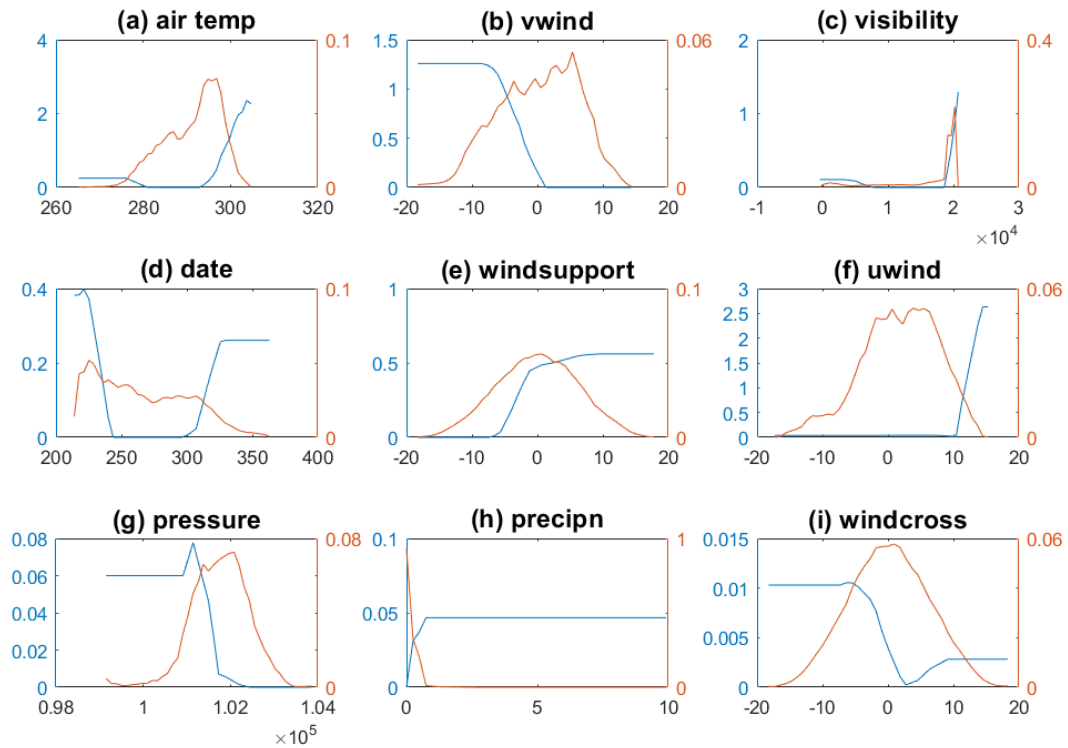


Figure 29. Predicted strength of marginal response to covariates in increasing likelihood of migratory departure into Federal waters

Blue lines depict relative likelihood of departing into Federal waters (with positive values indicating increased likelihood of departure) and red lines depict frequency of detection across conditions during migratory departure flights into Federal waters (n=59) and staging locations within the Study Area (sampled at dawn and dusk, n=6,523). Covariate responses are depicted in order of model influence (corresponding to Fig. JM3).

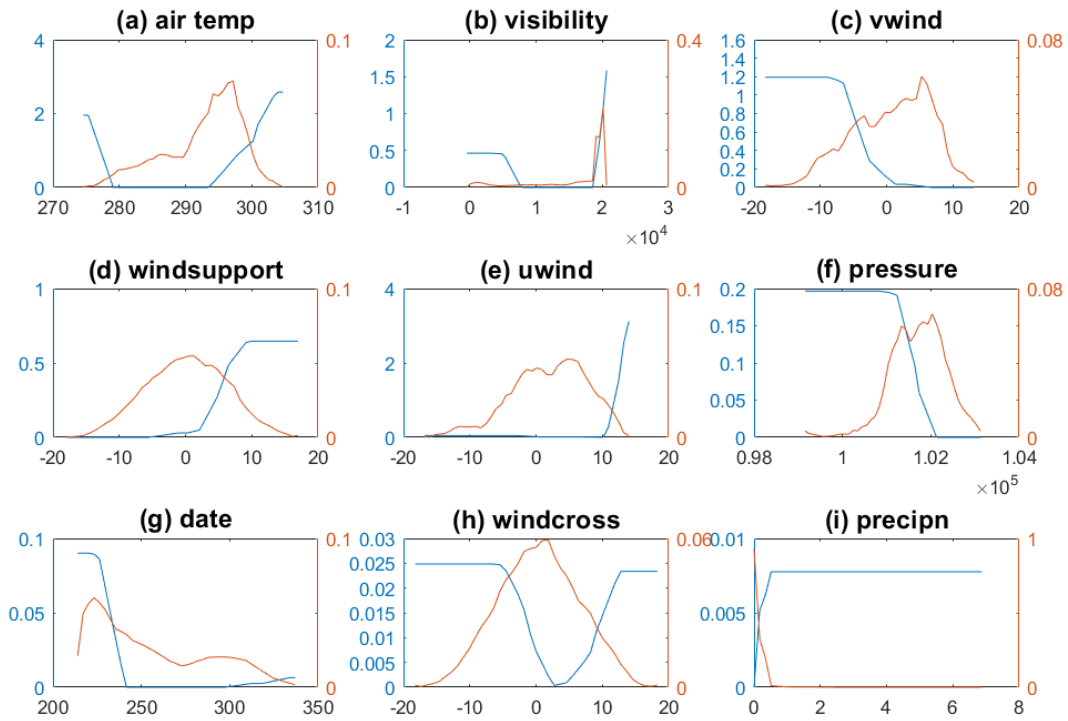


Figure 30. Predicted strength of marginal response to covariates in increasing likelihood of migratory departure into Federal waters by AHY females.

Blue lines depict relative likelihood of migratory departure into Federal waters (with positive values indicating increased likelihood) and red lines depict frequency of detection across conditions while individuals staged in the Study Area (sampled at dusk and dawn). Covariate responses are depicted in order of model influence.

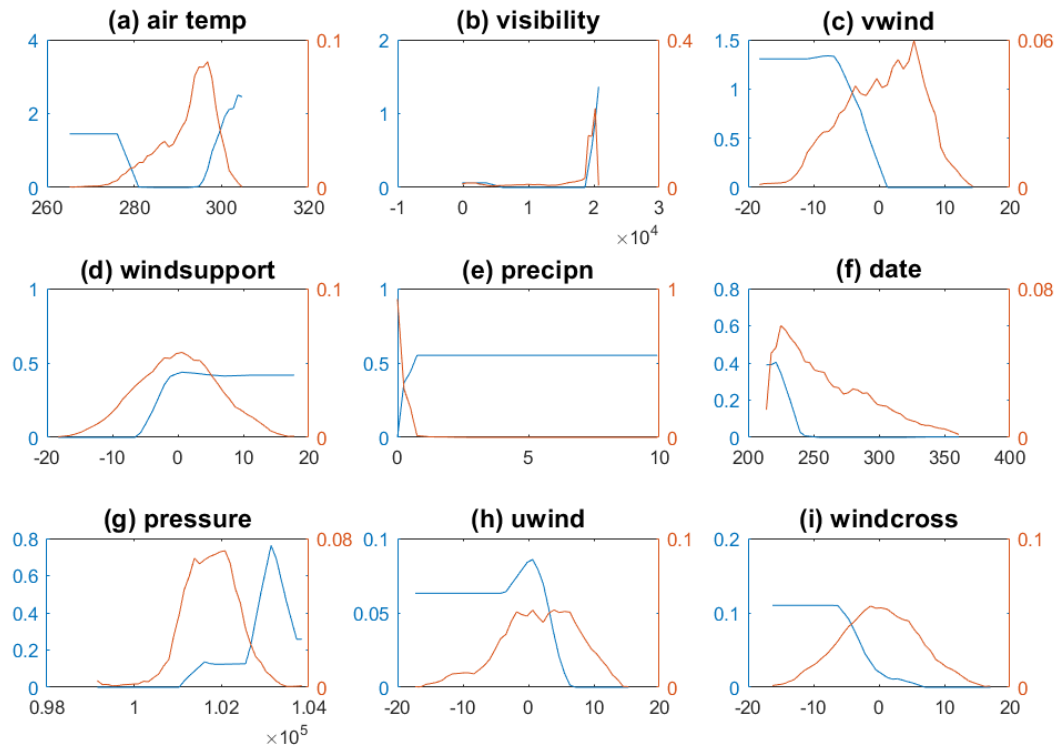


Figure 31. Predicted strength of marginal response to covariates in increasing likelihood of migratory departure into Federal waters among AHY males

Blue lines depict relative likelihood of migratory departure into Federal waters (with positive values indicating increased likelihood) and red lines depict frequency of detection across conditions while individuals staged in the Study Area (sampled at dusk and dawn). Covariate responses are depicted in order of model influence

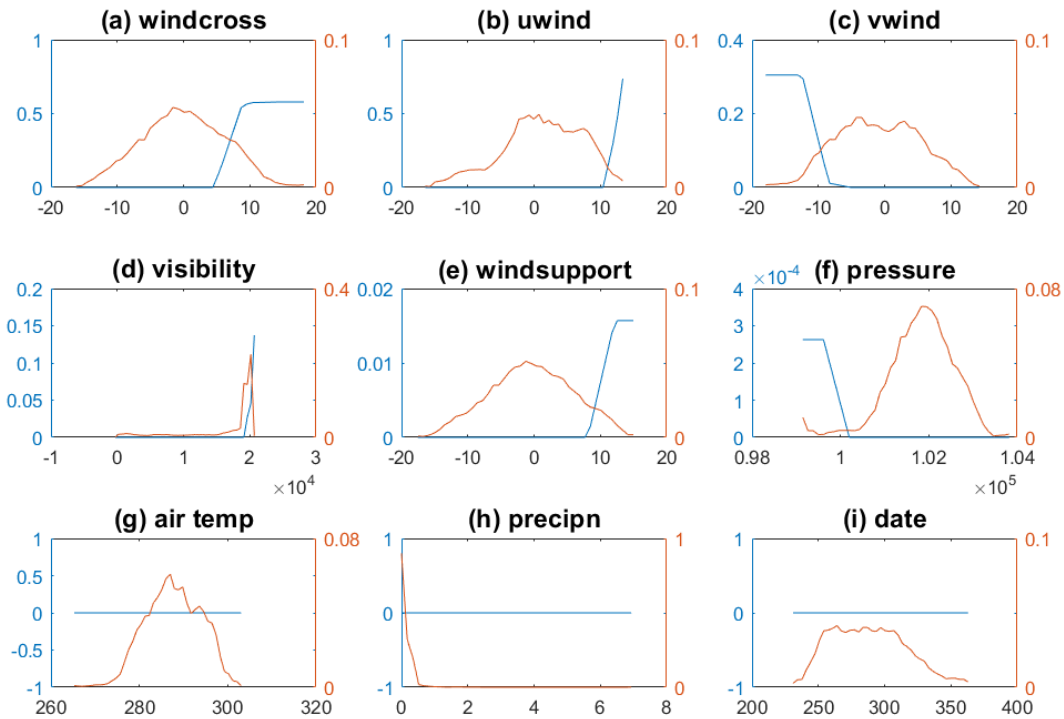


Figure 32. Predicted strength of marginal response to covariates in increasing likelihood of migratory departure into Federal waters among HY individuals

Blue lines depict relative likelihood of migratory departure into Federal waters, with positive values indicating increased likelihood) and red lines depict frequency of detection across conditions while individuals staged in the Study Area (sampled at dusk and dawn).

3.5.4 Altitude of Migratory Departure Flights Over Federal Waters

Estimated flight altitudes on initiation of migratory flights over Federal waters (n=59) was predicted to fall largely within rotor swept zones (83%), with a median flight altitude of 102 m, and range 56 to 775 m (Fig. 33). The interquartile range of mean predicted altitude (i.e. among all plausible solutions) also fell within this range 62 to 173 m and considering model uncertainty (error bars in Fig. 26), only 3 of 59 flights were predicted to fall outside rotor swept zones when departing on migration into Federal waters. However, these estimates may be biased towards low altitudes in the absence of simultaneous detections between towers when Red Knots departed directly offshore from staging areas.

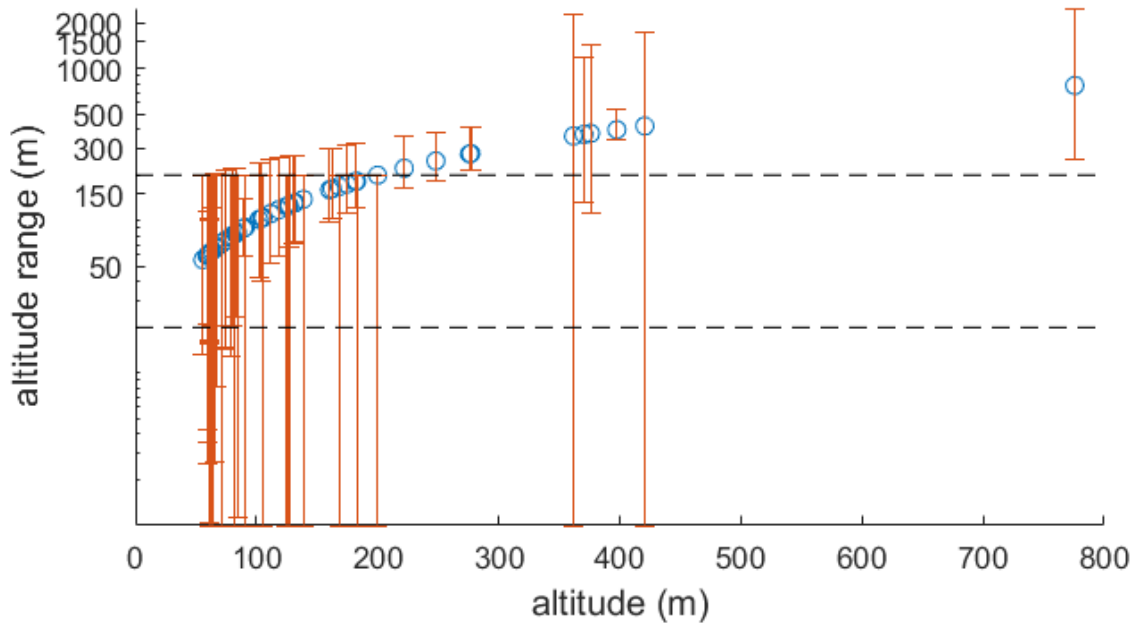


Figure 33. Predicted flight altitudes on initiation of migratory flights over Federal waters (n=59). The blue circles indicate frequency of occurrence based on the best estimated flight altitude from the location model, and the red error bars depict the overall mean model uncertainty (interquartile range). Dashed black lines represent the rotor-swept zone (20 to 200m).

4 Discussion

4.1 Movement Models

The movement model represents a prototype, but also to our knowledge the first application of radio propagation theory with measured signal strength applied to bird migration. It represents part of ongoing multidisciplinary research aiming to refine and improve analysis of Motus Wildlife Tracking Network data and thereby understanding of the migratory process and hazards involved. The development of information regarding altitudinal movements and being able to classify non-stop flights versus stopover are particularly novel (but see Poessel et al. 2018) and can facilitate estimation of spatial and temporal patterns in migratory and stopover movements.

Our study highlights the importance of accounting for the inherent uncertainty in received signal strength, here through combining information from sequences of near-simultaneous detections and single-beam detections. The relatively small discrepancy in the kite calibration between predicted and actual (GPS) locations and altitude (on the order of 1 km and 10 m, respectively) attests to the potential for future work

to verify that model accuracy, resulting in more confident assessment of both flight behavior and ensuing risks and hazards while airborne. Nonetheless, the spatial error in locations estimated by the model suggest that caution is advised in interpreting exact movements.

In the current study, we deployed a network of virtually identical (9-element Yagi) arrays in an effort to standardize detection probability among stations. However, broad applications of this model across the Motus network are challenged by the variety of receiver types and configurations used by various partners in the network, with differing numbers of antenna and signal gain, and differing signal strength measures (Sensorgnome dBm vs. Lotek SRX-600 0-255). Omnidirectional arrays may prove particularly useful since their short range of detection (500 m; Taylor et al. 2017) in the horizontal could help reduce location uncertainty when combined with near-simultaneous detections. A further potential improvement is to incorporate Sensorgnome signals into the current model framework in a more robust way; the model currently does so using a linear scaling factor.

4.2 Demographic Variation in Movements and WEA Exposure

Our results demonstrate substantial variation in the relative exposure of different segments of the *rufa* Red Knot population to potential effects from wind energy development. Two (22%, n=9) of the small sample of birds tagged in James Bay, ON, were detected passing through the Study Area in Nantucket Sound, and only six (3%, n=244) knots tagged in Mingan Islands, Quebec, were detected within the Study Area or over Atlantic OCS waters. All but one were detected in the Study Area for less than a day, suggesting that the majority were undertaking flights to areas farther south while they transited the region. Only two Canadian-tagged birds (both from Mingan Islands) were detected flying across WEAs in the mid-Atlantic, and both flights occurred on the same day (Nov 21). Many of the 244 birds tagged in the Mingan Islands were tracked departing continental North America (e.g., past Sable Island, Canada) on long-distance migratory routes that would take them beyond US Federal waters. This suggests that most of the birds heading south from the Mingan Islands are at little risk from potential wind energy development on the Atlantic OCS because they are well offshore while passing through the latitudes of the continental US. Although the tagged sample was small, conclusions are broadly similar for birds heading south from James Bay.

These results place the likelihood of exposure to wind energy development in context for the *rufa* Red Knot population as whole. Work is ongoing to understand the size of the passage populations at both the Mingan Islands (Lyons et al. *in review*), and the site in James Bay where we worked (Little Piskwamish; MacDonald, Smith et al. *in prep*). Preliminary estimates suggest that these two sites could harbor more than 15,000 knots or more than 35% of the current population estimate for *rufa*. Other sites in James Bay and Hudson Bay immediately to the north also hold substantial numbers of Red Knots. If results from our tagged birds are reflective of behavior for birds stopping in James and Hudson Bays generally, our results might extend to a substantially larger fraction (perhaps most) of the *rufa* population. However, a larger sample of tagged birds from James Bay would greatly increase the reliability of these conclusions.

Unsurprisingly, Red Knots tagged in Massachusetts and New Jersey were more likely to be detected within the Study Area. Among all individuals processed by the location model, 15 (43%, n=35) individuals from New Jersey and 57 of 99 (58%) individuals from Massachusetts were tracked crossing

Federal waters during staging or migration. Some of these differences are likely due to lower detection probability given the distribution of towers in coastal New Jersey versus coastal Massachusetts (Appendix C) but provided some indication that Red Knots from New Jersey departed from the Study Area following a more coastal trajectory.

The majority (93%) of Red Knots tagged on Cape Cod, Massachusetts were detected by the tracking array within the Study Area and remained in the area for an average of one month. Three females crossed WEAs one or more times during regional flights during the staging period. During migration, most Red Knots departed from Cape Cod to the southeast heading offshore, with lesser numbers departing southwest towards the mid-Atlantic. Six Red Knots departed to the southwest and intersected one or more WEAs migratory flights through the mid-Atlantic Bight. We expect that birds departing to the southeast from Cape Cod, Massachusetts are most likely traveling to South America, while birds departing to the southwest are most likely traveling shorter distances to more northerly wintering areas such as the southeast US coast and/or the Caribbean. Therefore, because of their flight trajectories, short-distance migrant Red Knots that staged on Cape Cod, Massachusetts are more likely to cross WEAs in the mid-Atlantic than mid or long-distance migrants and are thus at higher likelihood of exposure to potential effects from offshore wind development. Among Red Knots tagged in Massachusetts, the HY age class had a higher probability of WEA exposure relative to adults, but there were no differences in WEA exposure by sex.

Relative to Massachusetts, a lesser proportion of Red Knots tagged in New Jersey were detected in the Study Area (77%) and had a shorter length of stay following tagging (17 days). Just one individual (age and sex known) was detected crossing WEAs offshore of DE and MD during staging. During August, two AHYs migrated offshore and intersected WEAs off the coast of New Jersey, and three additional AHYs departed on similar trajectories and were last detected heading directly towards the New Jersey WEAs. In November, a HY female and a second individual of unknown age and sex intersected WEAs offshore of DE, MD, and VA while migrating along a nearshore trajectory.

Collectively, these results indicate that in the fall, WEA exposure occurs during both staging and migration. During migration, HY birds and AHY birds that remained at staging areas into late fall tended to make relatively short-distance flights across the mid-Atlantic Bight and were more susceptible to exposure to multiple WEAs throughout the Study Area. For AHY birds that migrated offshore, presumably on long distance flights to the Caribbean or South America, those departing to the southeast of Cape Cod, Massachusetts had low exposure to WEAs, whereas those departing southeast from New Jersey had a risk of intersecting with WEAs in adjacent Federal waters. These findings provide new information to support risk assessments of Red Knots from short-distance and long-distance wintering populations (Burger et al. 2011).

4.3 Timing, Meteorological, Conditions, and Altitude of Flights Across Offshore WEAs

4.3.1 Timing

Red Knots were exposed to WEAs during both staging and migratory flights that occurred from mid-August through late November, with the highest exposure during migratory flights in November. During both staging and migration, Red Knots primarily crossed WEAs at night. The highest number of flights across WEAs occurred after Red Knots departed from staging areas on nocturnal migratory flights. Timing of departure peaked around sunset, which is consistent with radar studies conducted during autumn that showed shorebirds departing from staging areas within 1 to 2 hours of sunset on migratory flights (Richardson 1979). Exposure to WEAs at night could increase the risk of collision with offshore wind turbines due to reduced visibility (Hüppop et al. 2006). Lights on turbines may also disorient nocturnally migrating birds and lead to increase collision risk (Hüppop et al. 2006, Drewitt and Langston 2008), although use of flashing lights (versus continuous lights) may help to reduce collision risk (Gehring et al. 2009).

4.3.2 Meteorological Conditions

During fall migration, Red Knots flew across WEAs under favorable meteorological conditions for long-distance offshore flights, including following winds (blowing towards the south/southeast) and high surface pressure, under clear skies with little to no precipitation. These results are consistent with weather conditions used by shorebirds departing from staging areas on flights across the Atlantic Ocean during fall (Richardson 1979). Collision risk with offshore wind turbines is reduced during fair weather conditions, when birds are better able to detect and avoid hazards in flight (Marques et al. 2014).

4.3.3 Altitude

From the perspective of understanding exposure to offshore wind turbines, flight altitudes are as important as flight routes. Red Knots and similar species of shorebirds are known to reach altitudes of over 2-km on long-distance migratory flights (Richardson 1976, Richardson 1979, Williams and Williams 1990). Our results indicate that, within our Study Area, both short-distance flights between adjacent coastal staging areas, as well as longer distance flights across the mid-Atlantic Bight, occurred at much lower altitudes (<500 m).

For Red Knots specifically, few studies have quantified the relationship between flight altitude relative to distance (Burger et al. 2011). However, information from offshore radar studies has recorded Red Knots and other species of shorebirds migrating at altitudes exceeding 1 to 2 km (Richardson 1976, Williams and Williams 1990), whereas nearshore studies documented local and migratory flights of shorebirds occurring at altitudes <100 m (Dirksen et al. 2000, Langston and Pullan 2003). The Northwest Atlantic Seabird Catalog had a total of 233 records of small-bodied shorebirds recorded during offshore surveys from 2003 to 2017 (USFWS 2018). Across all taxa groups, most flight altitudes were less than 100 m, with some individuals recorded up to 500 m (Fig. 34). Due to limitations of observers to detect and identify high flying birds, these survey data are inherently biased towards low altitude flights. However,

these data do provide additional evidence that shorebirds occur at low altitudes in offshore areas of the Atlantic OCS.

In the present study, altitude estimates were often subject to high levels of error (>100 m), so additional research is needed to more accurately assess exposure of Red Knots to the rotor swept zone (20 m to 200 m). Simultaneous detections from at least four spatially separated tracking towers are needed to improve accuracy of altitude estimates using this technology (Janaswamy et al, *in review*). Thus, VHF tracking technology is more suitable for estimating altitude using a dense array of tracking stations at finer spatial scales (e.g. through a single WEA). However, at the spatial scale of our Study Area, the lack of high-range (>100 km) simultaneous detections between towers when Red Knots crossed WEAs provides coarse evidence that these flights occurred at altitudes close to or within the rotor swept zone given the theoretical relationship between detection range of receiving stations and flight altitude of tagged birds. Further studies combining high density VHF arrays with radar-based tracking are recommended to more accurately estimate flights through WEAs and occurrence within rotor swept altitudes. GPS tracking technology may provide a viable alternative to collecting altitude data on small-bodied shorebirds in the near future, as light-weight transmitters become more widely available.

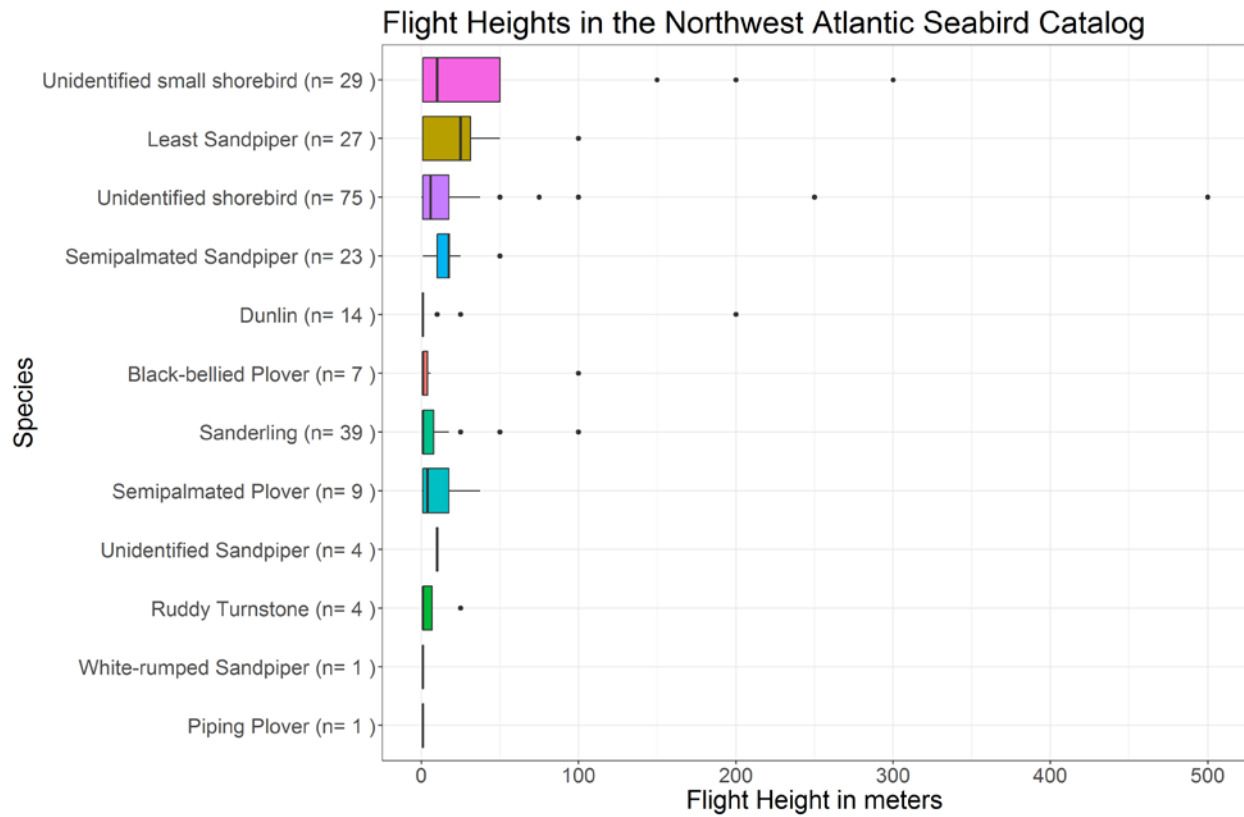


Figure 34. Distribution of flight height by taxa for 233 observations of shorebirds recorded during offshore surveys in the US Atlantic, from 2003 to 2017.

4.4 Covariate Analysis of Migratory Movements in Federal Waters

4.4.1 Temporal, Spatial, and Demographic Variation

Red Knots tagged in Massachusetts had a higher likelihood of departing on migration into Federal waters relative to Red Knots in New Jersey, which were more likely to be last detected along the coast. Within staging areas in southeastern Cape Cod, Massachusetts, *rufa* Red Knots exhibit differential use of foraging and roosting areas, depending on whether they are long-distance migrants that will winter in South America, or short distance migrants that will winter in southern North America and the Caribbean (Harrington et al. 2010). Long-distance migrants typically have a shorter stopover duration and leave southeastern Cape Cod by the end of August. In contrast, short distance migrants have a much longer stopover duration on Cape Cod and undergo flight feather molt before migrating further south. Generally, by early September, only short-distance migrating *rufa* Red Knots are using the area, and many may stay well into November (Harrington et al. 2010, S. Koch *pers. comm.*). In the present study, most Red Knots departed from Massachusetts to the southeast during from mid-August through early Sept, likely embarking on-long distance flights to South America (Niles et al. 2008). All departures from Massachusetts to the southwest across the mid-Atlantic Bight occurred in November, with many of these individuals arriving at stopovers in the southern portion of our Study Area, from New Jersey to Virginia. These were likely short-distance migrants that remain on staging areas through the late fall (Burger et al. 2012). Like Massachusetts, Red Knots from New Jersey initiated migration in two distinct periods (mid-August and mid-November), with most individuals that departed offshore heading in a southeast direction.

Previous observations suggest that migratory departures typically occur in the hours immediately prior to twilight on clear days (Alerstam et al. 1990). Our results are overall consistent with this finding, with the additional indication that initiation of long-distance flights into Federal waters occurred earlier in the day, sometimes several hours prior to dusk. This is further consistent with findings of passerine migrants in Europe which leave earlier when long-distance flights over water than otherwise (Müller et al 2016).

4.5 Meteorological Conditions

Both wind support (tail-wind) and winds blowing towards the southeast were found to play an important role overall in determining the likelihood of migratory flights in offshore waters. HY birds also seemed less flexible in reacting to meteorological conditions (e.g., in selecting stronger winds blowing to the South and enduring larger crosswinds), but this may also reflect the small sample size of flights into Federal waters among HY individuals (n=4 among 11 birds tracked while staging within the region). That birds initiate migration in response to specific wind conditions is well established, including for *rufa* Red Knots in the Study Area (Duijns et al. 2017). However, the influence of winds on the occurrence over particular portions of ocean are more subtle. Occurrence of AHY birds offshore was predicted in association with both positive and negative crosswind drift (winds blowing to the left and to the right), suggesting adaptive exploitation of wind to either avoid the longer coastal flight or avoid being blown too far offshore when undertaking non-stop flights. This is known to occur in regional movements across water, e.g. by lesser-black backed gulls (*Larus fuscus*; McLaren et al. 2016). Alternatively, this result could indicate that birds are being blown to the southwest when attempting longer barrier flights,

consistent with previous studies that have shown that Red Knots utilize “contingency stopover grounds” when confronted by unsupportive winds (Shamoun-Baranes et al. 2010). In any case, HY birds exhibited less clear relationships both with wind covariates and weather covariates generally, possibly reflecting a more general lack of control over their phenology due to their late-season arrival at staging areas. It may also be possible that conditions encountered and subsequent movements, particularly during the first fall migration, can greatly affect migration phenology in subsequent seasons (Cresswell 2014). Other weather covariates such as temperature, pressure and precipitation were found to be less influential in predicting offshore flights, but there was a small but significant tendency for offshore movements to occur in higher visibility.

Although our results are based on a comparatively small sample of tagged individuals, these observed patterns suggest that our detections likely reflected multiple as opposed to single individuals. For example, Red Knots typically migrate in single-species flocks of greater than 50 birds (Niles et al. 2008), with an observed mean flock size for *islandica* knots of 100 to 200 individuals (Alerstam et al. 1990). In addition, our results address some of the information gaps and assumptions employed in previous assessments of collision risk (e.g., Gordon and Nations 2016). Our analysis allows us to distinguish between the responses to correlated covariates, and as described above, and revealed that offshore movements were frequently initiated in southerly winds blowing to the southeast and near civil dusk. Results such as these can be used to adjust the assumptions of equal probability of departure with respect to time of day. Altitude and rates of ascent also play a crucial role in past assessments of risk. While model results strongly suggest that departing Red Knots often remained within rotor swept zones, due to the variable occurrence of near-simultaneous detections and the inherent ambiguity in inferring locations from VHF signals in three dimensions, our modeling framework may not have been able to reproduce possibly rapid climbs on initiation of these flights.

5 Future Directions

We have expanded 2-dimensional triangulation modeling techniques to resolve flight trajectories and flight altitude from detection data obtained by multiple tracking towers simultaneously, which both accounts for measurement uncertainty and behavioral characteristics of flight. This work has opened new possibilities for using individual-based tracking technology to model 3-dimensional flights of small-bodied species. However, the effectiveness of these techniques is limited by the coverage and configuration of automated radio telemetry stations.

Using the current land-based tower array, location model that we developed in this study represents a first prototype of a rigorous quantitative approach based on predicted signal strengths among non-simultaneous detections of migrating birds. This approach is particularly unique because it can resolve estimated location in three dimensions, and uncertainty in all three spatial coordinates. Identifying likely non-stop flight events allowed for dynamic smoothing of predictions based on signal strength. In the absence of subsequent detections during departure flights, final bearing (flight direction) can be used to predict subsequent movement, but separating non-migratory flights from final bearings is difficult when detection data are limited by receiver coverage. Filtering model output by ground speed improved estimated final flight directions, but further analysis of trajectories is needed to test how especially wind

might alter flight trajectories beyond straightforward projections based on final flight direction. One way to do this is by incorporating weather covariates dynamically using an Individual-based Modelling framework (e.g. McLaren et al. 2012).

The ability to estimate exposure to WEAs represents a novel and encouraging development, but there is considerable uncertainty from a technical standpoint. Central among these sources of uncertainty are (1) the challenge in distinguishing between plausible and probable locations, (2) the resolution of flight altitude, which can create large uncertainty in the horizontal range and (3) temporal gaps in the data, causing large uncertainty in interim flight trajectories. Another issue relating to flight altitude is that, since detections beyond 50 km offshore were sparse, many high-altitude flights remain unresolved, and best estimate (median) flight altitudes over exposure areas may well be underestimated. The first issue (large range uncertainty) deflates exposure estimates, whereas the latter issue may lead to an overestimate of direct exposure to rotor swept zones. There is indeed some evidence that migrating shorebirds, including Red Knots, make rapid climbs following departure. Covariate analysis provided some evidence that this may be the case, where offshore flights were predicted to be accompanied by higher altitudes. Regarding inclusion of covariates more generally, the marked heterogeneity in migration strategy and exposure among both individual migrants and within (sex and age) classes could be improved by including covariates related to migrant condition, e.g. weight at capture and total stopover duration.

From a location modeling perspective, improvement in three-dimensional location estimates is ongoing. Optimizing final flight trajectories with smoothing and incorporating vertical climbs was found to greatly improve the current version of the location model, in conjunction with three-dimensional estimates and error bounds from near-simultaneous detections. The Brownian Bridge model does inherently account for location uncertainty when extrapolating through time within maximal flight speeds in tangential directions, which can result in large estimated uncertainty in location, reducing exposure probability accordingly. However, this will also overestimate location uncertainty during periods of non-stop and directed flight, as during migration. A Brownian Bridge model accounting for heterogeneity in variance (Kranstauber et al. 2012) would therefore also be worth exploring. More generally, uncertainty in location estimates can also be addressed using a more fully ‘dynamic’ method which optimizes trajectories by adjusting each measured signal strength to account for model and measurement uncertainty, as opposed to within a one-minute time window as currently used. Ongoing research is being undertaken to develop these models, including from a state-space modelling approach using a Kalman filter (Janaswamy et al. *in review*). Incorporating the three-dimensional beam structure (Equations 1-2) may be key in the success of such endeavors.

Predicted occurrence of exposure can be further improved by developing our framework (Appendix C) of estimating overall detection probability, both on a spatial scale regionally, and depending on predicted signal strength, not only theoretically via horizontal and vertical range. Moreover, signal strength and detection probability may also vary with incidence of transmitter and receiver. These factors can potentially be integrated into the location model to utilize information from non-detections, given detection probability and candidate location within the model.

Within the current modeling framework, the land-based tower array within our Study Area generally provided data of sufficient spatial and temporal resolution for analyzing macro-level exposure of tagged individuals to offshore WEAs in the Atlantic OCS. The coastline of the southern New England and Long

Island region contains offshore islands and peninsulas that provide several key vantage points for triangulation across WEAs. Triangulation from land-based towers in the mid-Atlantic region is more limited due to the relatively linear coastline, and this results in variable detection probability and model accuracy across the Study Area (Appendix C).

Coordinated efforts of the Motus Wildlife Tracking System expand the geographic coverage and scope of digital VHF telemetry. Birds and bats that are tagged as part of BOEM-funded studies can be detected over a much broader spatial and temporal range through the extended Motus network. Additionally, Motus facilitates the sharing of tracking data from individuals of many different species that were tagged by cooperators in the network and subsequently detected by BOEM-funded automated radio telemetry stations. This greatly increases the sample size and diversity of individuals tracked throughout the Atlantic OCS. Overall, since Motus first began in 2012, partners have collectively tagged over 9,000 individuals representing over 87 species of birds, bats, and insects (Taylor et al. 2017). We have coordinated our tracking efforts with Motus since 2013, and to date have detected hundreds of individuals representing a variety of taxa, including shorebirds (e.g. Semipalmated Sandpipers [*Calidris pusilla*], Semipalmated Plovers [*Charadrius semipalmatus*], Black-bellied Plovers [*Pluvialis squatarola*]), coastally-migrating passerines (e.g. Blackpoll Warblers [*Setophaga striata*], the Ipswich subspecies of Savannah Sparrows [*Passerculus sandwichensis princeps*], and Saltmarsh Sparrows [*Ammodramus caudacutus*]), raptors (e.g. Merlin [*Falco columbarius*]), and Eastern red bats (*Lasiurus borealis*) that were tagged by collaborators throughout the network and passed through the BOEM telemetry array in the US Atlantic during migration (Appendix D).

These non-target data may be of significant future value to BOEM because many of the species tagged by Motus collaborators are of conservation concern. In 2017, a Cooperative Research and Development Agreement was finalized between the Department of the Interior and Motus Network leads at Bird Studies Canada to facilitate data-sharing. Motus is currently finalizing development of an online database enabling streamlined access to network-wide detection data through their website. This will provide BOEM access to summary-level data from many thousands of birds and bats that were tagged by partners and detected on BOEM-funded stations. This improved system, and the growing network of Motus stations, will facilitate additional opportunities to develop collaborative studies of shorebird movements throughout the Western Hemisphere. For example, data from tagging projects in South America could be used to estimate exposure of northbound migrants, provided towers are running in May.

Despite the expansion of Motus and potential for strategic deployment of offshore tracking stations, coverage of automated radio telemetry stations will likely limit broad-scale, global tracking efforts using digital VHF telemetry into the foreseeable future. Due to the vast amount of offshore area under consideration for the development of wind energy facilities, tracking technologies that offer more standardized, global coverage will help develop broader-scale assessments of exposure to multiple WEAs throughout a species' migratory range. Solar powered satellite transmitters, capable of collecting daily, relatively high accuracy (optimally 250 m) two-dimensional locations with an operating life of >2 years, are now becoming light enough (2-g) for deployment on shorebirds such as Red Knots. Lightweight (3.5 g) GPS loggers are becoming more widely available and are currently capable of acquiring 500 to 1,000 high accuracy (<10 m) locations according to a programmable schedule. However, similarly to geolocators, these units are archival and need to be recovered to access the data that is stored on board.

Due to the temporal and logistical limitations of satellite-based tracking technologies, digital VHF telemetry remains a viable option for high resolution tracking of small bodied birds and bats at local to regional spatial scales. To maximize spatial and temporal resolution of tracking data for addressing BOEM information needs, we suggest siting equipment on offshore infrastructure (such as buoys, platforms, or wind turbines) within WEAs, preferably during both construction and operational phases of offshore wind energy facilities. Ideally, these offshore stations would be arranged in a regular, grid-like pattern to standardize detection probability throughout target areas. During fall of 2017, an automated radio telemetry station was installed on an offshore wind turbine platform at the Block Island Wind Farm and will be used in an upcoming BOEM-funded study to assess detection rates and accuracy of movement models, based on simultaneous detections from two land-based tracking towers on Block Island (Fig. 35). These techniques could be expanded as additional wind energy facilities are developed throughout the AOCS given additional opportunities to integrate equipment with developing infrastructure.



Figure 35. Block Island offshore wind turbines

As seen from top of the telemetry tower located at the Southeast Lighthouse, Block Island, Rhode Island (photo: Brett Still).

In the future, digital VHF telemetry could be used with other types of tracking technologies to further refine these modeling techniques and improve local-scale exposure estimates through WEAs. For example, development of digital VHF transmitters with altitude sensors, such as those that have been developed for conventional VHF systems (Bowlin et al. 2015), would increase the accuracy of estimating occurrence in the rotor swept zone and would be useful for calibrating altitude estimates produced by the movement model. Other opportunities may exist to integrate digital VHF tracking systems with current

technologies for monitoring bird flight paths through offshore WEAs, including radar (three-dimensional tracking of unknown or targeted individuals) and infrared based imagery (used to assess collision). Strategic deployment of digital VHF tracking technologies on additional offshore wind turbines, as facilities are developed along the Atlantic coast, offers a promising opportunity to estimate the exposure of many different species of birds and bats throughout their migratory range. This is critical to addressing information needs to support conservation efforts and to assess cumulative effects as required by the NEPA process (Goodale and Milman 2016).

6 References

- Agostinelli C, Lund U. 2017. R package 'Circular': Circular Statistics (version 0.4-93); [accessed 2017 July 1]. <https://cran.r-project.org/web/packages/circular/>.
- Baker AJ, Gonzalez PM, Piersma T, Niles LJ, de Lima Serrano do Nascimento I, Atkinson, Clark NA, Minton CDT, Peck MK, Aarts G. 2004. Rapid population decline in Red Knots: Fitness consequences of decreased refueling rates and late arrival in Delaware Bay. *Proc. R. Soc. Lond. B* 271(1541): 875-882.
- Baker AJ, Gonzalez PM, Morrison RIG, Harrington BA. 2013. Red Knot (*Calidris canutus*), version 2.0. In *The Birds of North America* (P. G. Rodewald, editor). Cornell Lab of Ornithology, Ithaca, New York, USA. <https://doi.org/10.2173/bna.563>
- Bai, H. 2016. Estimation of Parameters in Avian Movement Models [Dissertation proposal], University of Massachusetts Amherst, Department of Electrical and Computer Engineering.
- Bivand R and Lewin-Koh N. 2016. R package 'Maptools' (version 0.9-2); [accessed 2017 July 1]. <https://cran.r-project.org/web/packages/maptools/>.
- BOEM (Bureau of Ocean Energy Management). 2017. Outer Continental Shelf Renewable Energy Leases Map Book; [accessed 2017 November 20]. <https://www.boem.gov/Renewable-Energy-Lease-Map-Book/>.
- BOEM. 2017b. Environmental Studies Program Studies Development Plan, 2018-2020; [accessed 2017 November 20]. <https://www.boem.gov/FY-2018-2020-SDP/>.
- BOEM. 2017c. Renewable Energy GIS Data (version 10 Apr 2017); [accessed 2017 August 20]. <https://www.boem.gov/Renewable-Energy-GIS-Data/>.
- Bowlin MS., Enstrom DA, Murphy BJ, Plaza E, Jurich P, Cochran J. 2015. Unexplained altitude changes in a migrating thrush: long-flight altitude data from radio-telemetry. *Auk* 132: 808-816.

- Brown JM, Taylor PD. 2017. Migratory Blackpoll Warblers (*Setophaga striata*) make regional-scale movements that are not oriented toward their migratory goal during fall. *Mov. Ecol.* 5(15).
- Brzustowski J. 2015. R package 'SensorGnome' (version 1.0.16); [accessed 2017 August 20]. <https://www.sensorgnome.org/>.
- Buidin C, Rochepault Y, Aubry Y. 2010. L'archipel de Mingan: une halte migratoire primordiale pour les oiseaux de rivage. *Le Naturaliste Canadien* 134(1): 73-81.
- Burger J, Gordon C, Niles L, Newman J, Forcey G, Vlietstra L. 2011. Risk evaluation for Federally listed (Roseate Tern, Piping Plover) or candidate (Red Knot) bird species in offshore waters: A first step for managing the potential impacts of wind facility development on the Atlantic Outer Continental Shelf. *Renewable Energy* 36: 338–351.
- Burger J, Niles LJ, Porter RR, Dey AD, Koch S, Gordon C. 2012a. Migration and over-wintering of Red Knots (*Calidris canutus rufa*) along the Atlantic coast of the United States. *Condor* 114: 302–313.
- Burger J, Niles LJ, Porter RR, Dey AD, Koch S, Gordon C. 2012b. Using a shorebird (Red Knot) fitted with geolocators to evaluate a conceptual risk model focusing on offshore wind. *Renewable Energy* 43: 370–377
- Burger J, Niles LJ. 2013. Shorebirds and stakeholders: Effect of beach closure and human activities on shorebirds at a New Jersey coastal beach. *Urban Ecosyst.* 16: 657-673.
- Clark KE, Niles LJ, Burger J. 1993. Abundance and distribution of migrant shorebirds in Delaware Bay. *Condor*: 694-705.
- Cochran WW, Warner DW, Tester JR, Kuechle VB. 1965. Automatic radio-tracking system for monitoring animal movements. *BioScience* 15: 98-100.
- Cochran WW. 1980. Wildlife telemetry. Pages 507-520 *in* *Wildlife Management Techniques* (S. P. Schemnitz, Ed.), 4th ed. The Wildlife Society, Inc., Washington, D.C.
- Cresswell W. 2014. Migratory connectivity of Palaearctic–African migratory birds and their responses to environmental change: the serial residency hypothesis. *Ibis* 156: 493-510
- Diffendorfer JE, Compton R, Kramer L, Ancona Z, Norton D. 2017. Onshore industrial wind turbine locations for the United States (version. 1.2): U.S. Geological Survey Data Series 817; [accessed 1 September 2017]. <https://doi.org/10.3133/ds817>.
- Dirksen S, Spaans AL, van der Winden J. 2000. Studies on Nocturnal Flight Paths and Altitudes of Waterbirds in Relation to Wind Turbines: A Review of Current Research in the Netherlands. In *Proceedings of the National Avian-Wind Power Planning Meeting III, San Diego, California, May 2000*. Prepared for the National Wind Coordinating Committee. Ontario: LGL Ltd.

- Drewitt AL, Langston RH. 2006. Assessing the impacts of wind farms on birds. *Ibis* 148:29-42
- Drewitt, AL, Langston, RH, 2008. Collision effects of wind-power generators and other obstacles on birds. *Annals of the New York Academy of Sciences* 1134(1): 233-266.
- Duijns S, Niles LJ, Dey A, Aubry Y, Friis C, Koch S, Anderson AM, Smith PA. 2017. Body condition explains migratory performance of a long-distance migrant. *Proc. R. Soc. B* 284: 20171374.
- Environment and Climate Change Canada. 2016. Recovery Strategy and Management Plan for the Red Knot (*Calidris canutus*) in Canada [Proposed]. Species at Risk Act Recovery Strategy Series. Environment and Climate Change Canada, Ottawa. ix + 54 pp
- Exo KM, Huppopp O, Garthe S. 2003. Birds and offshore wind farms: a hot topic in marine ecology. *Wader Study Group Bulletin* 100: 50-53.
- Fox AD, Desholm M, Kahlert J, Christensen TK, Petersen IBK. 2006. Information needs to support environmental impact assessment of the effects of European marine offshore wind farms on birds. *Ibis* 148: 129-144.
- Fedrizzi CE. 2008. Abundance, distribution and feeding ecology of shorebirds (Charadriiformes: Charadrii and Scolopaci) in the coastal zone of Rio Grande do Sul, Brazil. [Doctoral dissertation], Universidade Federal do Rio Grande, Rio Grande.
- Furness RW, Wade HM, Masden EA. 2013. Assessing vulnerability of marine bird populations to offshore wind farms. *Journal of Environmental Management* 110: 56-66.
- Gehring J, Kerlinger P, and Manville AM. 2009. Communication towers, lights, and birds: successful methods of reducing the frequency of avian collisions. *Ecological Applications*, 19(2): 505-514.
- Goodale MW, Milman A. 2016. Cumulative adverse effects of offshore wind energy development on wildlife, *Journal of Environmental Planning and Management* 59(1): 1-21.
- Gordon CE, Nations C. 2016. Collision Risk Model for “rufa” Red Knots (*Calidris canutus rufa*) Interacting with a Proposed Offshore Wind Energy Facility in Nantucket Sound, Massachusetts. US Department of the Interior, Bureau of Ocean Energy Management, Sterling, Virginia. OCS Study BOEM 2016-045.
- Green M, Alerstam T. 2002. The Problem of Estimating Wind Drift in Migrating Birds. *Journal of Theoretical Biology* 218: 485-496
- Harrington BA, Koch S, Niles LJ, Kalasz K. 2010. Red Knots with different winter destinations: differential use of an autumn stopover area. *Waterbirds* 33(3):357-363.
- Harrington BA. 2001. Red Knot (*Calidris canutus*). In Poole, A. & Gill, F.(eds.) *The Birds of North America*, No. 563. Philadelphia, PA, Academy of Natural Sciences, Washington DC, American Ornithologists' Union.

- Hastie T, Tibshirani R, Friedman J. 2009. Boosting and additive trees. In: *The Elements of Statistical Learning*. Springer, NY, p. 337-387.
- Horne JS, Garton EO, Krone SM, Lewis JS. 2007. Analyzing animal movements using Brownian bridges. *Ecology* 88: 2354-2363
- Huso MMP. 2010. An estimator of wildlife fatality from observed carcasses. *Environmetrics* 22: 318-329.
- Hüppop O, Dierschke J, Exo KM, Fredrich E, Hill R. 2006. Bird Migration Studies and Potential Collision Risk with Offshore Wind Turbines. *Ibis* 148: 90-109
- Janaswamy, R. 2001. *Radiowave Propagation and Smart Antennas for Wireless Communication*, Springer Science and Business Media, 312 p.
- Janaswamy R., Loring PH, McLaren JD. *In review*. A State Space Technique for Wildlife Position Estimation Using Non-Simultaneous Signal Strength Measurements.
- Kerns J, Erickson WP, Arnett EB. 2005. Bat and bird fatality at wind energy facilities in Pennsylvania and West Virginia. In: Arnett EB, editor. *Relationships between bats and wind turbines in Pennsylvania and West Virginia: An assessment of fatality search protocols, patterns of fatality, and behavioural interactions with wind turbines A final report prepared for the bats and wind energy cooperative*. Austin, Texas, USA: Bat Conservation International. p. 24-95.
- Kemp MU, Shamoun-Baranes J, van Loon EE, McLaren JD, Dokter AM, Bouten W. 2012. Quantifying flow-assistance and implications for movement research. *J Theor Biol* 308:56-67
- Kenward R. 1987. *Wildlife radio tagging*. Academic Press, San Diego, California.
- Kranstauber B, Kays R., LaPoint SD, Wikelski M, Safi K. 2012. A dynamic Brownian bridge movement model to estimate utilization distributions for heterogeneous animal movement. *Journal of Animal Ecology*, 81: 738-746.
- Korner-Nievergelt F, Korner-Nievergelt P, Behr O, Niermann I, Brinkmann R, et al. 2011. A new method to determine bird and bat fatality at wind energy turbines. *Journal of Wildlife Biology* 17: 350-363.
- Langston RH, Pullan JD. 2003. *Wind farms and birds: an analysis of the effects of wind farms on birds, and guidance on environmental assessment criteria and site selection issues*. Council of Europe.
- Langston RH. 2013. Birds and wind projects across the pond: a UK perspective. *Wildlife Society Bulletin* 37: 5-18.
- Lathrop R., Niles LJ, Mizrahi D, Dey A, Smith J. 2016. *Arctic Shorebird Habitat Climate Change Resilience Analysis For the Arctic Migratory Birds Initiative (AMBI) – the Americas Flyway Action Plan*. Report for the Commission for Environmental Cooperation.

- Loring PH. 2016. Evaluating digital VHF technology to monitor shorebird and seabird use of offshore wind energy areas in the Western North Atlantic. [Doctoral dissertation], University of Massachusetts, Amherst, MA.
- Loring PH, Goyert HF, Griffin CR, Sievert PR, Paton PWC. 2017. Tracking Movements of Common Terns, Endangered Roseate Terns, and Threatened Piping Plovers in the Northwest Atlantic: 2017 Annual Report to the Bureau of Ocean Energy Management.
- Lyons J. 2017. Red Knot Stopover Population Estimate for 2017. Report to Adaptive Resource Management Committee. Atlantic States Marine Fish Commission.
- Maloney KO, Schmid M, Weller DE. 2012. Applying additive modelling and gradient boosting to assess the effects of watershed and reach characteristics on riverine assemblages. *Methods Ecol. Evol.* 3: 116-128.
- Marques AT, Batalha H, Rodrigues S, Costa H, Pereira MJR, Fonseca C, Mascarenhas M, Bernardino J. 2014. Understanding bird collisions at wind farms: An updated review on the causes and possible mitigation strategies. *Biological Conservation*, 179: 40-52.
- McGowan CP, Hines JE, Nichols JD, Lyons JE, Smith DR, Kalasz KS, Niles LJ, Dey AD, Clark NA, Atkinson PW, Minton CD. 2011. Demographic consequences of migratory stopover: linking red knot survival to horseshoe crab spawning abundance. *Ecosphere* 2(6): 1-22.
- McLaren JD, Shamoun-Baranes J, and Bouten W. 2012. Wind selectivity and partial compensation for wind drift among nocturnally migrating passerines. *Behav. Ecol.* 23: 1089-1101.
- McLaren JD, Shamoun-Baranes J, Camphuysen CJ, Bouten W. 2016. Directed flight and optimal airspeeds: homeward-bound gulls react flexibly to wind yet fly slower than predicted. *J Avian Biol* 47: 476-490.
- Morrison RIG, Ross RK. 1989. Atlas of nearctic shorebirds on the coast of South America. Canada, 2 vols. Special Publication, Canadian Wildlife Service, Ottawa, Ontario.
- Morrison RIG, Harrington BA. 1992. The migration system of the Red Knot *Calidris canutus rufa* in the New World." *Wader Study Group Bulletin* 64: 71-84.
- Morrison RIG, Ross RK, Niles LJ. 2004. Declines in wintering populations of Red Knots in southern South America. *The Condor* 106 (1): 60-70.
- Morrison RIG, Davidson NC, Piersma T. 2005. Transformations at high latitudes: Why do Red Knots bring body stores to the breeding grounds? *The Condor* 107: 449-457.
- Motus Wildlife Tracking System. 2016. Motus Wildlife Tracking System Collaboration Policy. January 2016; [accessed 2017 August 20]. <https://motus.org/wp-content/uploads/2016/01/MotusCollaborationPolicy.January2016.pdf>.

- Müller F, Taylor PD, Sjöberg S, Muheim R, Tsvey A, Mackenzie SA, Schmaljohann H. 2016. Towards a conceptual framework for explaining variation in nocturnal departure time of songbird migrants. *Movement Ecology* 4(1): 24.
- Musial W, Beiter P, Schwabe P, Tian T, Stehly T, Spitsen P, Robertson A, Gevorgian V. 2017. 2016 Offshore Wind Technologies Market Report; [accessed 2017 November 20].
<https://energy.gov/sites/prod/files/2017/08/f35/2016%20Offshore%20Wind%20Technologies%20Market%20Report.pdf>
- Niles LJ, Dey AD, Douglass NJ, Clark JA, Clark NA, Gates AS, Harrington BA, Peck MK, Sitters HP. 2006. Red Knots wintering in Florida: 2005/6 expedition. *Wader Study Group Bull.* 111: 86-99
- Niles LJ, Sitters HP, Dey AD, Atkinson PW, Baker AJ, Bennett KA, Carmona R, Clark KE, Clark NA, Espoz C, et al. 2008. Status of the Red Knot (*Calidris canutus rufa*) in the Western Hemisphere. *Studies in Avian Biology* No. 36.
- Niles LJ, Bart J, Sitters HP, Dey AD, Clark KE, Atkinson PW, Baker AJ, Bennett KA, Kalasz KA, Clark NA, et al. 2009. Effects of Horseshoe Crab Harvest in Delaware Bay on Red Knots: Are Harvest Restrictions Working? *Bioscience* 59: 153-164
- Niles LJ, Burger J, Porter RR, Dey AD, Minton CDT, Gonzalez PM, Baker AJ, Fox JW, Gordon C. 2010. First results using light level geolocators to track red knots in the Western Hemisphere show rapid and long intercontinental flights and new details of migration pathways. *Wader Study Group Bull.* 117(2): 123-130.
- Niles LJ, Aubry y. 2014 Status of Migratory Shorebirds in French Guiana and Guadeloupe With Emphasis On Red Knots And Ruddy Turnstones. Report to Canadian Wildlife Service. 32 pp.
- National Oceanic and Atmospheric Administration. 2017. National Centers for Environmental Prediction North American Regional Reanalysis; [accessed 2017 May 20].
<http://www.esrl.noaa.gov/psd/data/gridded/data.narr.html>.
- Normandeau Associates. 2011. New insights and new tools regarding risk to roseate terns, piping plovers, and red knots from wind facility operations on the Atlantic Outer Continental Shelf. A Final Report for the U.S. Department of the Interior, Bureau of Ocean Energy Management, Regulation and Enforcement, Report No. BOEMRE 048-2011. Contract No. M08PC20060.
- Northeast Regional Ocean Council. 2017. Northeast Ocean Data Portal; [accessed 2017 May 20].
<https://www.northeastoceandata.org/data-explorer/>.
- O'Connell A, Spiegel CS, Johnston S. 2011. Compendium of Avian Occurrence Information for the Continental Shelf Waters along the Atlantic Coast of the United States, Final Report (Database Section - Shorebirds). Prepared by the U.S. Fish and Wildlife Service, Hadley, MD for the USGS Patuxent Wildlife Research Center, Beltsville, MD. U.S. Department of the Interior, Geological Survey, and Bureau of Ocean Energy Management Headquarters, OCS Study BOEM 2012-076.

- Poessel SA, Duerr AE, Hall JC, Braham MA, Katzner TE. Improving estimation of flight altitude in wildlife telemetry studies. *Journal of Applied Ecology*. 2018.
- R Development Core Team. 2017. R: a language and environment for statistical computing v. 3.3.2. R Foundation for Statistical Computing, Vienna, Austria; [accessed 2017 December 20]. <http://www.R-project.org/>.
- Richardson WJ. 1976. Autumn migration over Puerto Rico and the Western Atlantic: a radar study. *Ibis* 118(3): 309-332
- Richardson WJ. 1979. Southeastward shorebird migration over Nova Scotia and New Brunswick in autumn: a radar study. *Canadian Journal of Zoology* 57(1): 107-124.
- Robinson Willmott JC, Forcey G, Kent A. 2013. The Relative Vulnerability of Migratory Bird Species to Offshore Wind Energy Projects on the Atlantic Outer Continental Shelf: An Assessment Method and Database. Final Report to the U.S. Department of the Interior, BOEM Study BOEM 2013-207; [accessed 2017 December 20]. <http://www.data.boem.gov/PI/PDFImages/ESPIS/5/5319.pdf>
- Shamoun-Baranes J, Leyrer J, van Loon E, Bocher P, Robin F, Meunier F, Piersma T. 2010. Stochastic atmospheric assistance and the use of emergency staging sites by migrants. *Proc Biol Sci* 277:1505-1511
- Sitters H. 2017. Red Knots in Monomoy Refuge and Atlantic Coast NJ. Unpublished Report 5 pp.
- Smith JAM, Niles LJ, Modjeski A, Hafner S, Dillingham T. *In prep*. Beach restoration to improve habitat quality for horseshoe crabs and shorebirds in the Delaware Bay.
- Smolinsky JA, Diehl RH, Radzio TA, Delaney DK, Moore FR. 2013. Factors influencing the movement biology of migrant songbirds confronted with an ecological barrier. *Behav Ecol Sociobiol*. 67: 2041-2051.
- Taylor PD., Crewe TL, Mackenzie SA, Lepage D, Aubry Y, Crysler Z, Finney G, et al. 2017. The Motus Wildlife Tracking System: A Collaborative Research Network to Enhance the Understanding of Wildlife Movement. *Avian Conservation and Ecology* 12(1).
- USFWS. 2014. Endangered and Threatened Wildlife and Plants; Threatened Species Status for the rufa Red Knot; Final Rule. Department of the Interior, Fish and Wildlife Service, 50 CFR Part 17. 79 Federal Register (FR) 238: 73706-73748; [accessed 12 December 2017]. <http://www.gpo.gov/fdsys/pkg/FR-2014-12-11/pdf/2014-28338.pdf>.
- USFWS. 2018. Northwest Atlantic Seabird Catalog, Version 2; Accessed through U.S. Department of Interior; [accessed 13 Apr. 2018].
- Woodworth BK, Mitchell GW, Norris DR, Francis CM, Taylor PD. 2015. Patterns and correlates of songbird movements at an ecological barrier during autumn migration assessed using landscape- and regional-scale automated radiotelemetry. *Ibis* 157: 326-339.

7 Appendix A. Metadata for all Red Knots included in this study.

As supplementary material to this report, we have provided tag deployment data and results of exposure analysis for each Red Knots in this study submitted to BOEM, in separate files for each Project Number and tagging site ('Appendix A-Proj#-tag-site-metadata.csv').

Descriptions of each field appear below:

Fields:

projId: Motus network Tag Project ID number (#14 - New Jersey, USA Fall; #88 - Massachusetts, USA fall 2016 deployments; #15 - Mingan Islands, Canada fall 2016 deployments, #38 - includes James Bay and Mingan Islands fall 2016 deployments; #47 - Delaware Bay, USA spring 2016 deployments)

nanoId: nanotag ID number

spp: species (Red Knot)

depLoc: geographic location of tag deployment

depLat: Latitude of tag deployment (decimal degrees)

depLon: Longitude of tag deployment (decimal degrees)

depDate: Date of tag deployment

age: age of bird (where available). HY, AHY, U=unknown (not determined)

sex: sex of bird (where available). M = male, F = female, U = unknown (not determined)

band: US Geological Survey (USGS) issued band number, where available

flag: code and color of uniquely coded leg flag, where available

model: model of nanotag

period: burst rate of nanotag (in seconds)

det_US: 1=detected by one or more automated radio telemetry stations on US Atlantic coast, 0=not detected on US Atlantic coast (separated by spring and fall migration Delaware Bay spring deployments)

first_date_US: date of first detection on US Atlantic coast (separated by spring and fall migration Delaware Bay spring deployments)

last_date_US: date of last detection on US Atlantic coast (separated by spring and fall migration Delaware Bay spring deployments)

days_US: total number of days detected on US Atlantic coast (separated by spring and fall migration Delaware Bay spring deployments)

det_fed_waters: 1 = movement model estimated locations in Federal waters of US Atlantic, 0 = movement model did not estimate locations in Federal waters of US Atlantic (separated by spring and fall migration Delaware Bay spring deployments)

boem_lease: lists all BOEM wind energy lease areas (and the Block Island Wind Farm in state waters of Rhode Island) that movement model estimated exposure to. For Delaware Bay spring deployments, these columns are separated by spring and fall migration.

boem_plan: lists all BOEM wind energy planning areas that movement model estimated exposure to. For Delaware Bay spring deployments, these columns are separated by spring and fall migration

8 Appendix B. Metadata for BOEM automated radio telemetry stations in 2016

Site	Code	Lat	Long	Install Date	Installation
Race Point, Provincetown, MA	RCPT	42.0658	-70.2440	05/01/2016	12.2-m, six antenna tower
Marconi Station, Wellfleet, MA	WELL	41.9147	-69.9720	04/24/2016	12.2-m, six antenna tower
Monomoy NWR - N, Chatham, MA	MNYN	41.6088	-69.9870	05/30/2016	12.2-m, six antenna tower
Monomoy NWR - S, Chatham, MA	MNYS	41.5526	-70.010	05/30/2016	12.2-m, six antenna tower
Waquoit Bay, Mashpee, MA	WAQT	41.5518	-70.5070	05/31/2016	12.2-m, six antenna tower
Wings Neck, Bourne, MA	WING	41.6807	-70.6615	06/06/2016	11-m observation tower with two antennas
Sachuest Point NWR, Middletown, RI	SACH	41.4787	-71.2440	04/11/2016	12.2-m, six antenna tower
Shearwater (Boat), Nantucket, MA	SHEA	41.4431	-69.8850	05/24/2016	Single 200-W omnidirectional antenna
Nantucket NWR (Great Point), Nantucket, MA	GTPT	41.3906	-70.0490	05/12/2016	12.2-m, six antenna tower
Trustom Pond NWR, South Kingston, RI	TRUS	41.3734	-71.5760	04/07/2016	12.2-m, six antenna tower
Muskeget Island, Nantucket Sound, MA	MUSK	41.3373	-70.3050	05/14/2016	12.2-m, six antenna tower
Coatue Point, Nantucket, MA	CTPT	41.3073	-70.0640	05/12/2016	12.2-m, six antenna tower
Napatree Point, Westerly, RI	NAPA	41.3063	-71.8840	04/13/2016	12.2-m, six antenna tower
Old Saybrook, CT	OSCT	41.2875	-72.3240	07/01/2016	8-m, three antenna tower
Nomans Land Island NWR, MA	NOMA	41.2613	-70.8150	04/25/2016	12.2-m, six antenna tower
Nomans Land Island NWR, MA - Summit	NOMS	41.2531	-70.8130	04/25/2016	One antenna on 3-m mast on summit of Noman's Land Island (34 ft ASL)

Site	Code	Lat	Long	Install Date	Installation
Great Gull Island, NY	GGIS	41.2018	-72.1190	06/18/2016	11-m observation tower with four antennas
Plum Island, Orient, NY	PLIS	41.1894	-72.1630	04/20/2016	12.2-m, six antenna tower
Southeast Light, Block Island, RI	BISE	41.1532	-71.5530	04/22/2016	12.2-m, six antenna tower
Montauk Point, Montauk, NY	MNTK	41.0723	-71.8560	04/07/2016	12.2-m, six antenna tower
Fire Is, NY	FRIS	40.6328	-73.2160	05/05/2016	12.2-m, six antenna tower
Coney Is, NY	CONY	40.5738	-73.9770	05/21/2016	4 antennas on 3-m tower atop 12 m building
Jamaica Bay, NY	JMBY	40.6163	-73.8240	09/17/2016	12.2 m utility pole with 4 antennas
Sandy Hook, NJ	SHNJ	40.4301	-73.9868	08/01/2016	12.2-m, six antenna tower
Rutgers Station, NJ	RTNJ	39.5090	-74.3240	07/29/2016	Four antennas attached to roof of 12-m building
Brigantine, NJ	NBNJ	39.4218	-74.3477	07/28/2016	12.2-m, six antenna tower
Avalon, NJ	AVNJ	39.0919	-74.7179	08/23/2016	Four antennas attached to 7-m mast
Cape Henlopen State Park, DE	CHSP	38.7702	-75.0852	07/27/2016	12.2-m, six antenna tower
Parramore Is, VA	PARR	37.5737	-75.6174	07/22/2016	Four six-element antennas on existing 21-m tower
Chincoteague NWR, VA	CHIN	37.8627	-75.3703	07/20/2016	12.2-m, six antenna tower
Skidmore Island, VA	SKID	37.1340	-75.9258	07/19/2016	12.2-m, six antenna tower
Back Bay NWR, VA	BBVA	36.6718	-75.9156	07/15/2016	12.2-m, six antenna tower

9 Appendix C. Detection probability of BOEM automated radio telemetry stations

We strategically installed our BOEM-funded tower array with the objective to maximize the number of detections of our target species in the Study Area. Due to the tradeoffs involved in siting a limited number of towers, we set up a high-density array near high-use staging and migratory areas for *rufa* Red Knots that are adjacent to BOEM Lease and Planning Areas throughout the Study Area. To aid in this effort, we developed a coverage map to identify areas of low-to-high detection probability within our study region.

First, we depicted the radiation pattern of a single antenna (Fig. C-1), to illustrate the relationship between transmitter altitude and detection range of automated radio telemetry towers. There are two relationships to note here: 1.) altitude (z) and range (r) are positively related (i.e., the higher a bird, the farther away it can be detected); and 2.) for a given radial angle from the receiving antenna, signal strength is inversely related to horizontal range (Eqns 1-2), i.e. a bird flying closer to an antenna at a given radial angle will have a relatively stronger signal.

Second, we calculated each tower's probability of detecting a tagged target, given the target's height and signal strength value of corresponding detection (unitless, range 1 to 255). We used the calibration surveys (conducted by flying a test tag from a kite that was towed behind a boat) to determine an overall detection rate $p = 0.5$ (given target height = 30 m), where p = the proportion of test-tag locations that were detected by the towers. Across the calibration surveys, the overall detection rate was highest along the main beam axis, i.e., bearing close to zero degrees, and varied marginally with the angle of transmitter to receiver. Next, we calculated the probability of detection by all antennas on a single tower. This probability varied depending on the location of the target within the radiation pattern, because side lobes from one antenna overlapped with the main beam and side lobes from other antennas. The probability of detection at any point in the radiation pattern = P , where $P = 1 - (1-p)^n$, and n = the number of overlapping beams at that location (maximum = 6 for a six-antenna tower).

Third, we mapped the overlapping detection probabilities of the BOEM tower array, given the target's height (20 m, 200 m, 1000 m, Fig. C-2). We assumed the same detection rate, $p = 0.5$, across all heights. Towers from the global Motus network that detected our tagged birds provide extended coverage, which is not depicted here, due to variability in tower detections set up using different configurations. At higher flight altitudes, tower coverage overlaps due to increased detection range; in these cases, we display the maximum detection probability. Such overlapping ranges indicate where one target is likely to be detected simultaneously by multiple towers. Simultaneous detections provide more accurate estimates of altitude and spatial coordinates than what can be estimated from single detections. This information can help to provide guidelines for further research, based on the average flight height and Study Area of target species. Future studies should aim to maximize the number of overlapping tower ranges, to improve the altitude and location accuracy of their target estimates, given greater potential for simultaneous detections.

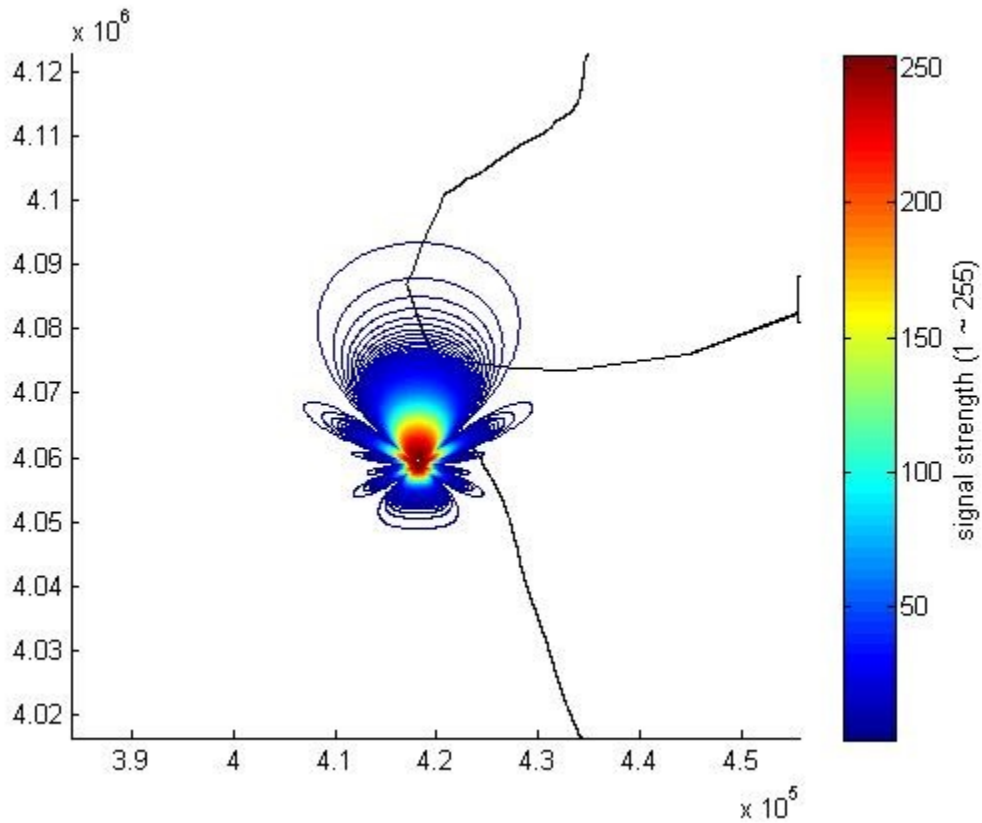
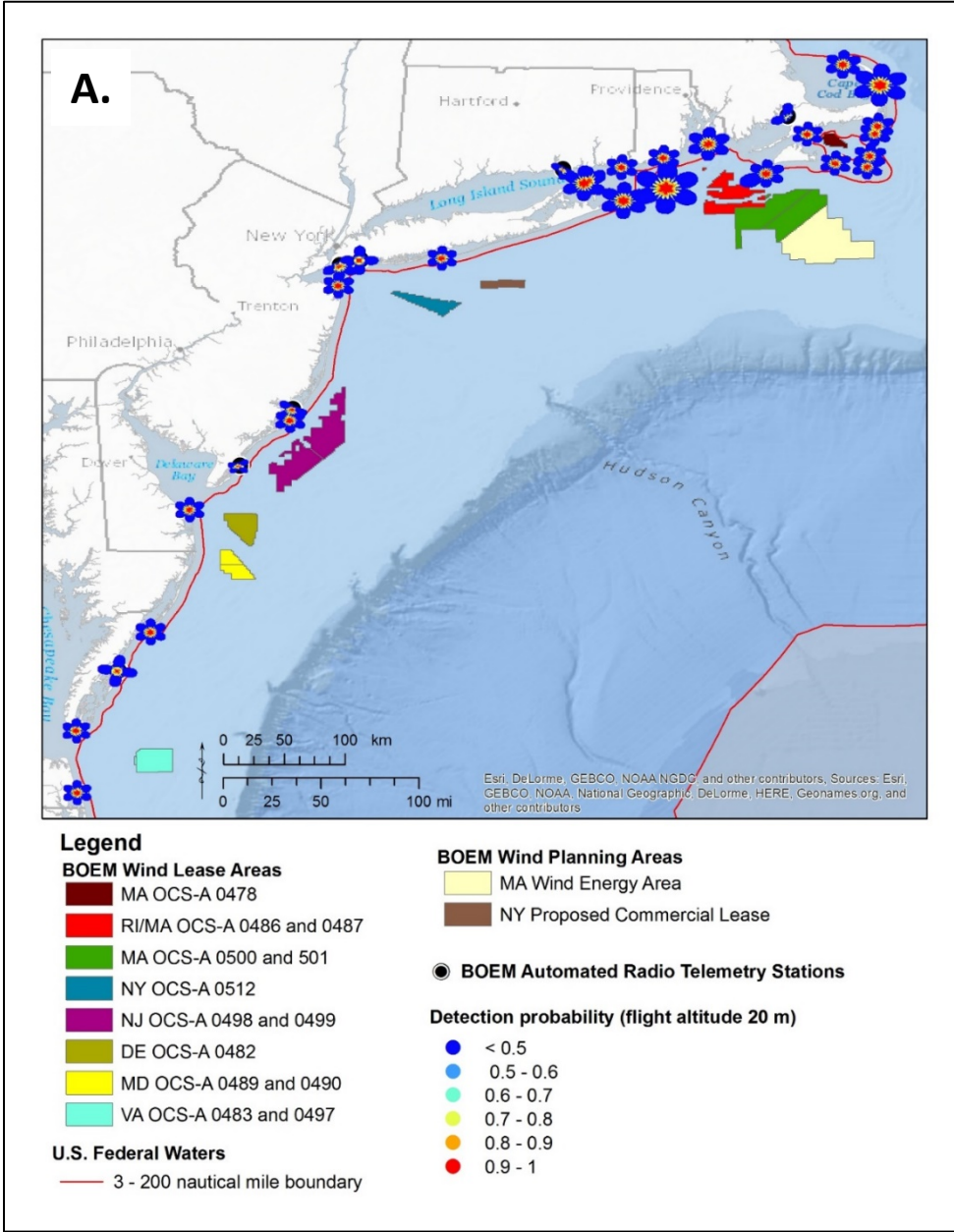
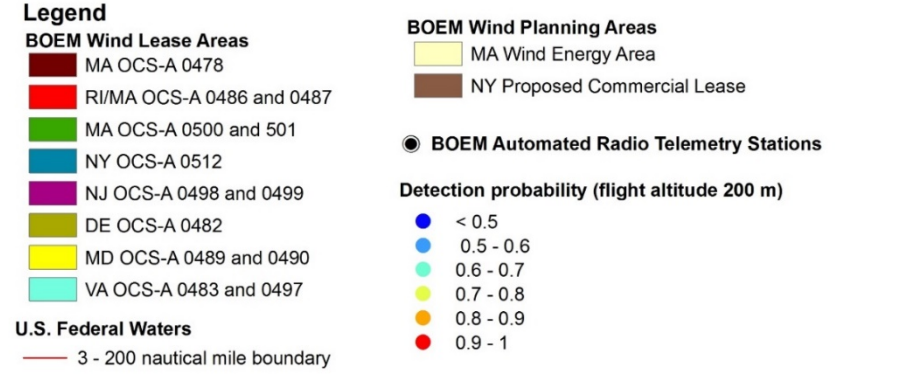
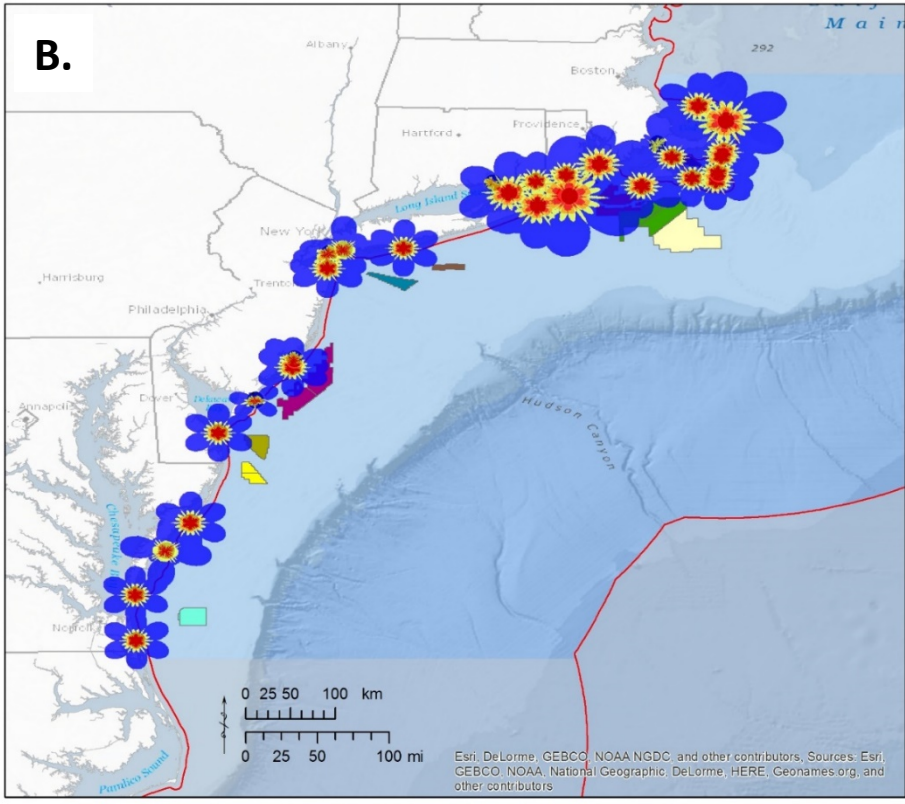


Figure C-1. Two-dimensional radiation pattern of 9-element Yagi antenna.

Example main beam (pointed upwards) and side lobes (e.g., from backscatter) associated with a tower antenna, given a target's range of signal strengths (1-255, scale bar), height (100 m), and map resolution (100 m). Each line represents a signal strength, where the outermost value = 1 and the innermost value = 255. The heat map scaling indicates a higher density of signal strengths closer to the tower, where a bird is most likely to be detected at high signal strength values. The x- and y-axes are in meters, such that this antenna has a range of approximately 40 km. Note that each signal strength has an equal probability of occurrence.





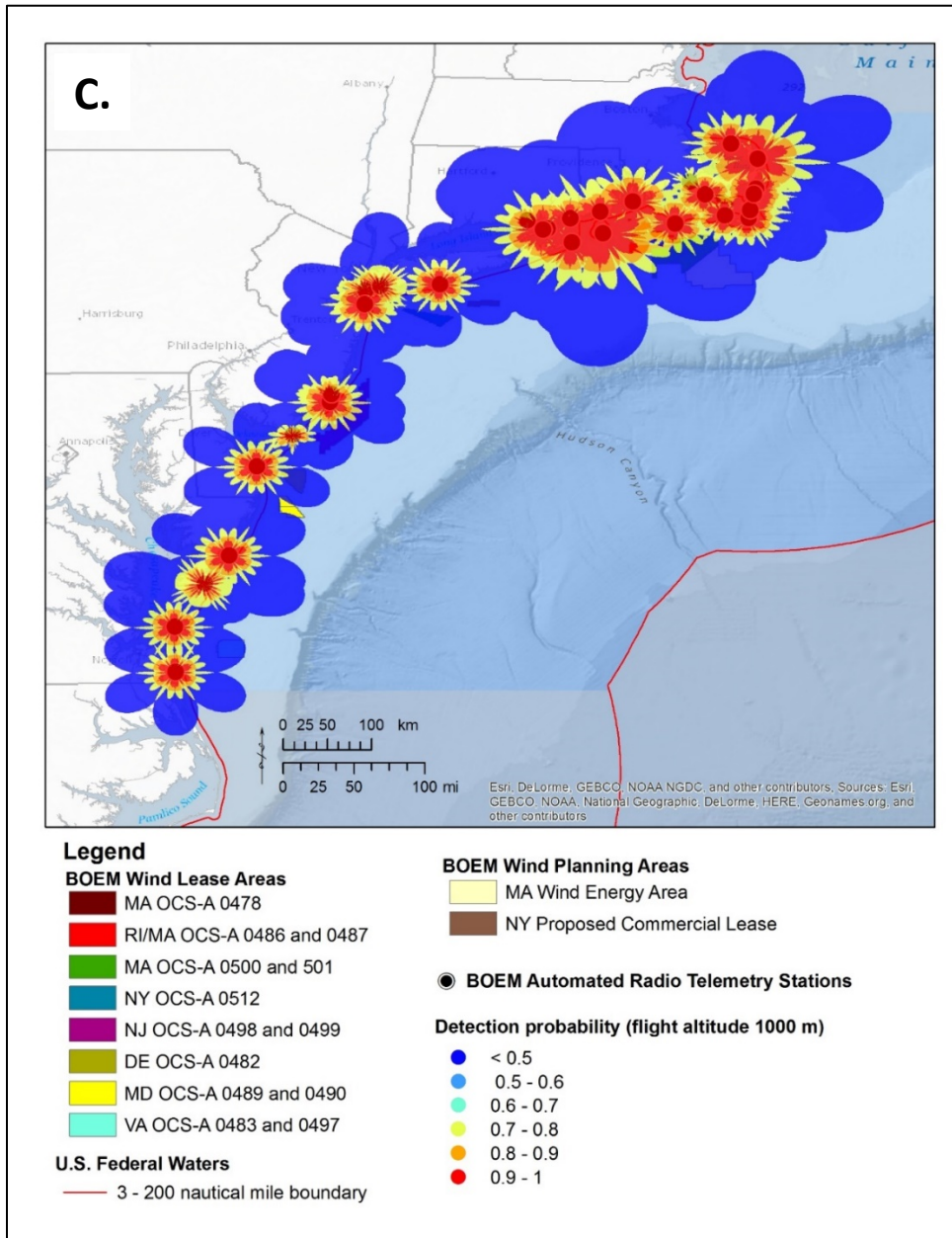


Figure C-2. Coverage map from 2016 BOEM-funded towers showing the probability of detecting a bird flying at (a) 20m, (b) 200m, or (c) 1000m.

Coverage assumes signal strength value (5). Higher signal strengths would be likely to show a similar probability distribution, but with contracted coverage consistent with Fig. C-1. Overlapping tower ranges indicate the capacity for simultaneous detections to provide more accurate estimates of the target's altitude and spatial coordinates than what can be estimated from the single detections

10 Appendix D: Summary of data from nano-tagged birds that were tagged by partners in the Motus network and detected by BOEM radio telemetry stations in 2016

We compiled the total number of nano-tagged birds that were tagged by partners in the Motus network and detected by BOEM-funded radio telemetry stations in 2016 and calculated the total number of individuals detected per day at each site. We conservatively removed false detections by retaining only individuals with ≥ 10 detections per tower per day. This resulted in 33 detected species of shorebirds, passerines, and raptors (Table D-1) from 40 projects (Table D-2); no bats were detected. The sex and age of most individuals detected on BOEM-funded towers were either not recorded or unknown, due to incomplete metadata available through Motus for non-target tags. Of those individuals of known sex and/or age, seven were immature (Swainson's Thrush, American Woodcock, Gray-cheeked Thrush, and Dunlin), three were after hatch year (American Woodcock, Gray-cheeked Thrush, and Bicknell's Thrush), three were male (American Woodcock, Bicknell's Thrush), and two were female (American Woodcock).

The entire non-target dataset for BOEM funded towers, consisting of the number of individuals detected per species and tower by date, is provided as supplementary material to this report (Appendix_D_Non-Target_Detection_Data_BOEM_2016.csv'.)

Table D-1. Total number of nano-tagged individuals per species detected by BOEM-funded radio telemetry stations in 2016, including sex and age data where available

Common name	Scientific name	Num. Individ.	Sex		Age				Project
			M	F	Juv	HY	SY	AHY	
Semipalmated Sandpiper	<i>Calidris pusilla</i>	65							38, 47, 58, 59, 66, 78, 103, 110, 124
Saltmarsh Sparrow	<i>Ammodramus caudacutus</i>	42							25, 29, 33
Sanderling	<i>Calidris alba</i>	34							47, 63, 68
Hermit Thrush	<i>Catharus guttatus</i>	21							83
Semipalmated Plover	<i>Charadrius semipalmatus</i>	19							38, 40, 67, 78
Blackpoll Warbler	<i>Setophaga striata</i>	17							74, 83
Red-eyed Vireo	<i>Vireo olivaceus</i>	15							83
White-rumped Sandpiper	<i>Calidris fuscicollis</i>	15							38, 66, 68
Least Sandpiper	<i>Calidris minutilla</i>	13							38, 78
Yellow-rumped Warbler	<i>Setophaga coronata</i>	13							74, 87
Merlin	<i>Falco columbarius</i>	12							45
Swainson's Thrush	<i>Catharus ustulatus</i>	11				1			35, 49, 74, 104
Ruddy Turnstone	<i>Arenaria interpres</i>	10							38, 47
American Woodcock	<i>Scolopax minor</i>	7	2	2		3		1	43, 82
Black-bellied Plover	<i>Pluvialis squatarola</i>	4							66, 68
Pectoral Sandpiper	<i>Calidris melanotos</i>	4							38
Whimbrel	<i>Numenius phaeopus</i>	4							40
Gray-cheeked Thrush	<i>Catharus minimus</i>	3				1		1	49, 57
Lincoln's Sparrow	<i>Melospiza lincolnii</i>	3							74
Rusty Blackbird	<i>Euphagus carolinus</i>	3							64
Dunlin	<i>Calidris alpina</i>	2			2				67
Barn Swallow	<i>Hirundo rustica</i>	1							92
Bicknell's Thrush	<i>Catharus bicknelli</i>	1	1					1	49
Black-backed Woodpecker	<i>Picoides arcticus</i>	1							42
Eastern Whip-poor-will	<i>Antrostomus vociferus</i>	1							119
Northern Saw-whet Owl	<i>Aegolius acadicus</i>	1							118
Northern Waterthrush	<i>Parkesia noveboracensis</i>	1							74
Piping Plover	<i>Charadrius melodus</i>	1							77
Prairie Warbler	<i>Setophaga discolor</i>	1							95
Red Knot	<i>Calidris canutus</i>	1							65

Common name	Scientific name	Num. Individ.	Sex		Age				Project
			M	F	Juv	HY	SY	AHY	
Savannah Sparrow	<i>Passerculus sandwichensis</i>	1							100
Swamp Sparrow	<i>Melospiza georgiana</i>	1							104
Wood Thrush	<i>Hylocichla mustelina</i>	1							74

Table D-2. Projects with nano-tagged birds detected by BOEM radio telemetry array in 2016.

ID	Project Name	Short Description
1	Motus Ontario Array	Array of 70+ towers maintained by Bird Studies Canada in support of all projects.
25	obrien	Shorebird work on the Gulf of Maine. Saltmarsh Sparrow migration project.
29	R5_SALS	Currently only winter/spring deployments on Saltmarsh Sparrow (SALS) in South Carolina
32	Dowling	Migratory season tracking of eastern red, hoary, and silver-haired bats to inform migration ecology and offshore wind development
33	Ernst	Fall deployments on Saltmarsh Sparrows in Rhode Island
35	Powdermill Nature Reserve	Studies investigating stopover ecology of migrant songbirds at Carnegie Museum of Natural History's Powdermill Avian Research Center (PARC).
38	James Bay Shorebirds	Multi-agency shorebird monitoring on the western coast of James Bay.
40	EC - Arctic Shorebirds	Collective of stations throughout the Canadian arctic and subarctic in support of shorebird ecology research.
42	Tremblay - Boreal Woodpeckers as forest indicators	Description not available
43	Eastern Shore of Virginia National Wildlife Refuge	1 Motus Station maintained by ESV - NWR - USFWS
45	BI_MERL	Digitally-coded tags on southward migrating Merlins captured during fall on Block Island, Rhode Island
47	Red Knot staging and migration ecology.	Stopover and migration ecology of Red Knots at Delaware Bay, NJ.
49	Thrush post-breeding ecology in Quebec	PIs: Andre Derochers (U Laval), Junior Tremblay & Yves Aubry (Env Canada) Breeding, post-breeding, and migratory ecology of BITH, SWTH, GCTH.
57	Selva Colombia	1) Winter habitat use of Canada Warbler and Swainson's Thrush. 2) Landscape use and continental movement patterns of Gray-cheeked Thrush.
58	Semipalmated Sandpiper stopover in Plymouth, MA	A joint project between Manomet and MassWildlife will be deploying nanotags on SESAs in Plymouth Bay to learn more about their local stopover ecology.
59	NJ Audubon - Delaware Bay Shorebirds	Track Semipalmated Sandpipers staging in Delaware Bay during spring migration
63	Saskatchewan Migratory Shorebirds	Shorebird stopover timing and habitat use in Saskatchewan
64	Ohio State University	Rusty Blackbird stopover ecology and Black-crowned Night Heron post-fledging survival

ID	Project Name	Short Description
65	Texas Gulf Coast Migratory Shorebirds	Stopover and migration ecology of migratory REKN and SAND on the Texas Coast.
66	New project (#66)- EBM_Coats	Description not available
67	Nol - Churchill Shorebirds	Assessing Departure and Stopover Ecology of Two Species of Migrating Shorebirds
68	Arctic Shorebirds - CWS Yellowknife	Shorebird study at the Polar Bear Pass National Wildlife Area on Bathurst Island, Nunavut.
71	Lake Erie Bats	Study of bat migration, post-breeding dispersal and habitat use in Norfolk County and Long Point, Ontario.
73	Mississippi Clapper Rail	Using automated telemetry to estimate seasonal and annual survivorship of Clapper Rails in emergent marshes of the northern Gulf of Mexico
74	CT River Valley Migratory Songbird Study	Migratory passerine use of the Connecticut river valley in Massachusetts, Vermont, and New Hampshire.
77	NJ Chick Survival	This project will examine factors limiting reproductive success in New Jersey.
78	Atlantic Canada Shorebirds	Assessing movement, habitat use and length of stay of migrating shorebirds during stop-over in Atlantic Canada.
82	Maine - American Woodcock	American Woodcock
83	BIMYWA	Digitally-coded tags on southward migrating warblers (Yellow-rumped and Blackpoll) captured during fall on Block Island, Rhode Island
87	Post-breeding Movements of BLPW and MYWA	Examining the scope and scale of post-breeding movements of two related species with alternate life-history strategies nesting on islands in NS.
92	Ontario Barn and Cliff Swallows	Description not available
95	BellVagrantsNS	Studying reorientation of vagrant passerines and near-passerines in Nova Scotia, CA
100	Stutchbury - Ontario Savannah Sparrow	Dispersal and onset of fall migration of juvenile and adult Savannah Sparrow in Southern Ontario.
103	NYC Audubon	NYC Audubon will be using VHF NanoTags in order to track movements of Semipalmated Sandpipers stopping over in Jamaica Bay, NY during their migration.
104	Perlut - Maine Forest Birds	Banding station deploying nanotags on migrant songbirds in a coastal forest in southern Maine (Biddeford).
109	Nova Scotia SWTH Post-breeding Dispersal	Post-breeding dispersal of Swainson's Thrush on Bon Portage and Seal Island in Nova Scotia. Research conducted by Lucas Berrigan and Phil Taylor.
110	Holberton 2015-16	Description not available
118	Tadoussac NSW0	We want to monitor the migration pattern(s) of NSW0 from Tadoussac, Quebec till the wintering areas of the species in eastern North-America.
119	Missouri - E. Whip-poor-will	Description not available

ID	Project Name	Short Description
124	NJA - South America Shorebirds	Description not available

11 Appendix E. Summary of geospatially referenced detection data from all Red Knots in this study submitted to BOEM as a supplemental material to this report.

As supplementary material to this report, we have provided movement model output and associated meteorological covariate data on a 10-minute time step for all Red Knots in this study (Appendix E - Red_knot_location_estimates_and_weather_data_2016_boem_study.csv). In addition, we provide all processed data from the Motus Wildlife Tracking System for all Red Knots in this study (Appendix E - Red_knot_motus_detection_data_2016_boem_study.csv).

Field descriptions of each file appear below:

File name: Appendix E-Red_knot_location_estimates_and_weather_data_2016_boem_study.csv

Fields:

bird_id: unique identifier of each tagged bird, where prj = Motus project number and id = id of transmitter

ts_gmt: time stamp of estimated location, in Greenwich Mean Time (GMT)

x: mean x-coordinate of location estimate in UTM Zone 18N (units in m)

y: mean y-coordinate of location estimate in UTM Zone 18N (units in m)

z: mean altitude estimate (units in m)

stdx: standard deviation of x-coordinate of location estimate in UTM Zone 18N (units in m)

stdy: standard deviation of y-coordinate of location estimate in UTM Zone 18N (units in m)

lqz: lower quartile of z (units in m)

uqz: upper quartile of z (units in m)

wind_sp: wind at a pressure level of 1000 mb (about 100 m above sea level), quantified as wind speed (m/s), Zonal (Eastward) and Meridional (Northward) wind components (m/s)

wind_dirn: the direction wind blows toward, measured in degrees clockwise from geographic North

air_temp: air temperature (units in Kelvins, surface level)

precipn: precipitation accumulation kg/m², surface level)

visibility: visibility (units in m, surface level)

pressure: barometric pressure (units in Pa, surface level)

windSupport: the tailwind component (units in m/s) in a bird's flight direction (where negative values are headwinds), which can be considered as supportive under the assumption that birds fully compensate for drift, i.e. that flight directions represent intended (goal) directions.

windCross: crosswind component (units in m/s) relative to a bird's flight direction, i.e. under the presumption of full compensation for crosswind, i.e. that flight directions represent intended (goal) directions. Positive values are to the left (clockwise) relative to the flight direction.

groundSp: magnitude of ground speed (units in m/s)

airSp: magnitude of a bird's airspeed vector (units in m/s), i.e. excluding any wind effect. The airspeed vector is derived by vector subtraction of the wind vector (at 1000 mb) from the bird's ground speed vector.

File name: Appendix E-Red_knot_motus_detection_data_2016_boem_study.csv

Fields:

id: id of transmitter

ts_gmt: time stamp of detection, in GMT

site: name of automated radio telemetry station that recorded detection

siteant: combination of automated radio telemetry station name and receiving antenna number

sig: signal strength of detection

lat: latitude of automated radio telemetry station (in decimal degrees)

lon: longitude of automated radio telemetry station (in decimal degrees)

tsOrig: original format of time stamp (in seconds, origin = 1970-01-01 00:00.00 GMT)

projID: id number of project that deployed automated radio telemetry station in Motus

tagProjectID: id number of project that deployed transmitter in Motus

period: burst rate of transmitter (in seconds)

motusEnglishName: common name of species

depTsGmt: time stamp of tag deployment (in GMT)

depLoc: site name of tag deployment

depLat: latitude of tag deployment (in decimal degrees)

depLon: longitude of tag deployment (in decimal degrees)

12 Appendix F. Maps of flights that intersected one or more WEAs in Atlantic OCS. Inset plots show estimated altitude (pts) and error quartiles (bars, in m) over time (in min, Eastern Standard Time)

during WEA exposure event. Shading shows altitude range in Rotor Swept Zone of offshore wind turbines (20 to 200 m).

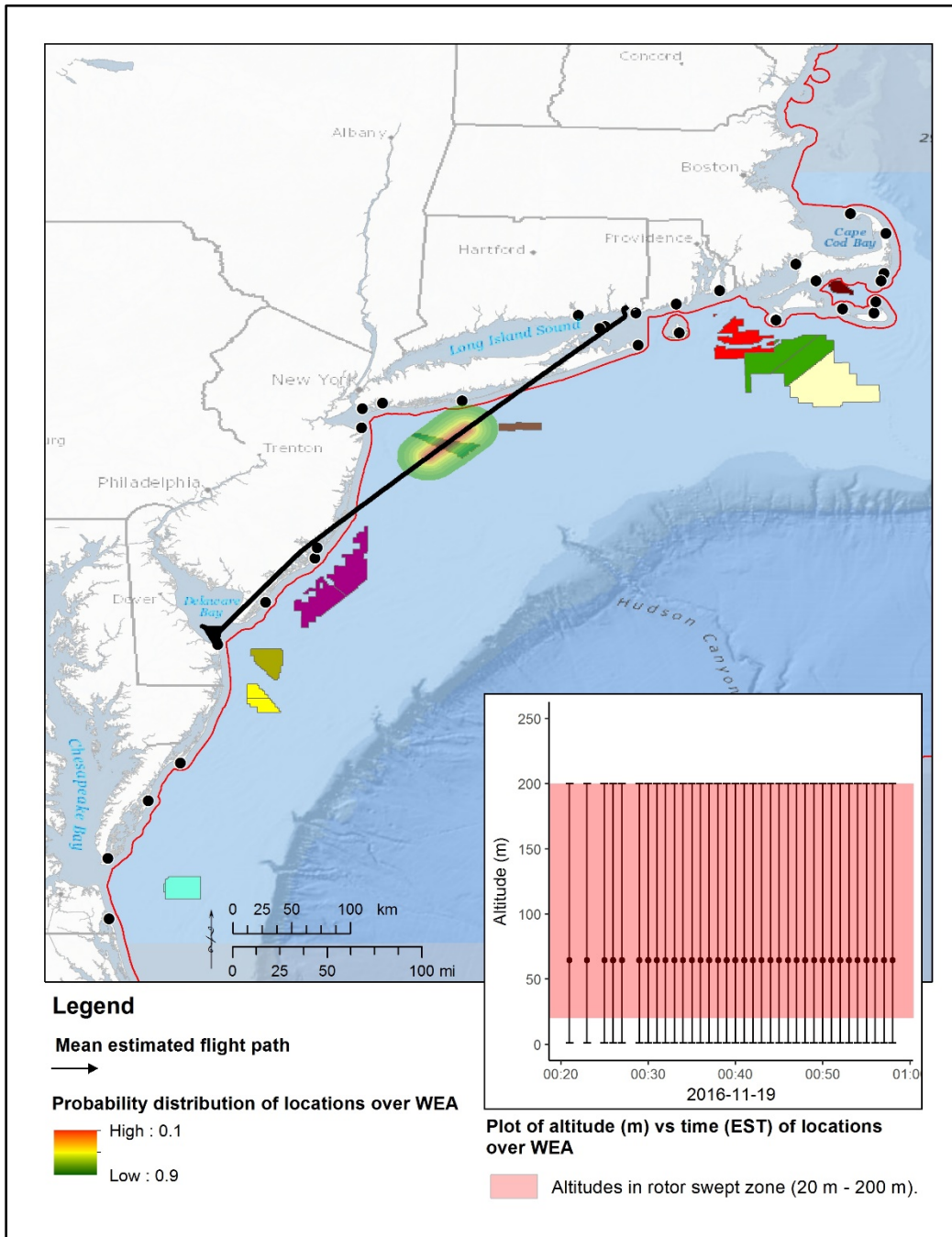


Figure F-1. Estimated flight path of Red Knot ID 316, Hatch Year (HY) male, tagged in the Mingan Islands, Canada.

Probability bands show spatial error around locations during estimated exposure to BOEM Lease Area NY OCS-A 0512 on November 19, 2016.

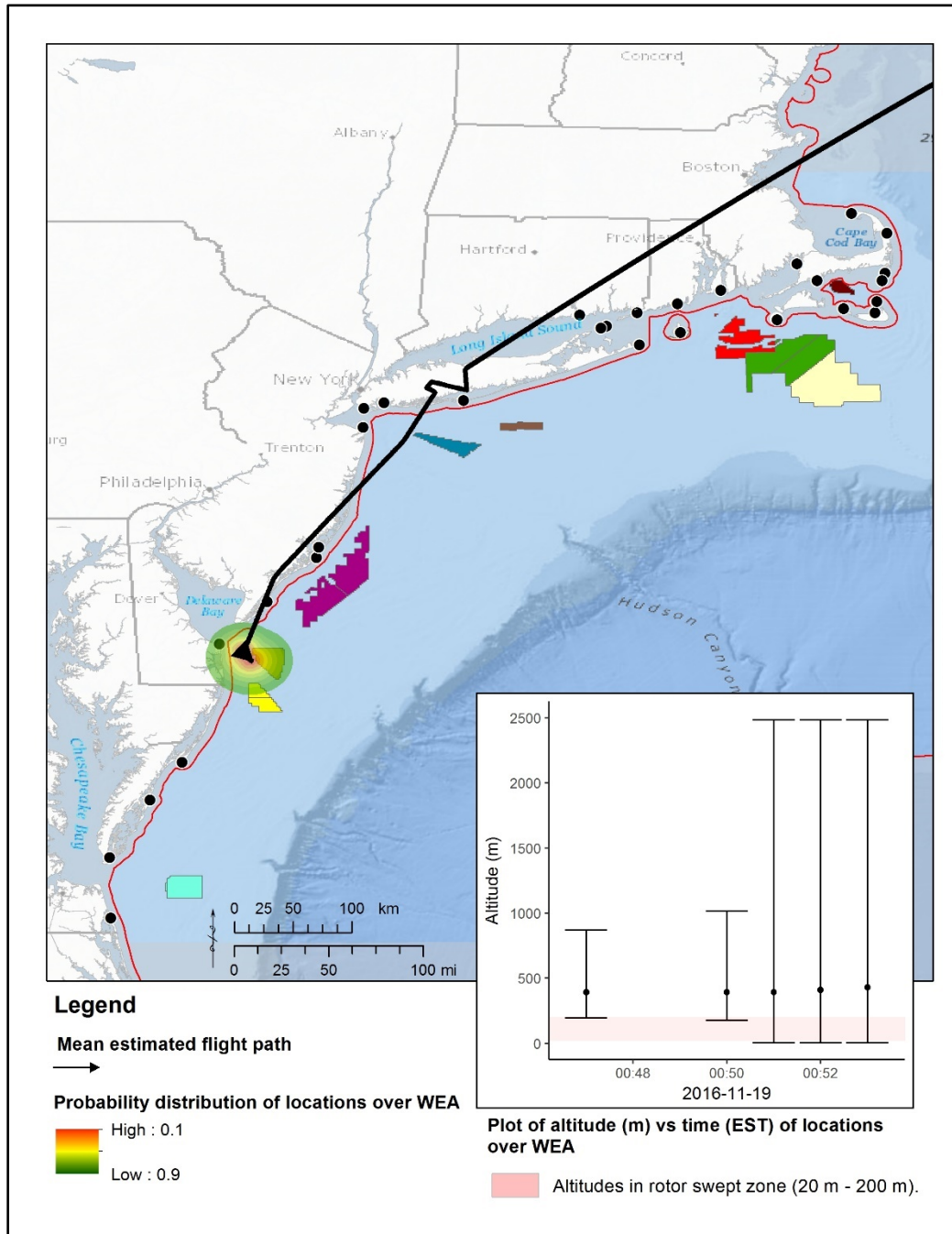


Figure F-2. Estimated flight path of Red Knot ID 328, After Hatch Year (AHY) male, tagged in the Mingan Islands, Canada.

Probability bands show spatial error around locations during estimated exposure to BOEM Lease Area DE OCS-A 0482 on November 19, 2016.

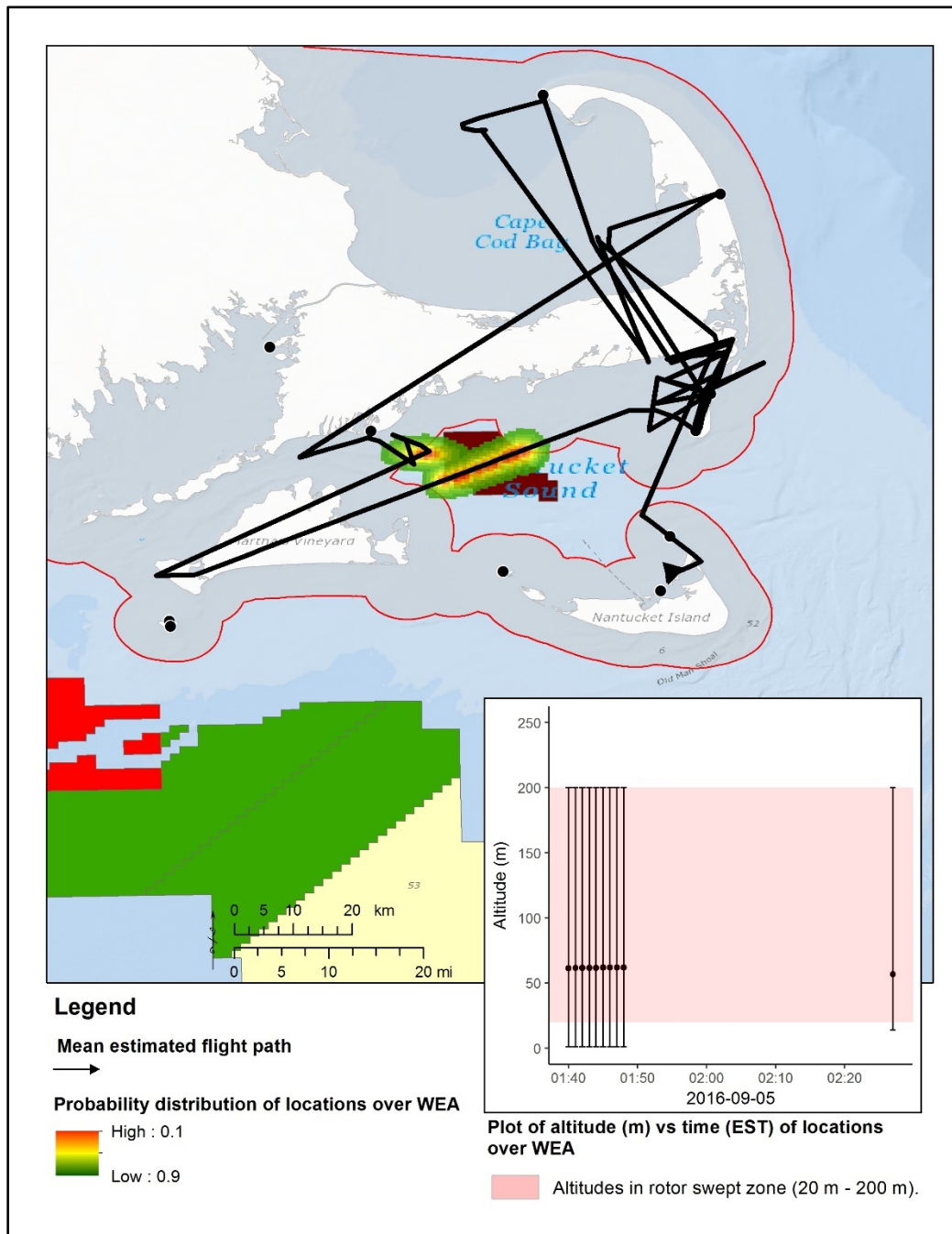


Figure F-3. Estimated flight path of Red Knot ID 471, HY female, tagged in Massachusetts, USA. Probability bands show spatial error around locations during estimated exposure to BOEM Lease Area MA OCS-A 0478 on September 5, 2016.

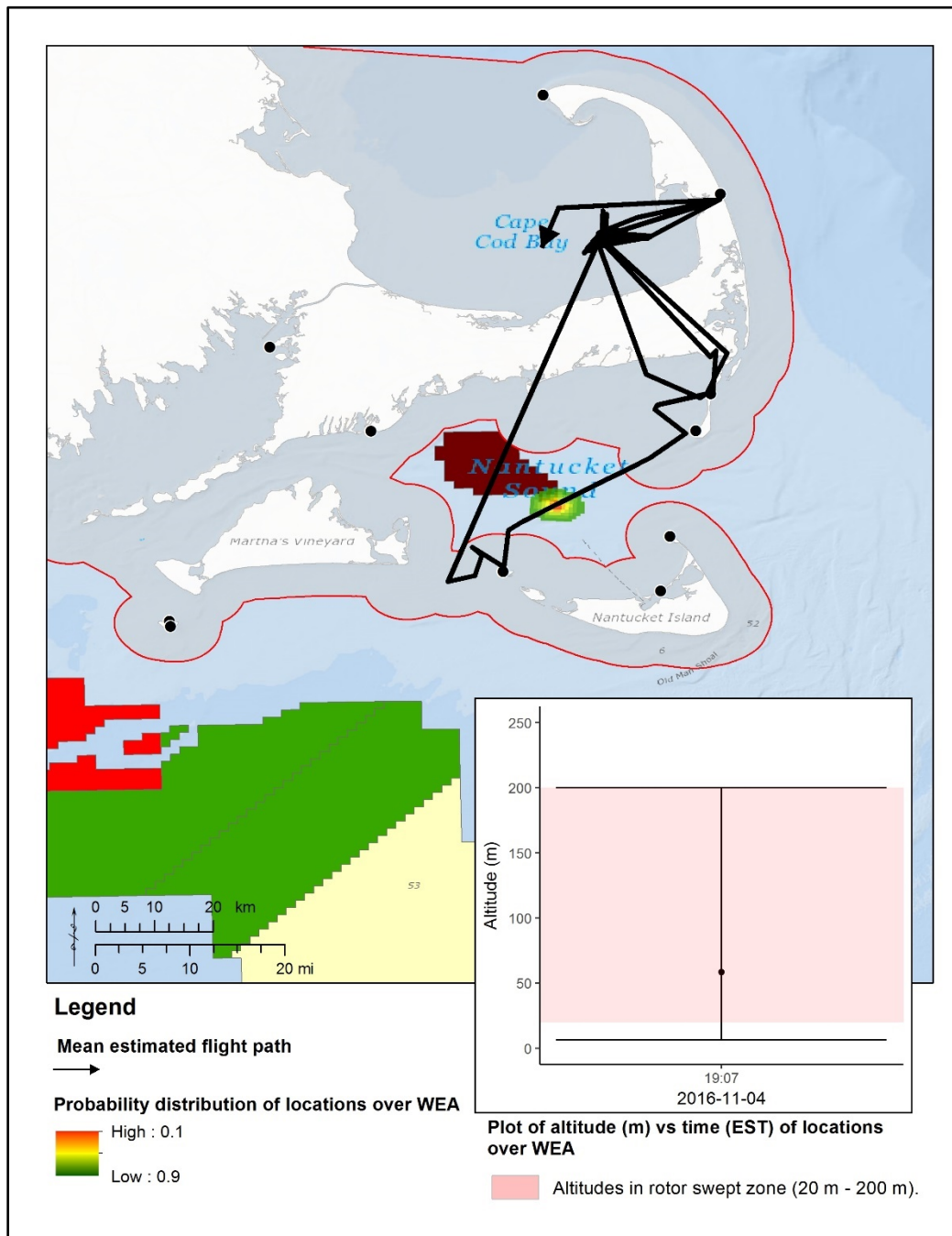


Figure F-4. Estimated flight path of Red Knot ID 464, SY female, tagged in Massachusetts, USA.

Probability bands show spatial error around locations during estimated exposure to BOEM Lease Area MA OCS-A 0478 on November 4, 2016.

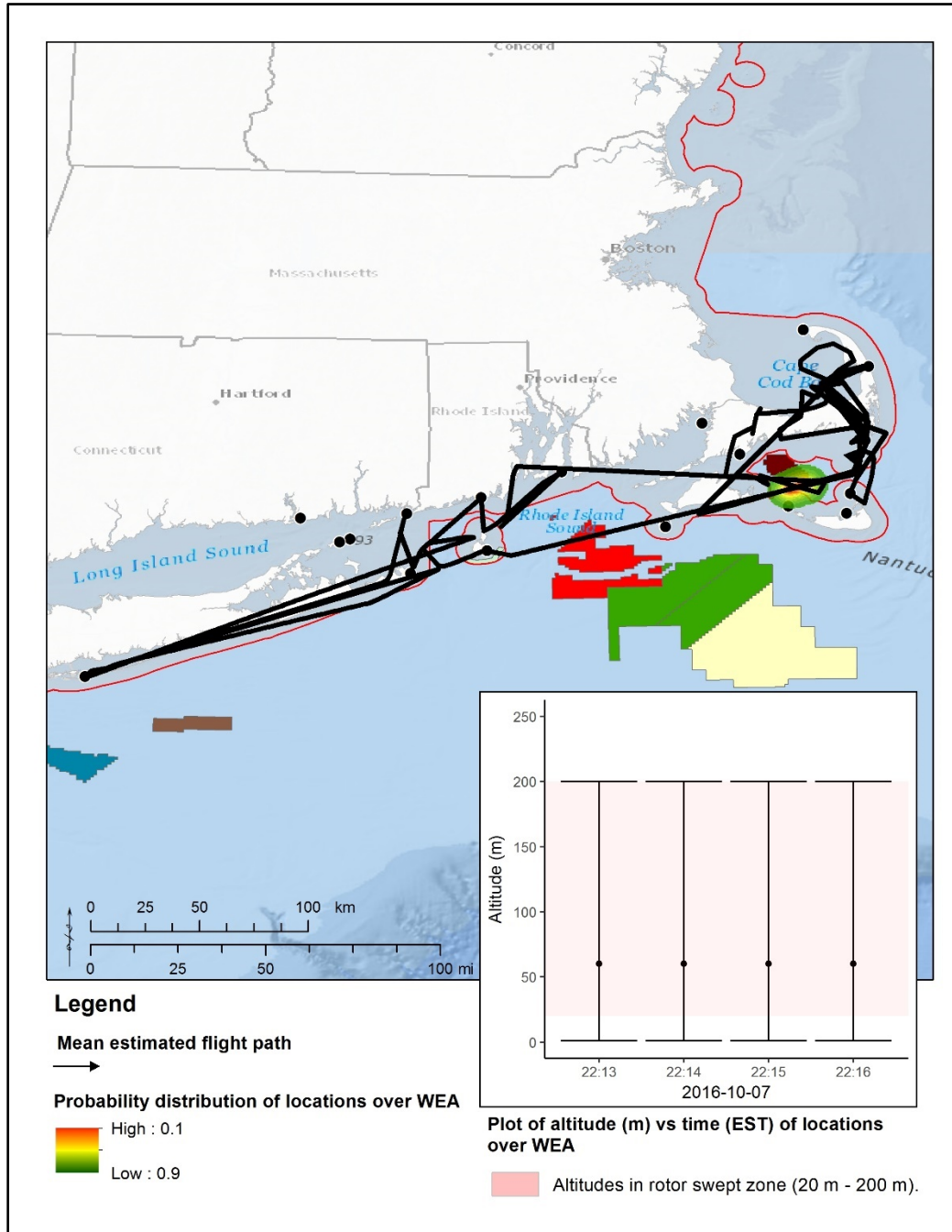


Figure F-5. Estimated flight path of Red Knot ID 453, SY female, tagged in Massachusetts, USA.

Probability bands show spatial error around locations during estimated exposure to BOEM Lease Area MA OCS-A 0478 on October 7, 2016.

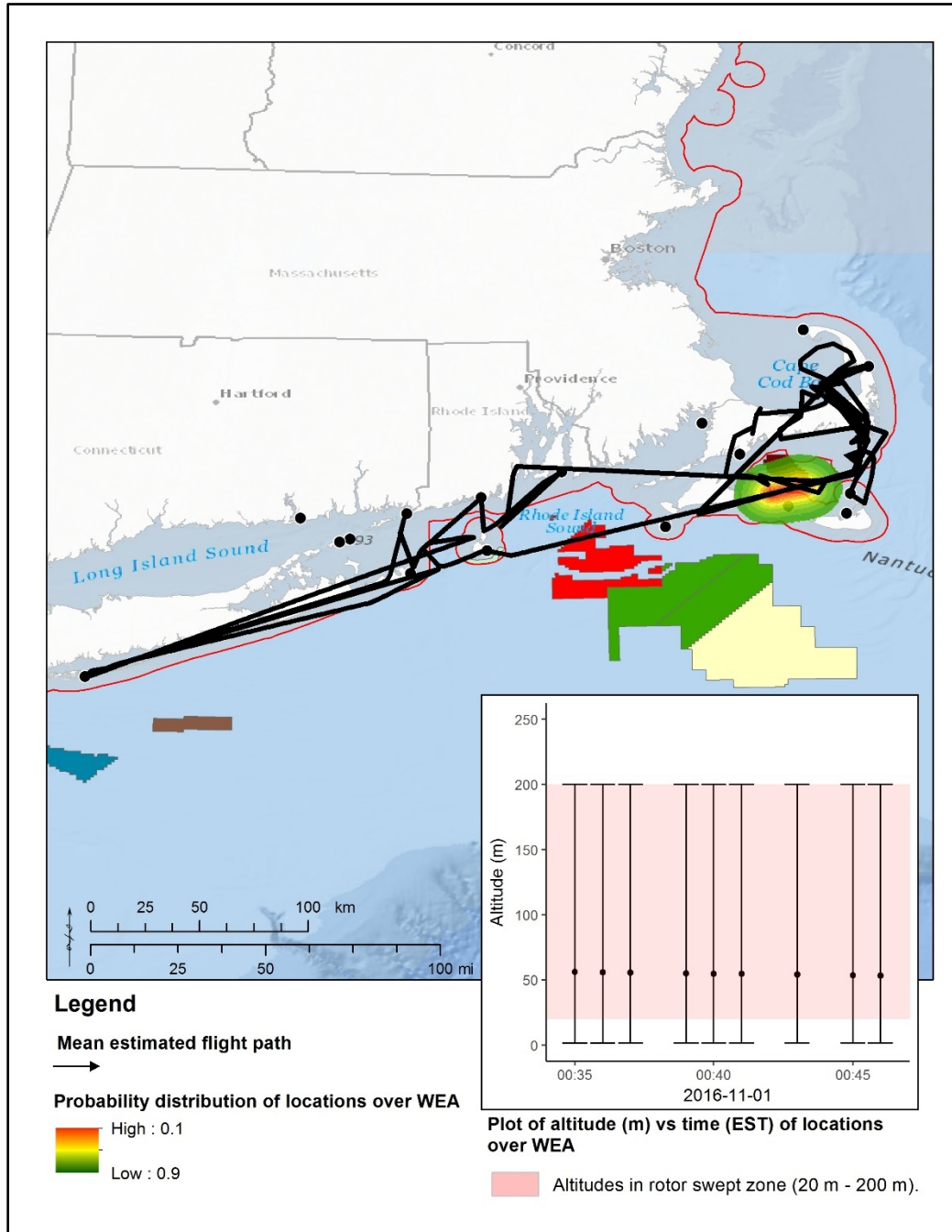


Figure F-6. Estimated flight path of Red Knot ID 453, SY female, tagged in Massachusetts, USA.

Probability bands show spatial error around locations during estimated exposure to BOEM Lease Area MA OCS-A 0478 on November 1, 2016.

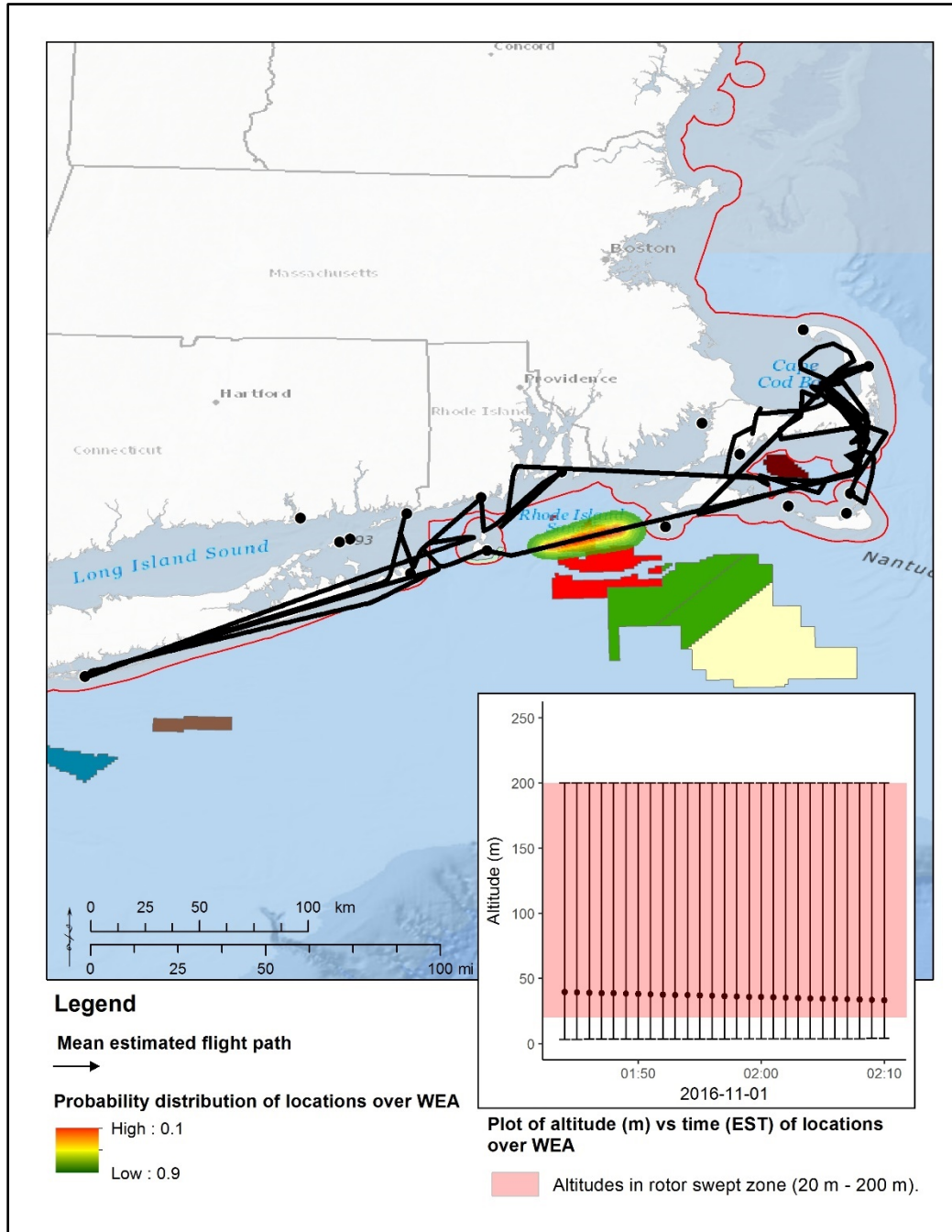


Figure F-7. Estimated flight path of Red Knot ID 453, SY female, tagged in Massachusetts, USA.

Probability bands show spatial error around locations during estimated exposure to BOEM Lease Area RI / MA OCS-A 0486 on November 1, 2016.

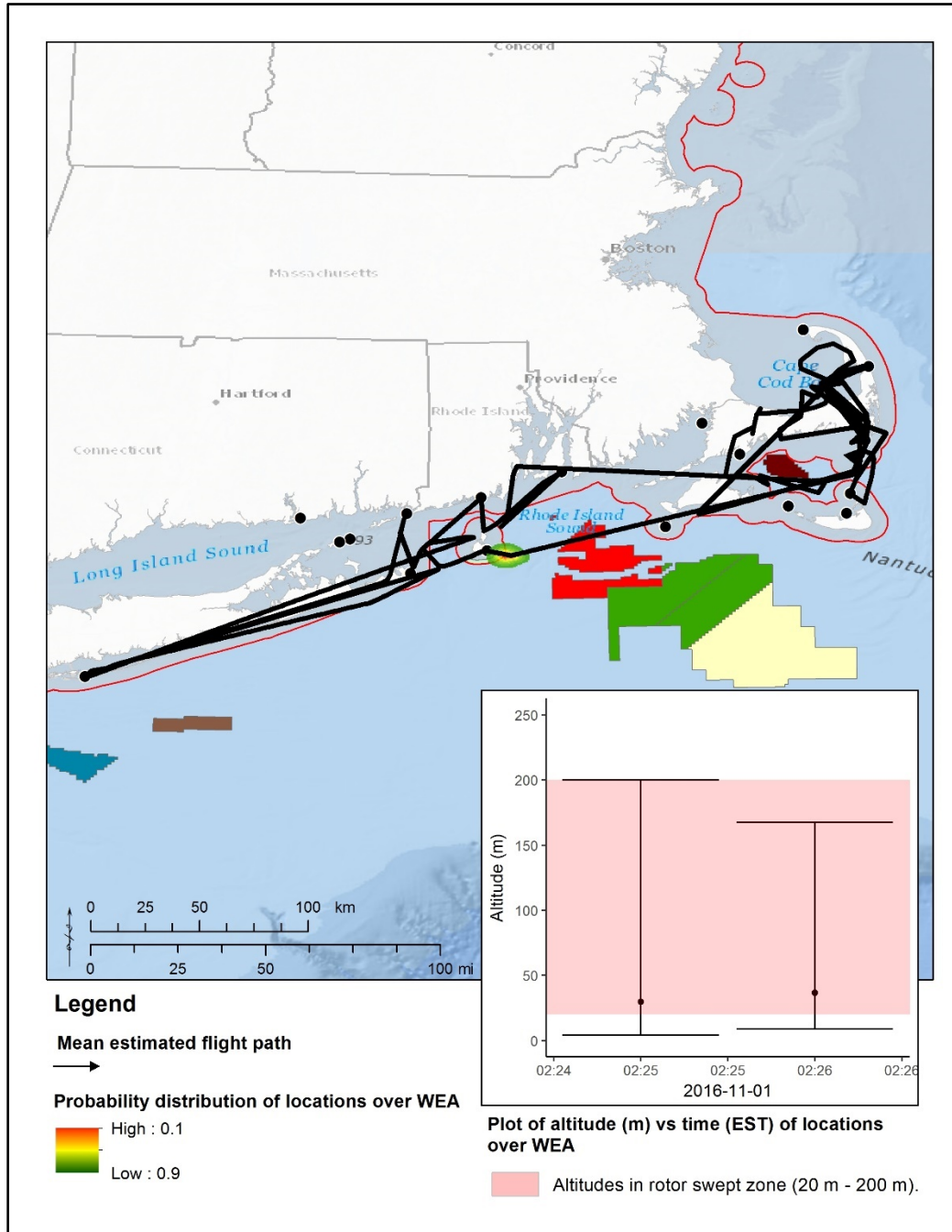


Figure F-8. Estimated flight path of Red Knot ID 453, SY female, tagged in Massachusetts, USA.

Probability bands show spatial error around locations during estimated exposure to the Block Island Wind Farm in Rhode Island state waters on November 1, 2016.

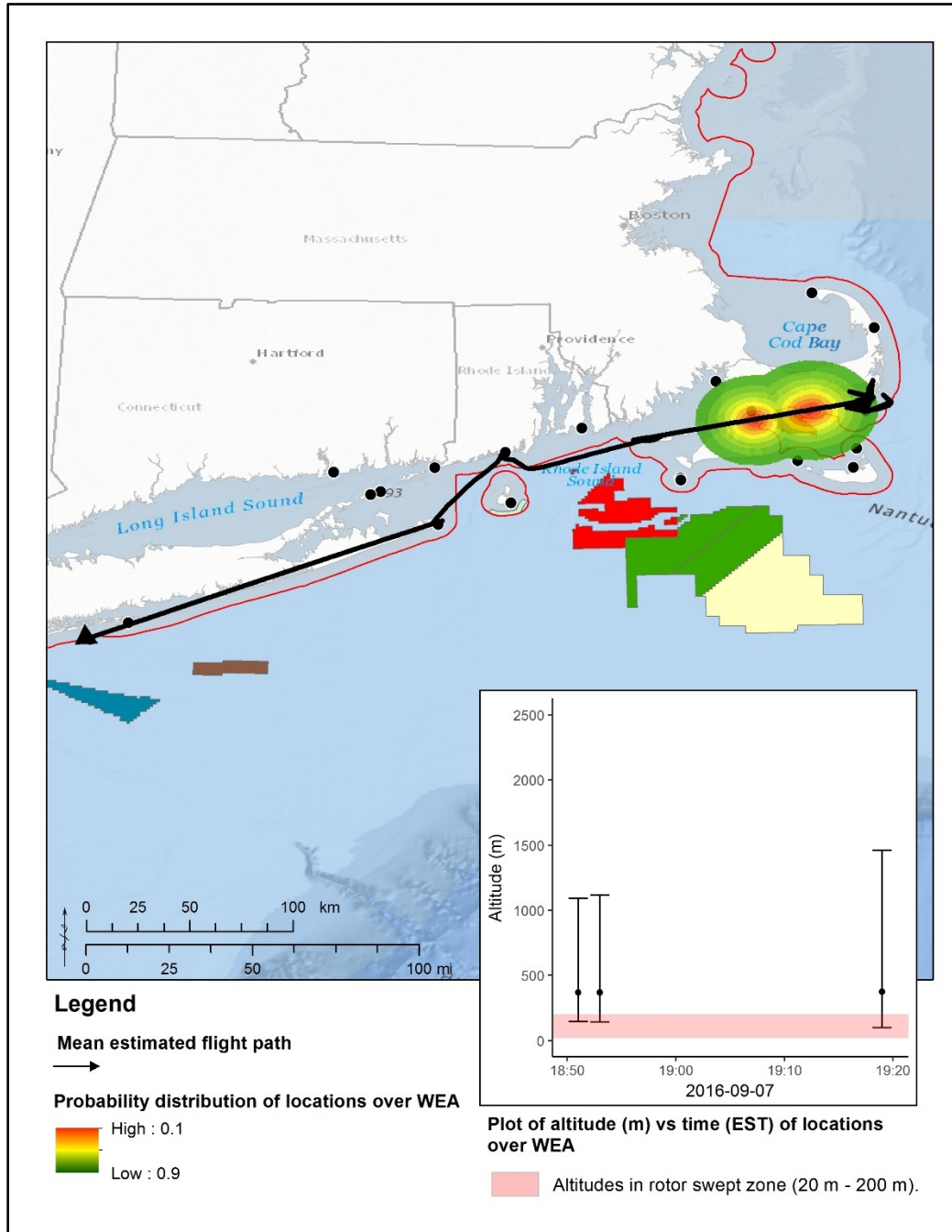


Figure F-9. Estimated flight path of Red Knot ID 434, Second Year (SY) female, tagged in Massachusetts, USA.

Probability bands show spatial error around locations during estimated exposure to BOEM Lease Area MA OCS-A 0478 on September 7, 2016.

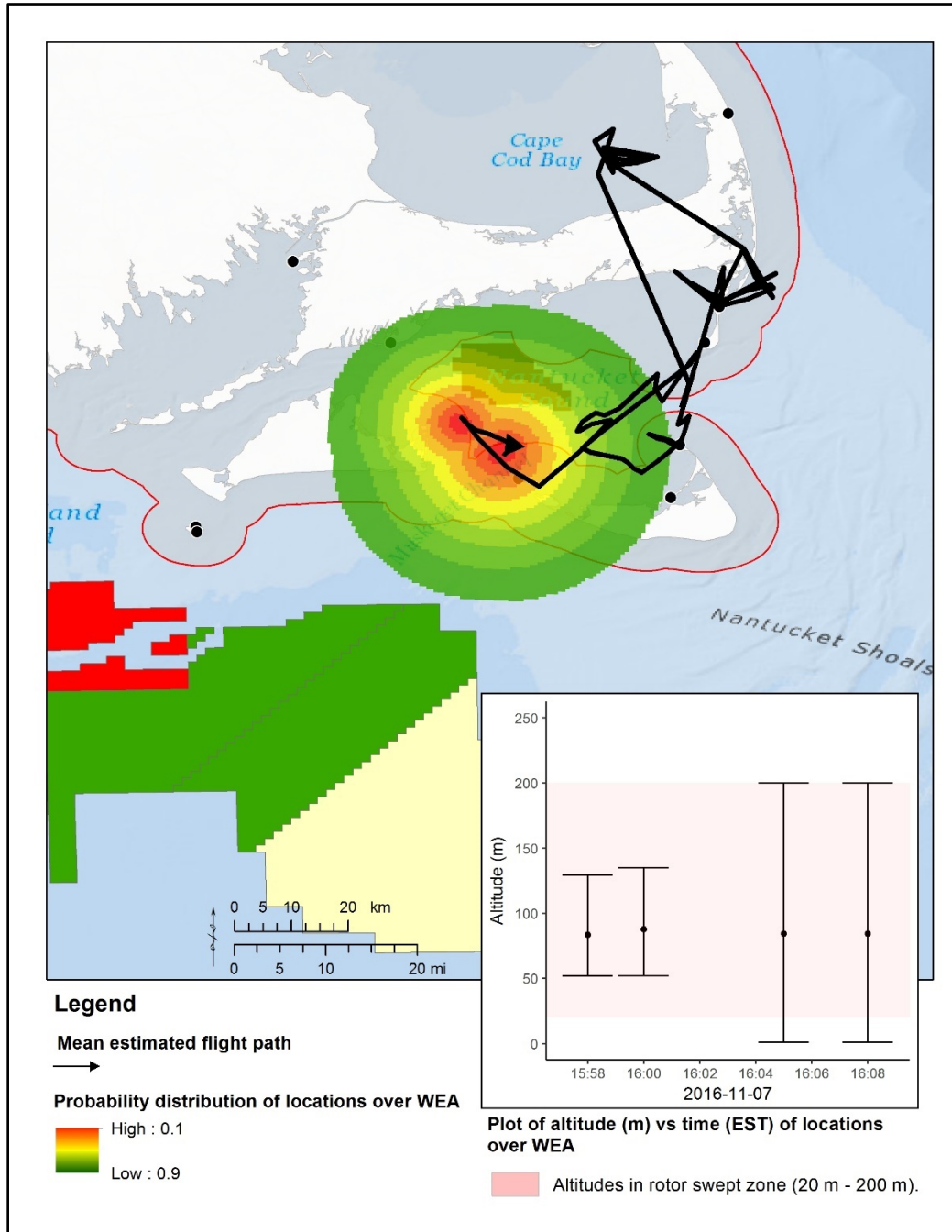


Figure F-10. Estimated flight path of Red Knot ID 454, SY male, tagged in Massachusetts, USA.

Probability bands show spatial error around locations during estimated exposure to BOEM Lease Area RI / MA OCS-A 0486, and the Block Island Wind Farm in Rhode Island state waters on September 12, 2016.

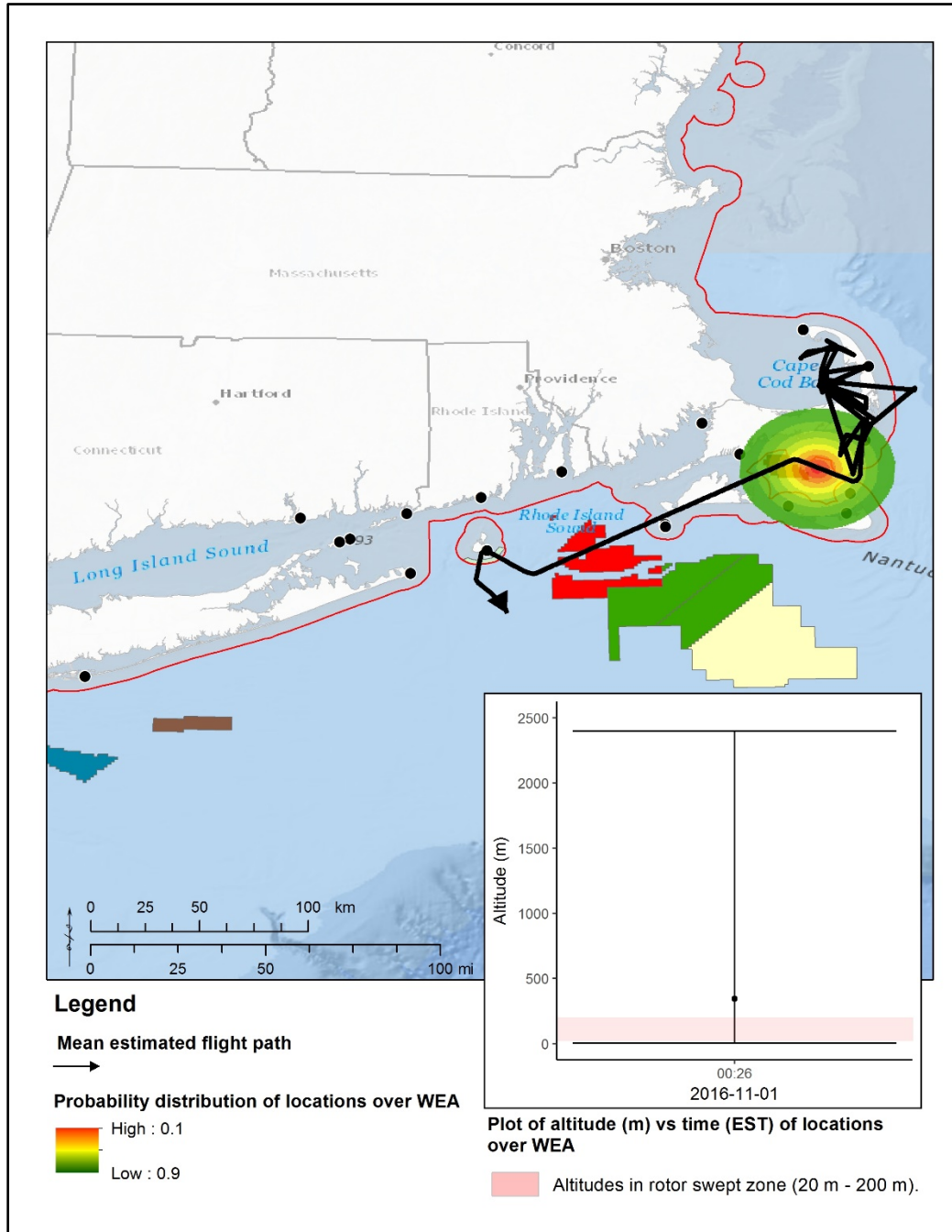


Figure F-12. Estimated flight path of Red Knot ID 449, SY female, tagged in Massachusetts, USA.

Probability bands show spatial error around locations during estimated exposure to BOEM Lease Area MA OCS-A 0478 on November 1, 2016.

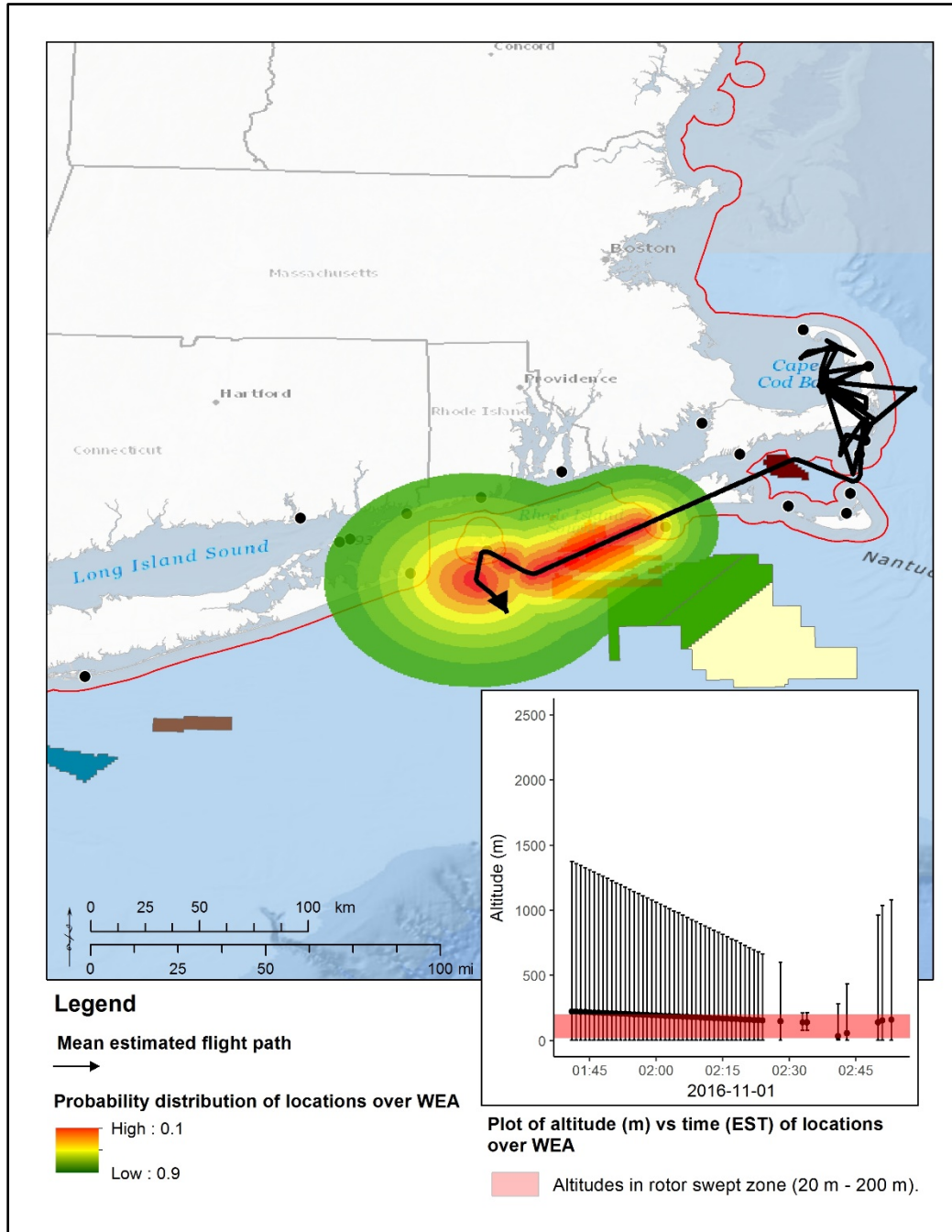


Figure F-13. Estimated flight path of Red Knot ID 449, SY female, tagged in Massachusetts, USA.

Probability bands show spatial error around locations during estimated exposure to BOEM Lease Area RI / MA OCS-A 0486, and the Block Island Wind Farm in Rhode Island state waters on November 1, 2016.

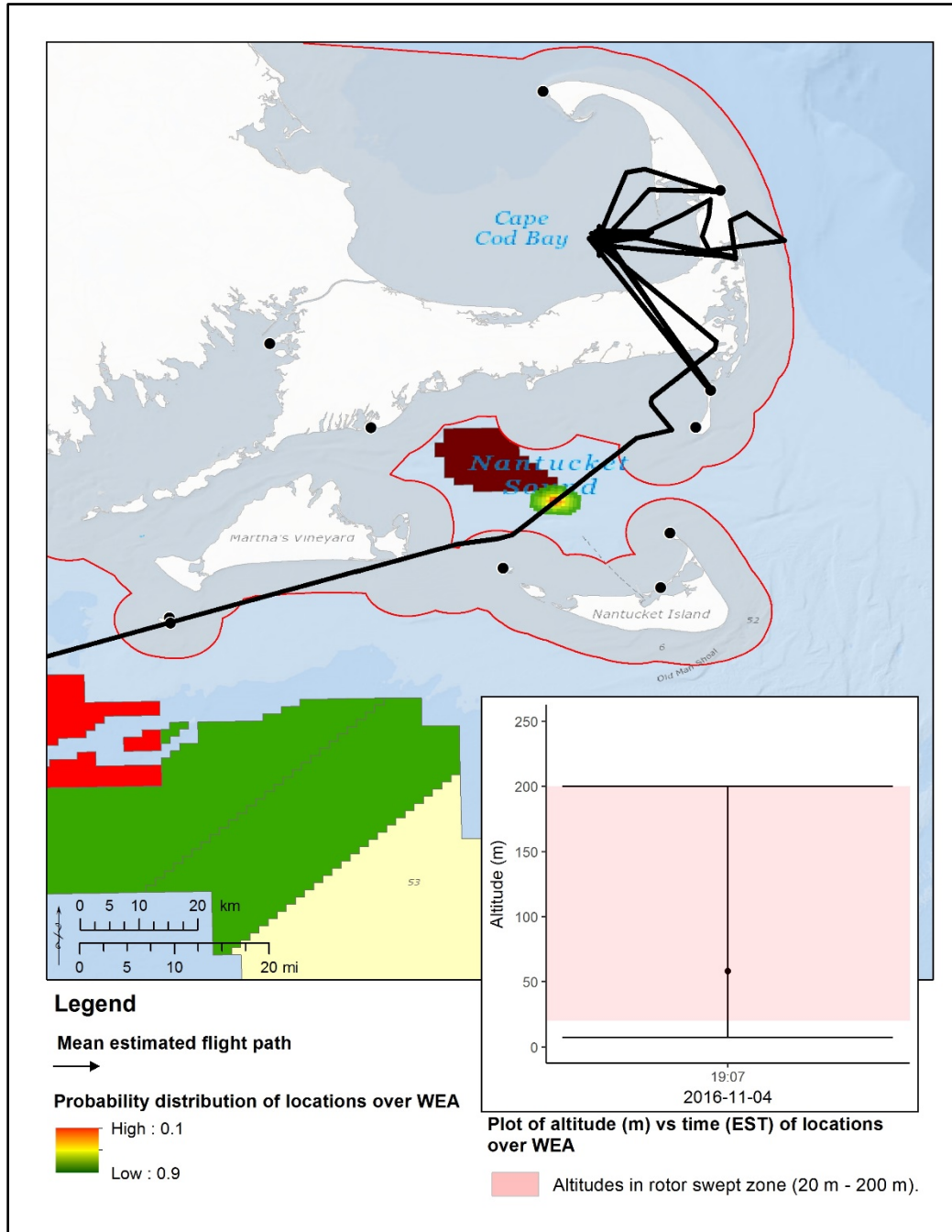


Figure F-14. Estimated flight path of Red Knot ID 470, HY female, tagged in Massachusetts, USA.

Probability bands show spatial error around locations during estimated exposure to BOEM Lease Area MA OCS-A 0478 on November 4, 2016.

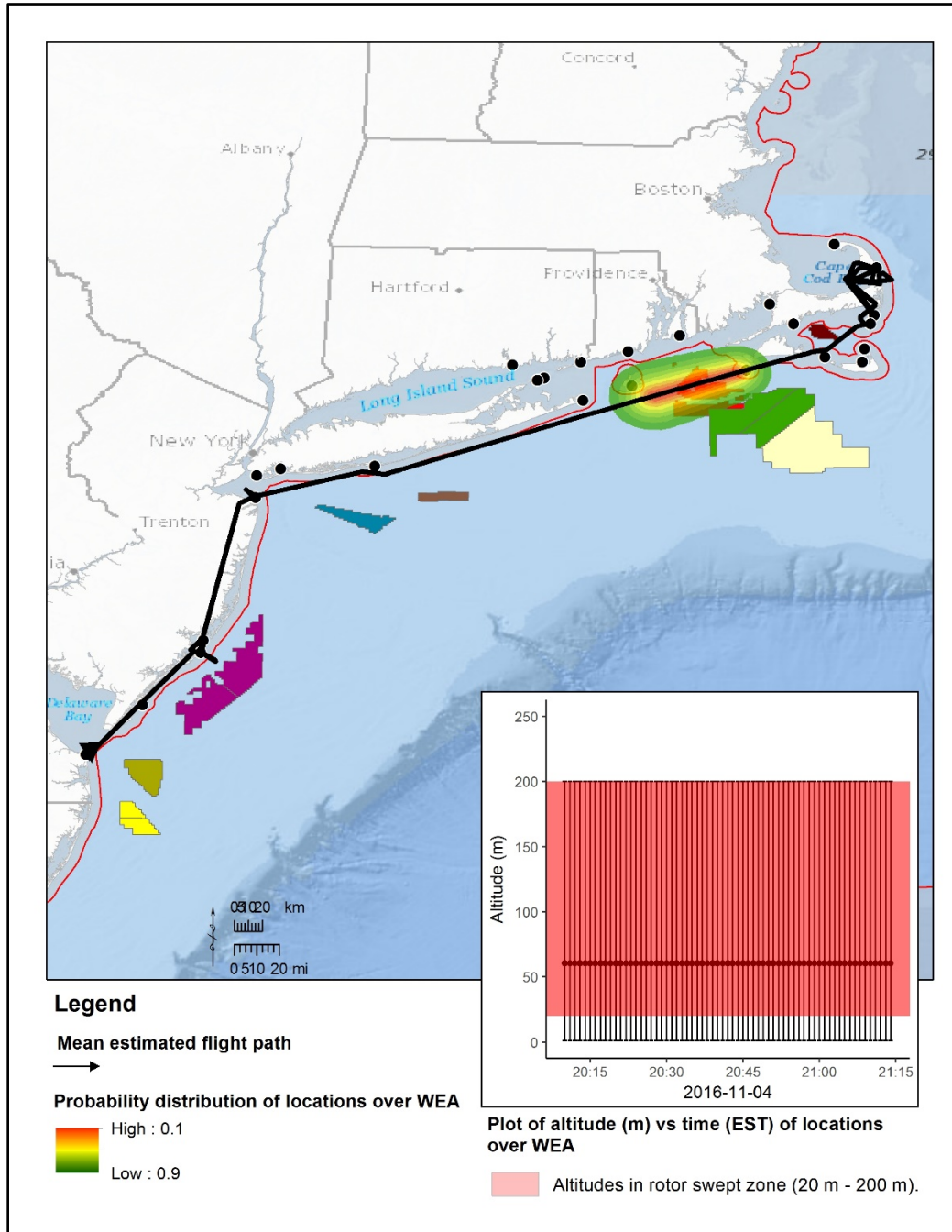


Figure F-15. Estimated flight path of Red Knot ID 470, HY female, tagged in Massachusetts, USA.

Probability bands show spatial error around locations during estimated exposure to BOEM Lease Area RI / MA OCS-A 0486, and the Block Island Wind Farm in Rhode Island state waters on November 4, 2016.

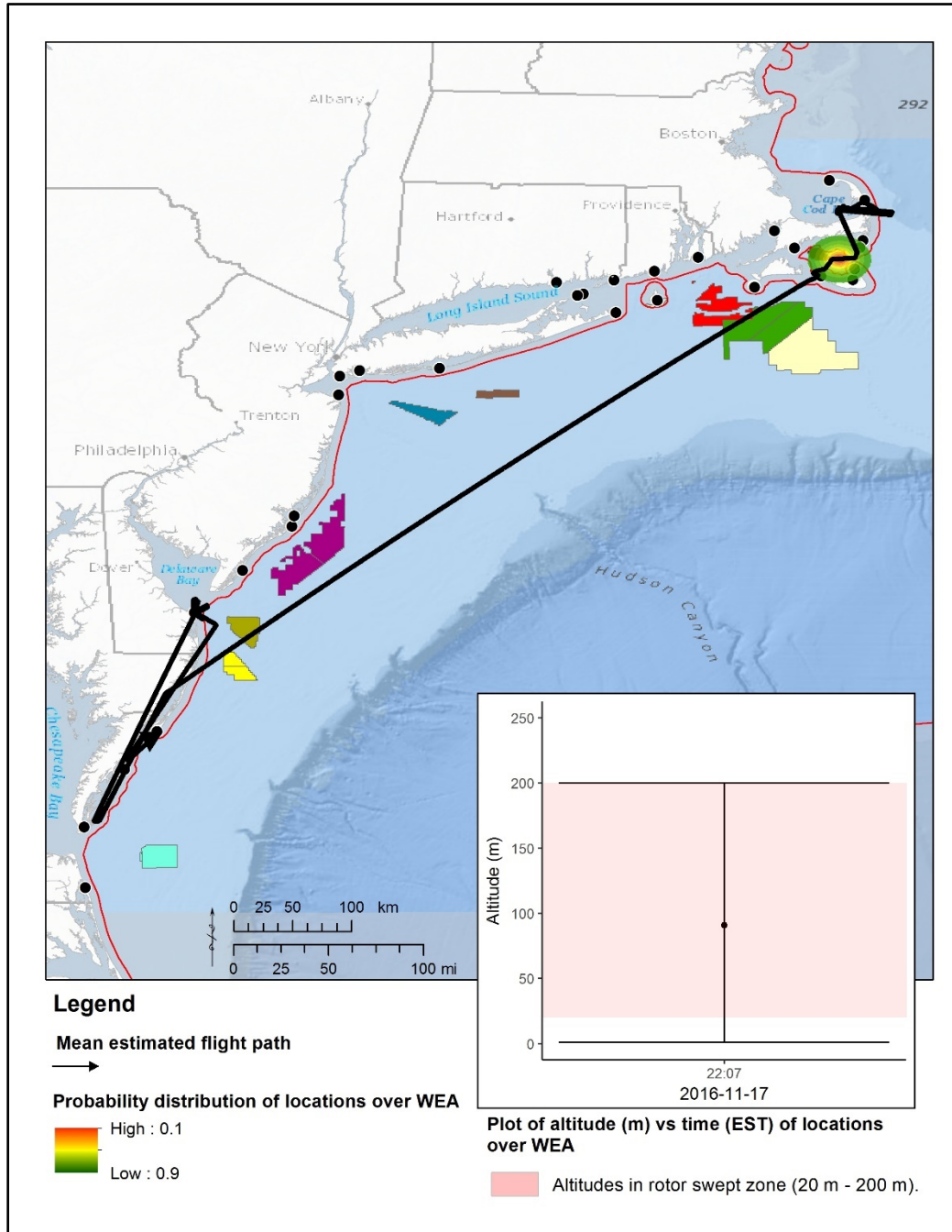


Figure F-16. Estimated flight path of Red Knot ID 458, HY female, tagged in Massachusetts, USA.

Probability bands show spatial error around locations during estimated exposure to BOEM Lease Area MA OCS-A 0478 on November 17, 2016.

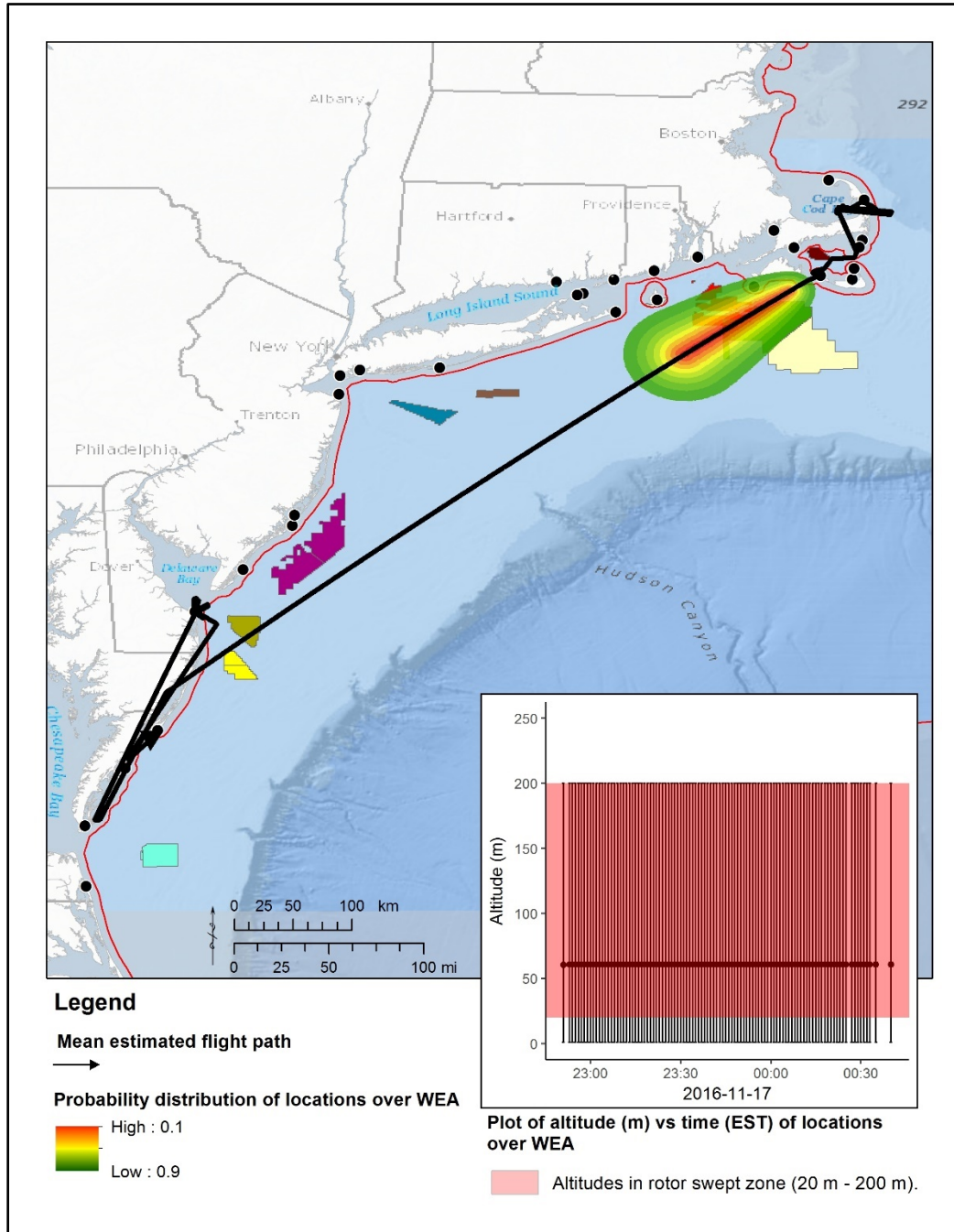


Figure F-17. Estimated flight path of Red Knot ID 458, HY female, tagged in Massachusetts, USA.

Probability bands show spatial error around locations during estimated exposure to BOEM Lease Areas RI / MA OCS-A 0486 and MA OCS-A 0500 and 501 on November 17, 2016.

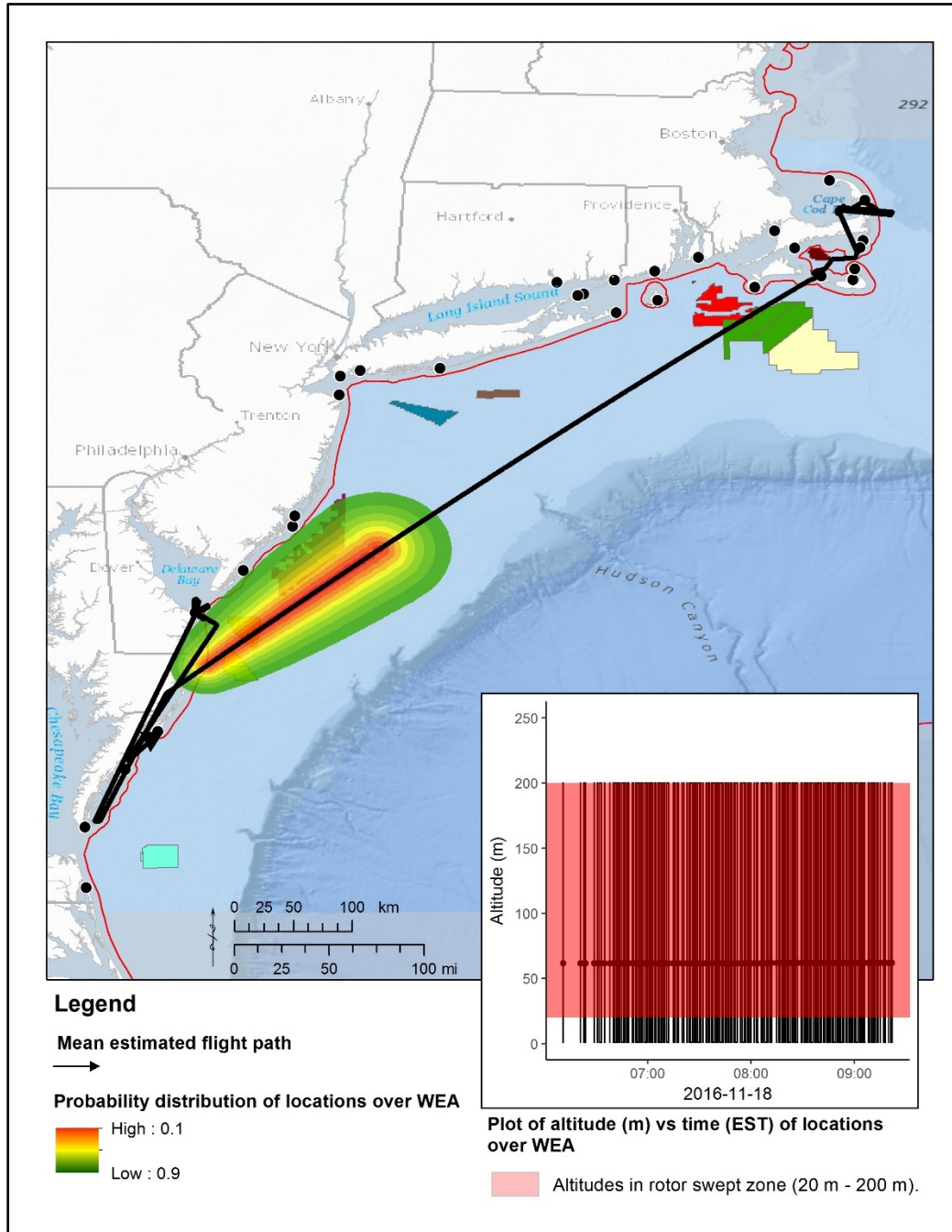


Figure F-18. Estimated flight path of Red Knot ID 458, HY female, tagged in Massachusetts, USA.

Probability bands show spatial error around locations during estimated exposure to BOEM Lease Areas NJ OCS-A 0498 and 0499, DE OCS-A 0482, and MD OCS-A 0489 and 0490 on November 18, 2016.

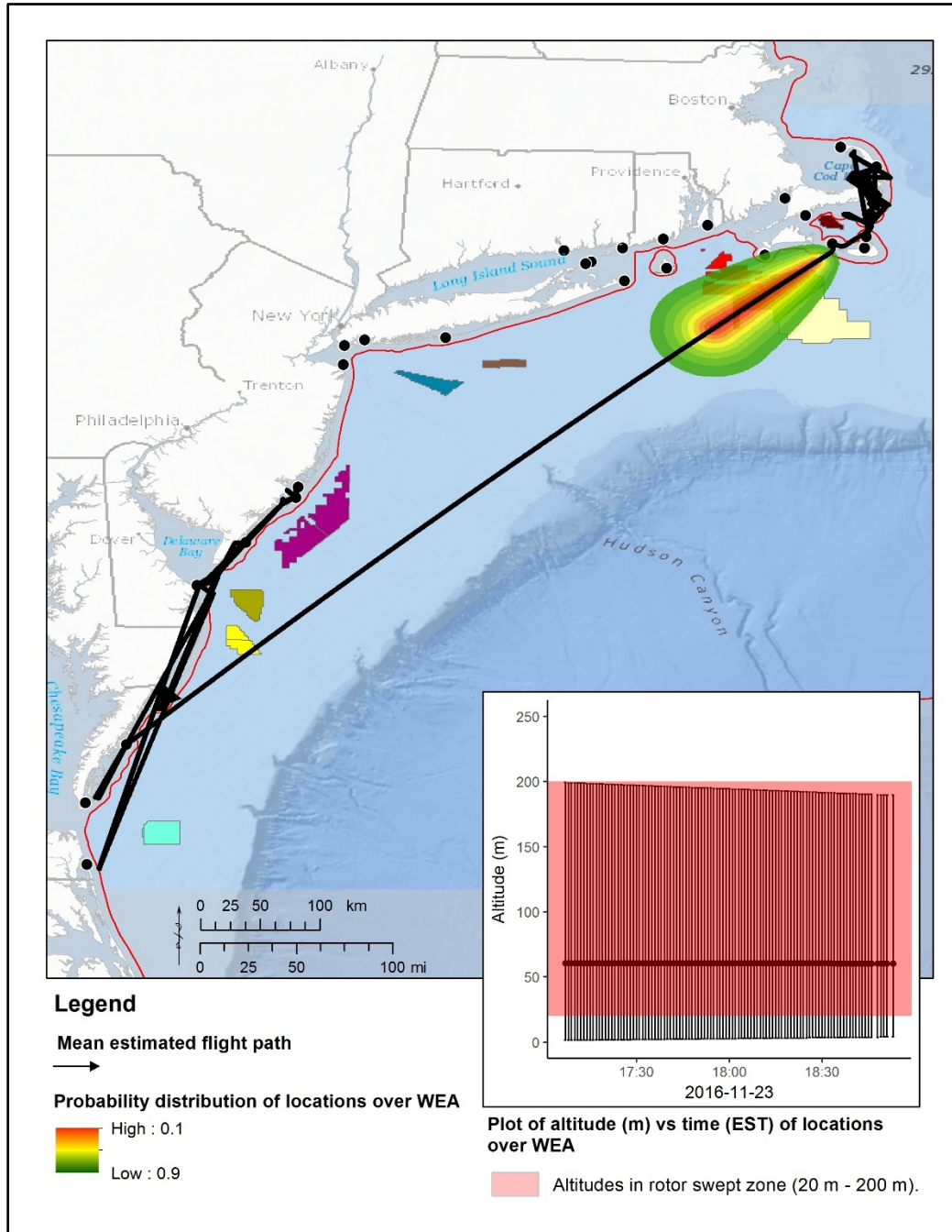


Figure F-19. Estimated flight path of Red Knot ID 451, SY male, tagged in Massachusetts, USA.

Probability bands show spatial error around locations during estimated exposure to BOEM Lease Areas MA OCS-A 0500 and 501 on November 23, 2016.

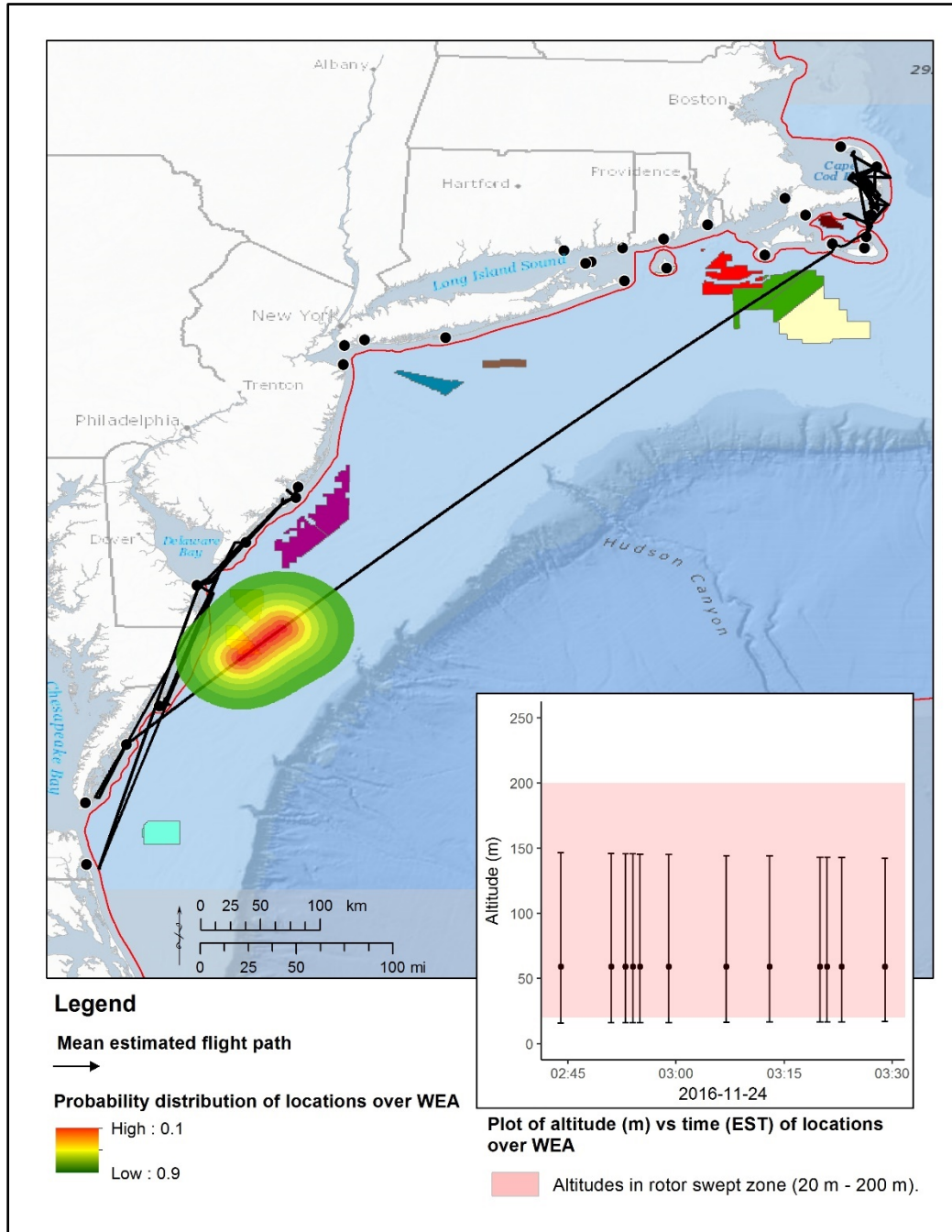


Figure F-20. Estimated flight path of Red Knot ID 451, SY male, tagged in Massachusetts, USA.

Probability bands show spatial error around locations during estimated exposure to BOEM Lease Areas DE OCS-A 0482, MD OCS-A 0489 and 0490 on November 24, 2016.

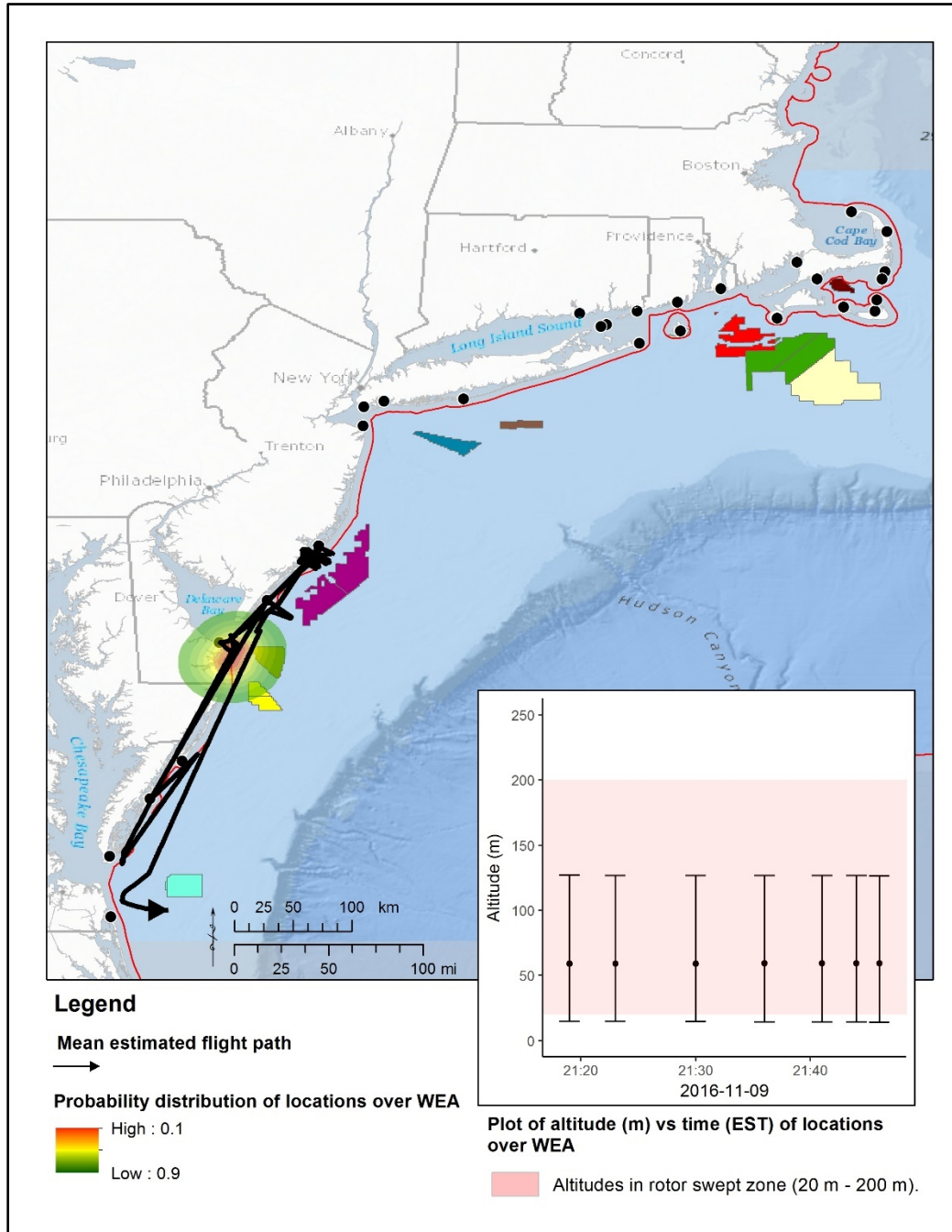


Figure F-21. Estimated flight path of Red Knot ID 47, age and sex unknown, tagged in New Jersey, USA.

Probability bands show spatial error around locations during estimated exposure to BOEM Lease Areas DE OCS-A 0482 and MD OCS-A 0489 and 0490 on November 9, 2016.

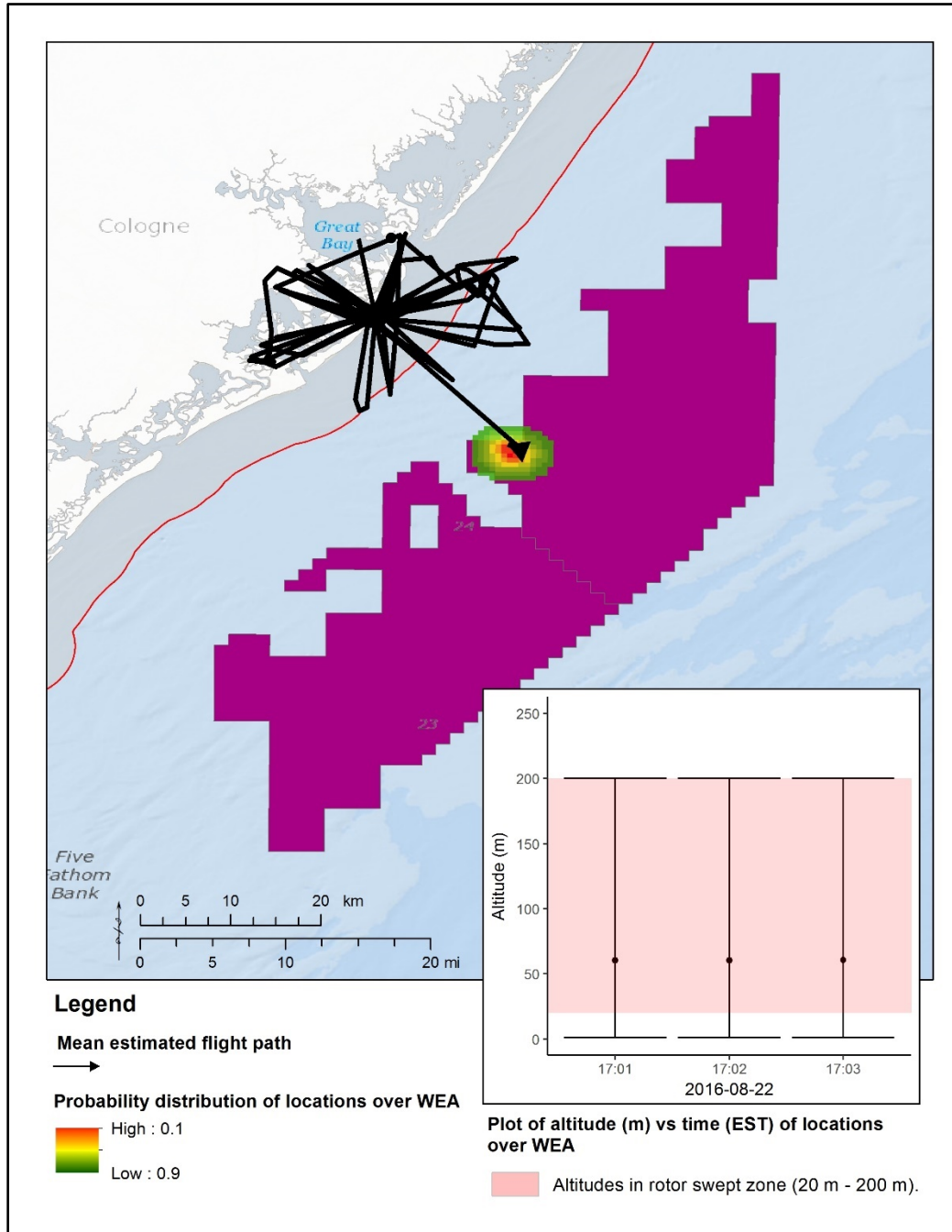


Figure F-22. Estimated flight path of Red Knot ID 101, AHY male, tagged in New Jersey, USA.

Probability bands show spatial error around locations during estimated exposure to BOEM Lease Areas NJ OCS-A 0498 and 0499 on August 22, 2016.

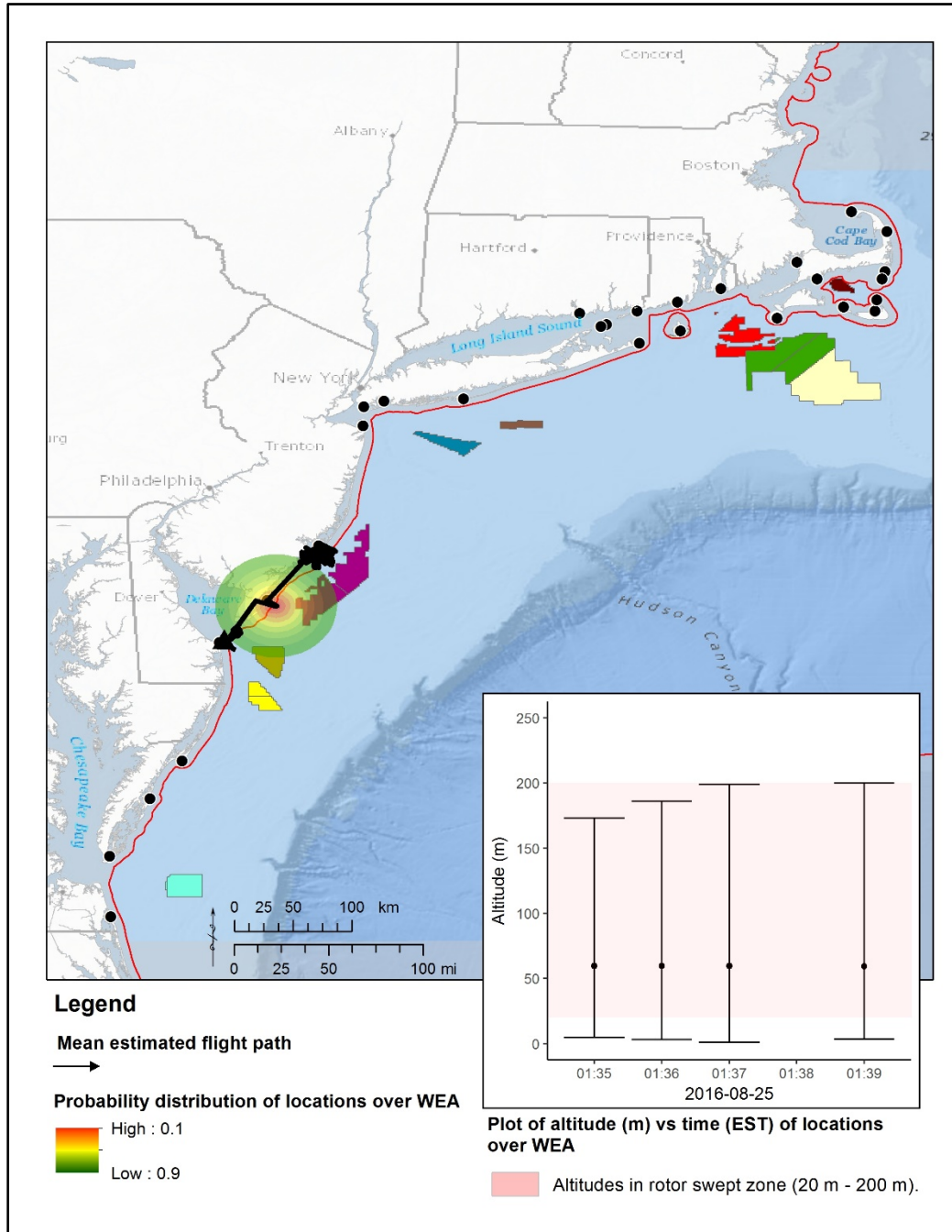


Figure F-23. Estimated flight path of Red Knot ID 478, AHY female, tagged in New Jersey, USA.

Probability bands show spatial error around locations during estimated exposure to BOEM Lease Areas NJ OCS-A 0498 and 0499 on August 25, 2016.

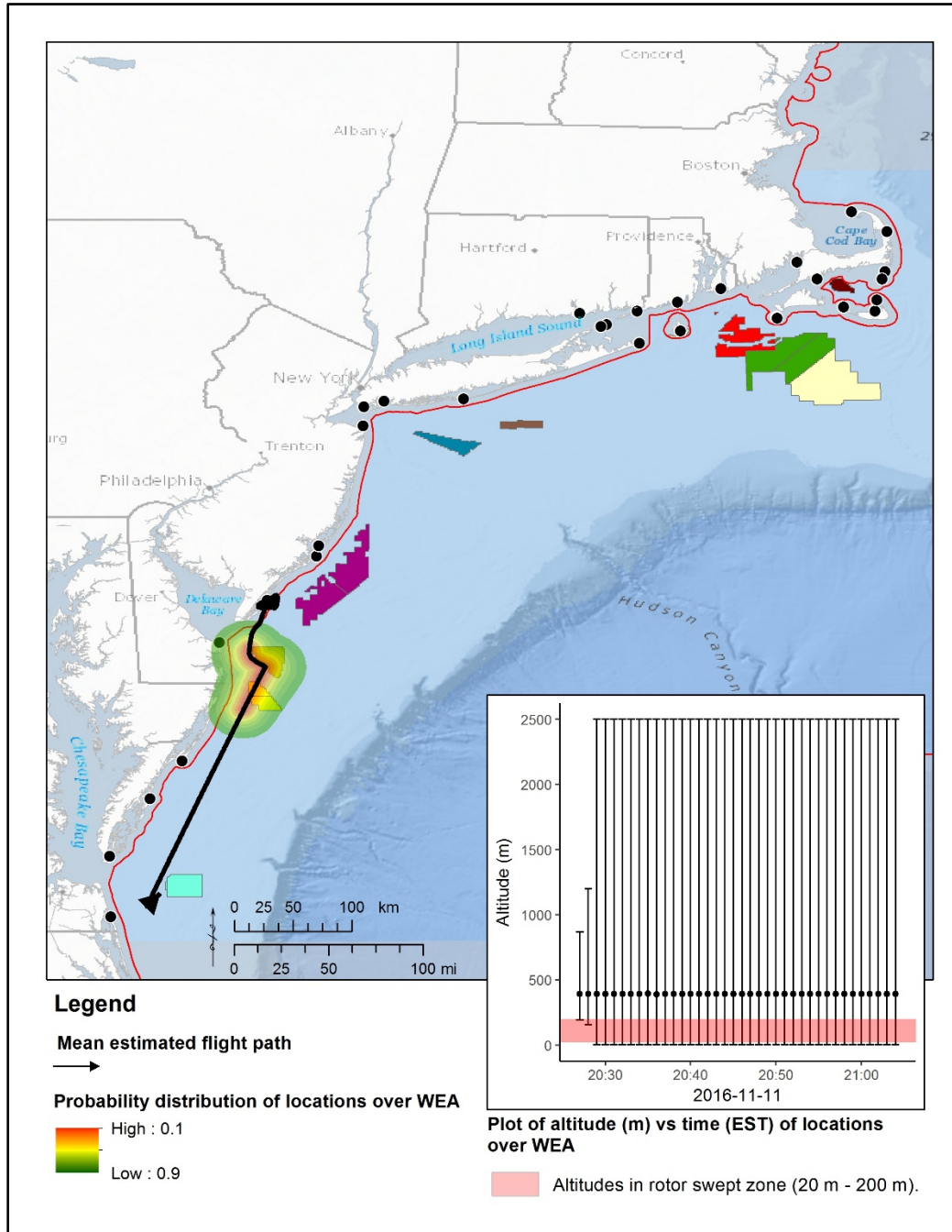


Figure F-24. Estimated flight path of Red Knot ID 48, HY female, tagged in New Jersey, USA.

Probability bands show spatial error around locations during estimated exposure to BOEM Lease Area DE OCS-A 0482 and MD OCS-A 0489 and 0490 on November 11, 2016.

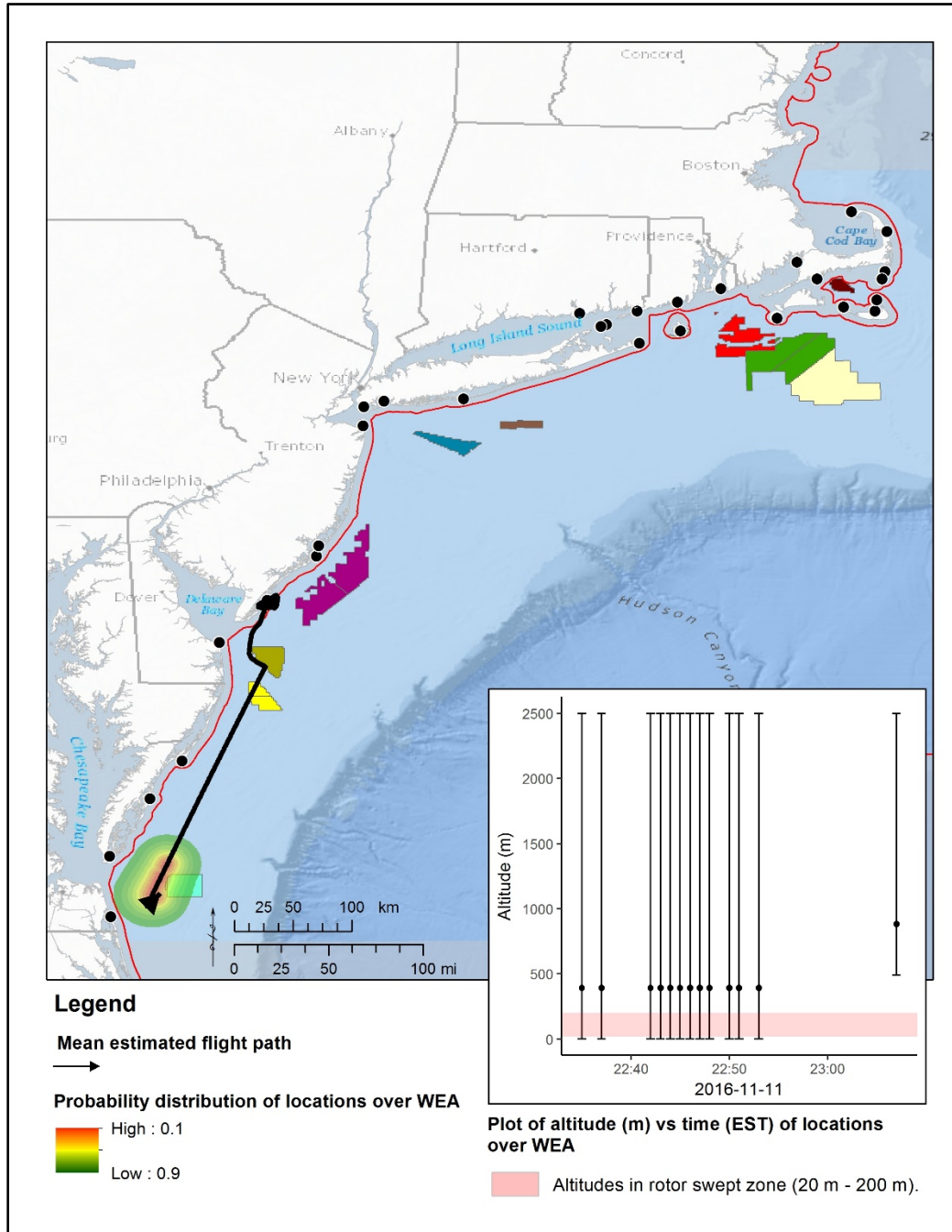


Figure F-25. Estimated flight path of Red Knot ID 48, HY female, tagged in New Jersey, USA.

Probability bands show spatial error around locations during estimated exposure to BOEM Lease Areas VA OCS-A 0483 and 0497 on November 11, 2016.

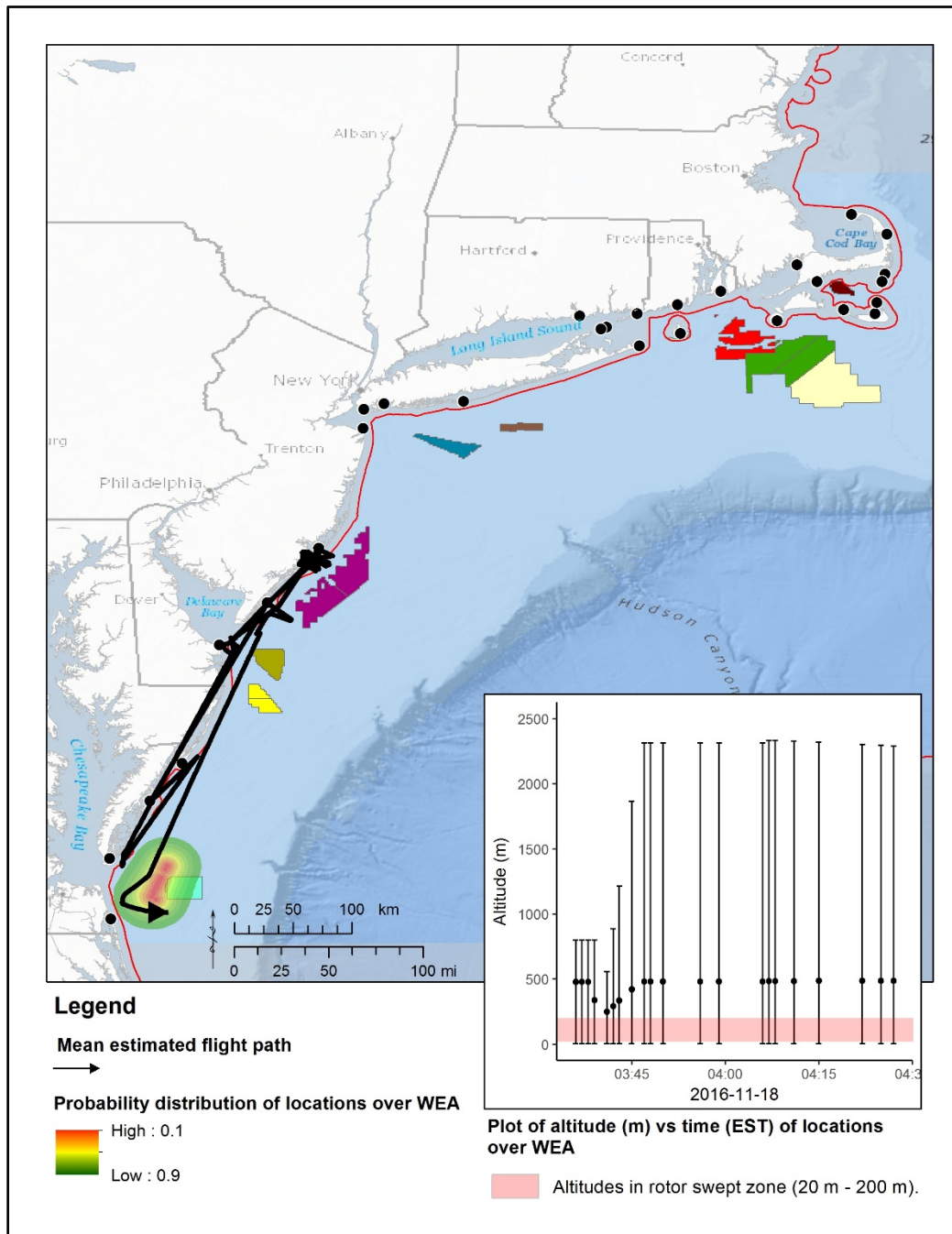


Figure F-26. Estimated flight path of Red Knot ID 47, age and sex unknown, tagged in New Jersey, USA.

Probability bands show spatial error around locations during estimated exposure to BOEM Lease Areas VA OCS-A 0483 and 0497 on November 18, 2016.

13 Appendix E. Summary of supplemental data from Red Knots tagged during spring of 2016 in Delaware Bay, USA

This Appendix summarizes supplemental data from *rufa* Red Knots that were tagged during spring migration at staging areas in Delaware Bay, USA as part of a study on Red Knot migration ecology funded by Environment and Climate Change Canada in partnership with Conserve Wildlife Foundation of New Jersey. These supplemental data provide additional information on movements of Red Knots tagged in at a major stopover area, Delaware Bay, during spring (northbound) migration, with some individuals detected within our Study Area during fall (southbound) migration. We did not include these spring-tagged Red Knots within analyses of the main report because we assumed that their detection probability was lower as there were less towers operating in the Motus network during spring of 2016 relative to fall of 2016. We also assumed that, in the fall, detection probability of spring-tagged birds was lower than that of fall-tagged birds due to increased tag loss over time. Despite these shortcomings, these data provide some interesting insights into the movements of Red Knots tagged during spring at the largest stop-over site on the US Atlantic coast.

During spring migration, most *rufa* Red Knots wintering in South America stopover in Delaware Bay between late April and early June, where they feed primarily on the eggs of horseshoe crabs (*Limulus polyphemus*). The Delaware Bay northbound shorebird stopover includes most of the shoreline of Delaware Bay in both Delaware and New Jersey from just north of the mouth of the bay extending to Bombay Hook National Wildlife Refuge in Delaware and to the Cohansey River in New Jersey. Recent shorebird numbers in the stopover have ranged from 17,000 to 24,500 by 1-day aerial count and over 45,000 using capture-recapture methods to estimate total passage population (Lyon et al 2012). The number of birds wintering in closer areas such as southeast US and the Caribbean islands that come to the Delaware Bay depends on birds' body condition, weather and resources in more southerly stopovers.

13.1 Tag deployment and movement summaries

The tagging areas for this study were located entirely on the New Jersey side of Delaware Bay, centered primarily on four beaches from Reeds Beach to Pierce's Point beach. From May 14 to 25, study partners captured and nano-tagged a total of 110 ASY Red Knots (sex unknown) within these tagging areas. Local movements were tracked using an array seven telemetry towers throughout the Delaware Bay region, and the broader Motus network that included up to 19 additional telemetry stations within the BOEM Study Area, from coastal Massachusetts to Virginia.

A total of 52 individuals were detected within the BOEM Study Area. Of these, 49 individuals were detected during spring (northbound) migration, primarily from stations within Delaware Bay. Red Knots departed Delaware Bay from May 22 to June 2. Seventeen Red Knots were tracked flying northwest from Delaware Bay to the James Bay and Hudson Bay regions of Canada, and five Red Knots departed Delaware Bay to the northeast and entered Federal waters of the US Atlantic OCS.

Of the five Red Knots tracked through in Federal waters during spring, two individuals (id 310 and id 354) were exposed to WEAs on the morning of May 30. Id 310 flew across RI / MA OCS-A 0486 on May 30 at between 3:00 and 4:00 EST (1-2 hours prior to sunrise; Fig. E-1). The flight over the WEA occurred under low visibility conditions (116 m) and rain (precipitation accumulation 0.38 kg/m²), with

wind blowing to the north at 2.5 m/s (wind support 1.1 m/s). Mean flight altitude above the WEA was 502 m (range 300 m to 554 m), indicating that this flight was above the rotor swept zone. Id 354 flew across RI / MA OCS-A 0486 at 6:00 hrs (Fig. E-2) and MA OCS-A 0478 at 7:00 hrs (Fig. E-3). These WEA crossings also occurred poor weather conditions, with low visibility (4,497 m, range 585 m to 6,868 m), rain (precipitation accumulation 2.16 kg/m²), and wind blowing to the north at 7.9 m/s (wind support 6.5 m/s). Mean altitudes of flights across the WEAs were above the rotor swept zone, at 683 m across RI / MA OCS-A 0486 and 383 m across MA OCS-A 0478.

During fall migration, seven Red Knots were detected in the Study Area and arrived between July 23 and August 22. Of these, six individuals passed through Federal waters, including two of the same birds detected moving through Federal Waters in the spring. Four were detected for less than one day as they passed through Study Area, and one (id 169) flew across MA OCS-A 0478 on Aug 8 at 6:00 hrs (sunrise; Fig. E-4). This southbound flight occurred during high visibility conditions (20,000 m) and no precipitation, with wind blowing to the southeast at 3.7 m/s (wind support 3.6 m/s). Mean flight altitude above the WEA was 475 m (range 204 m to 582 m), indicating that this flight was above rotor swept zone.

Two individuals staged within the Cape Cod, Massachusetts region during fall. One arrived on July 26, remained for 8 days and departed to the southeast on August 3. The other arrived on August 22, remained for 43 days, and departed to the southwest towards the mid-Atlantic on Oct 4.

13.2 Discussion

Detections of spring tagged Red Knots were highly variable, only 47% of the birds tagged in Delaware Bay detected by stations on the US Atlantic coast. This could be due to a limited number of towers running in spring of 2016 along the US Atlantic coast (for a map of deployed towers by date, see <https://motus.org/data/receiversMap?lang=en>). From this subset of birds tagged during spring (n=110), only six percent (n=7) were detected during fall, with a maximum tracking duration of 132 days. This is likely due to variable tag retention for glue on-transmitters, ranging from weeks to months (Warnock and Takekawa 2003).

Despite variable detection probability, these data provide new insights on the movements of individual Red Knots within the US Atlantic OCS during both spring and fall migration. Length of stay during spring migration was much shorter relative to fall migration, and most birds with detection data outside of Delaware Bay appeared to fly directly from Delaware Bay towards breeding grounds in Canada. Despite having fewer tracking towers up and running along the US Atlantic coast during spring, we did track flights of some individuals into Federal waters after departing Delaware Bay. While only two individuals were estimated to cross WEAs during spring, these flights both occurred near sunrise on May 30, during poor weather conditions (heavy precipitation and low visibility). Shorebirds may be subjected to more inclement weather during spring migration versus fall (O'Reilly and Wingfield 1995), and this may result in exposure to WEAs under higher-risk conditions for collision.

During spring migration, Red Knots may be exposed to offshore WEAs during flights from wintering areas into Delaware Bay and other stopover areas along the US Atlantic coast (Burger et al. 2012). Delaware Bay is the single most important spring migratory staging site on the US Atlantic coast, likely

bringing a large majority of the *rufa* population near the Atlantic OCS (Niles et al. 2009). Long- and mid-distance northbound migrants can arrive to the US Atlantic coast landing anywhere from Florida to Long Island, New York. However, nearly all pass through Delaware Bay (Clark et al. 1993, Watts and Truitt 2015). Most short-distance migrants also come to Delaware Bay (Burger et al. 2012 a, Niles et al. 2013), but unpublished geolocator tracks show some knots flying directly to breeding areas from southeast US stopovers, bypassing Delaware Bay in some years. Additional exposure may occur when Red Knots move between other important stopover sites in the US Atlantic (e.g. Cape Cod, Massachusetts), and these movements may largely be driven by habitat conditions at stopover sites, such as density of horseshoe crab eggs (Lyons 2017). A focused study examining the exposure of Red Knots to WEAs during spring migration is recommended to more fully assess risk to this species from wind energy development in the US Atlantic OCS.

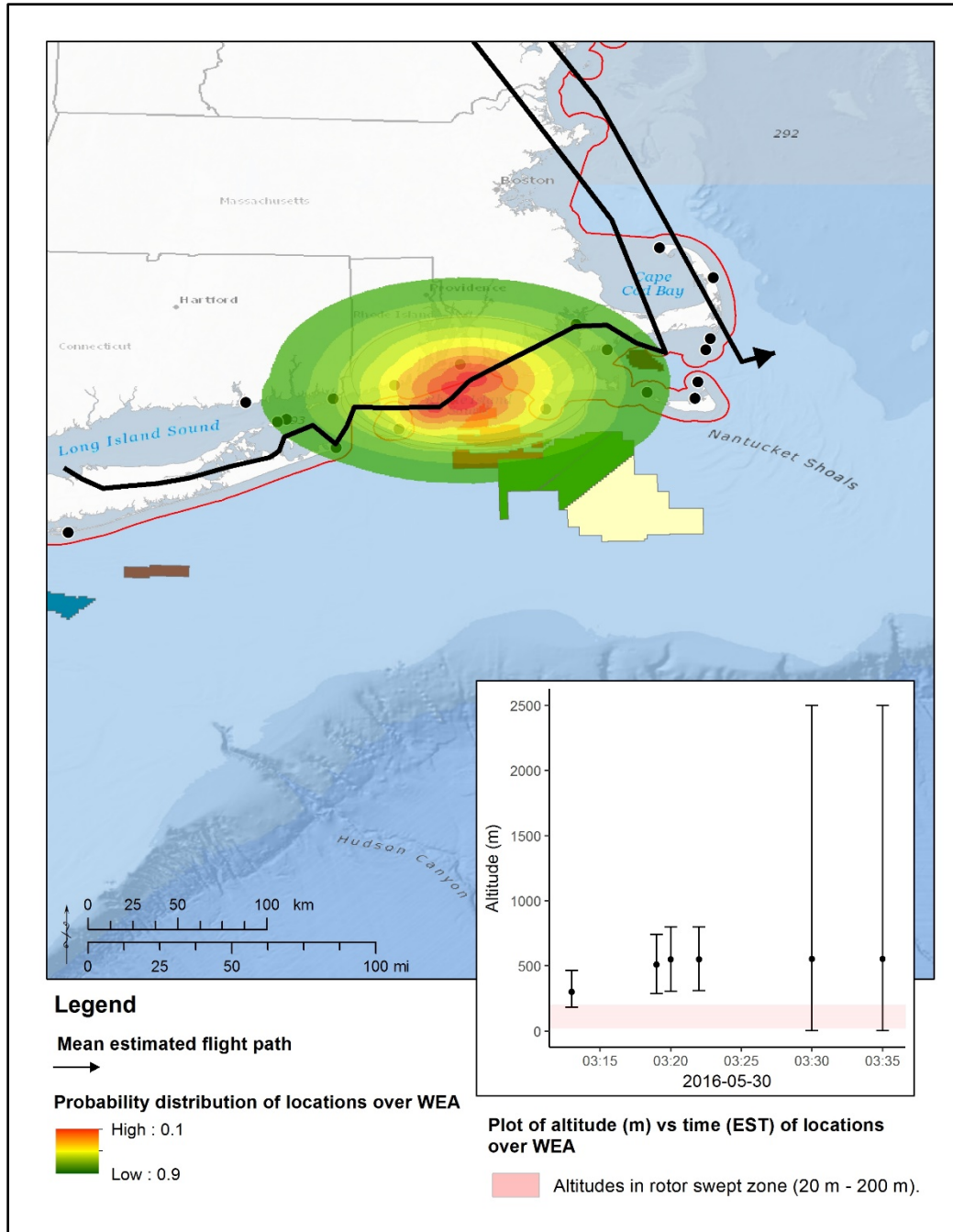


Figure E-1. Estimated flight path of Red Knot ID 310 (AHY, unknown sex), tagged in Delaware Bay, USA during May 2016.

Probability bands show spatial error around locations during estimated exposure to BOEM Lease Area MA OCS-A 0478 on May 30, 2016.

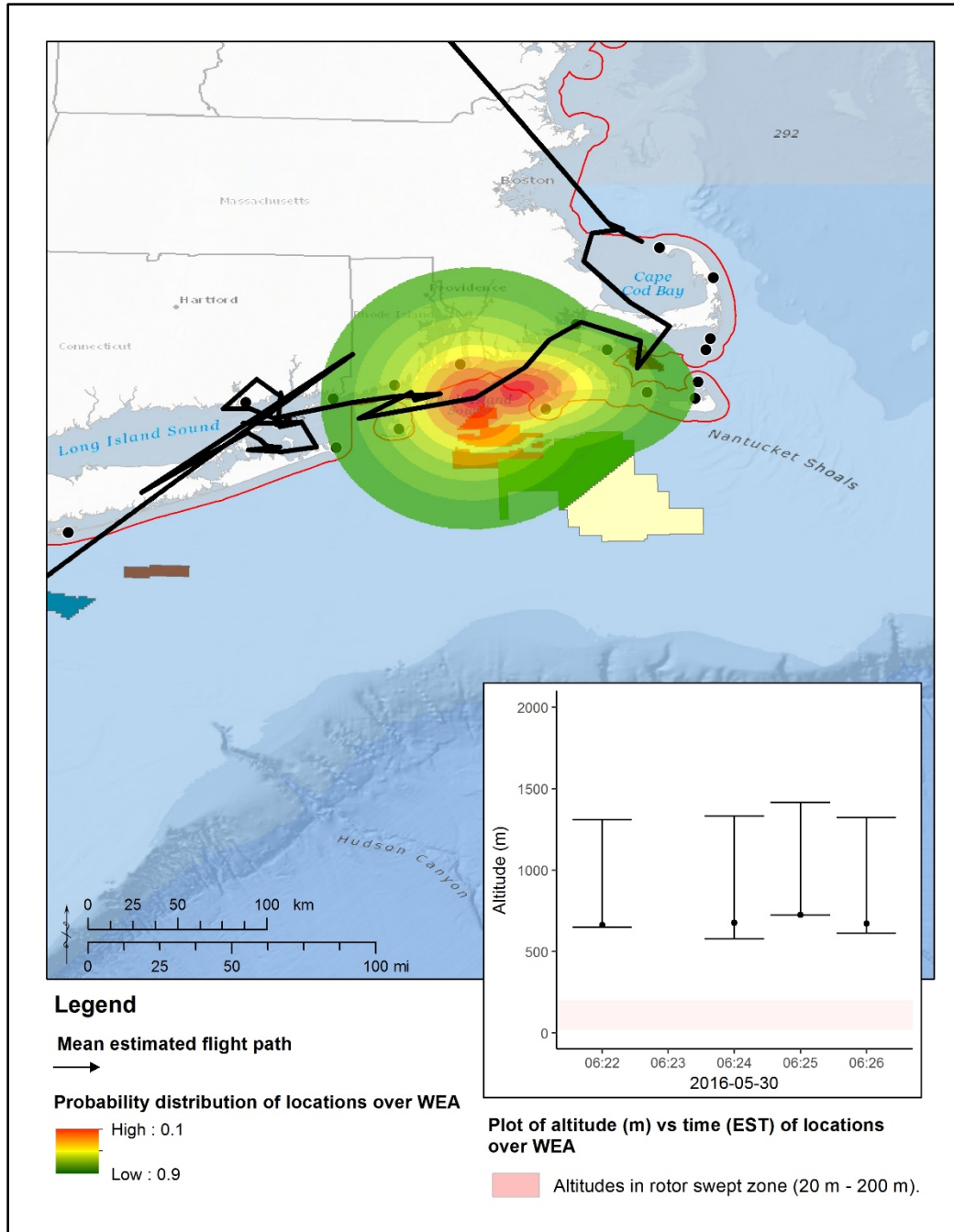


Figure E-2. Estimated flight path of Red Knot ID 354 (AHY, unknown sex), tagged in Delaware Bay, USA during May 2016.

Probability bands show spatial error around locations during estimated exposure to BOEM Lease Area RI / MA OCS-A 0486 on May 30, 2016.

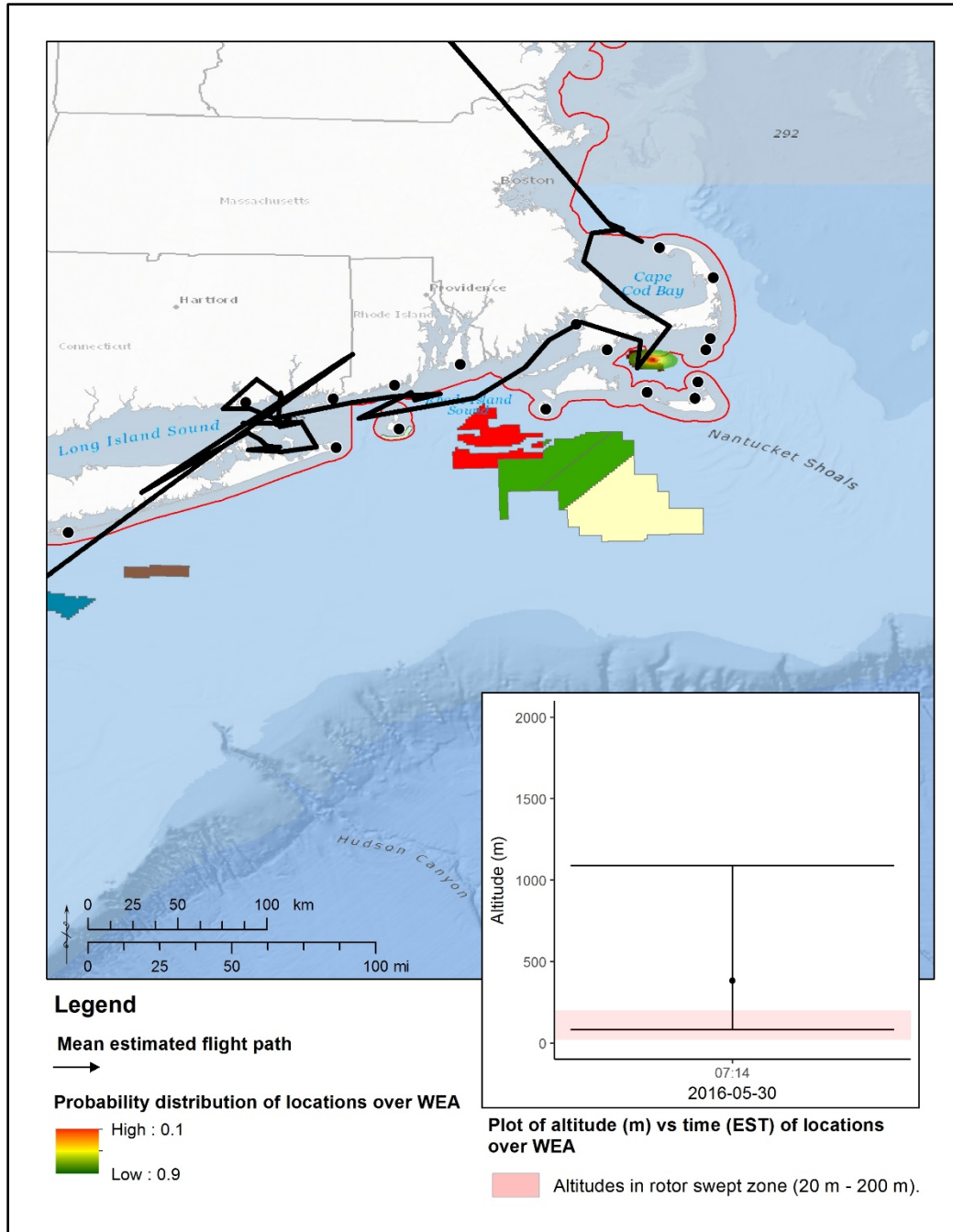


Figure E-3. Estimated flight path of Red Knot ID 354 (AHY, unknown sex), tagged in Delaware Bay, USA during May 2016.

Probability bands show spatial error around locations during estimated exposure to BOEM Lease Area MA OCS-A 0478 on May 30, 2016.

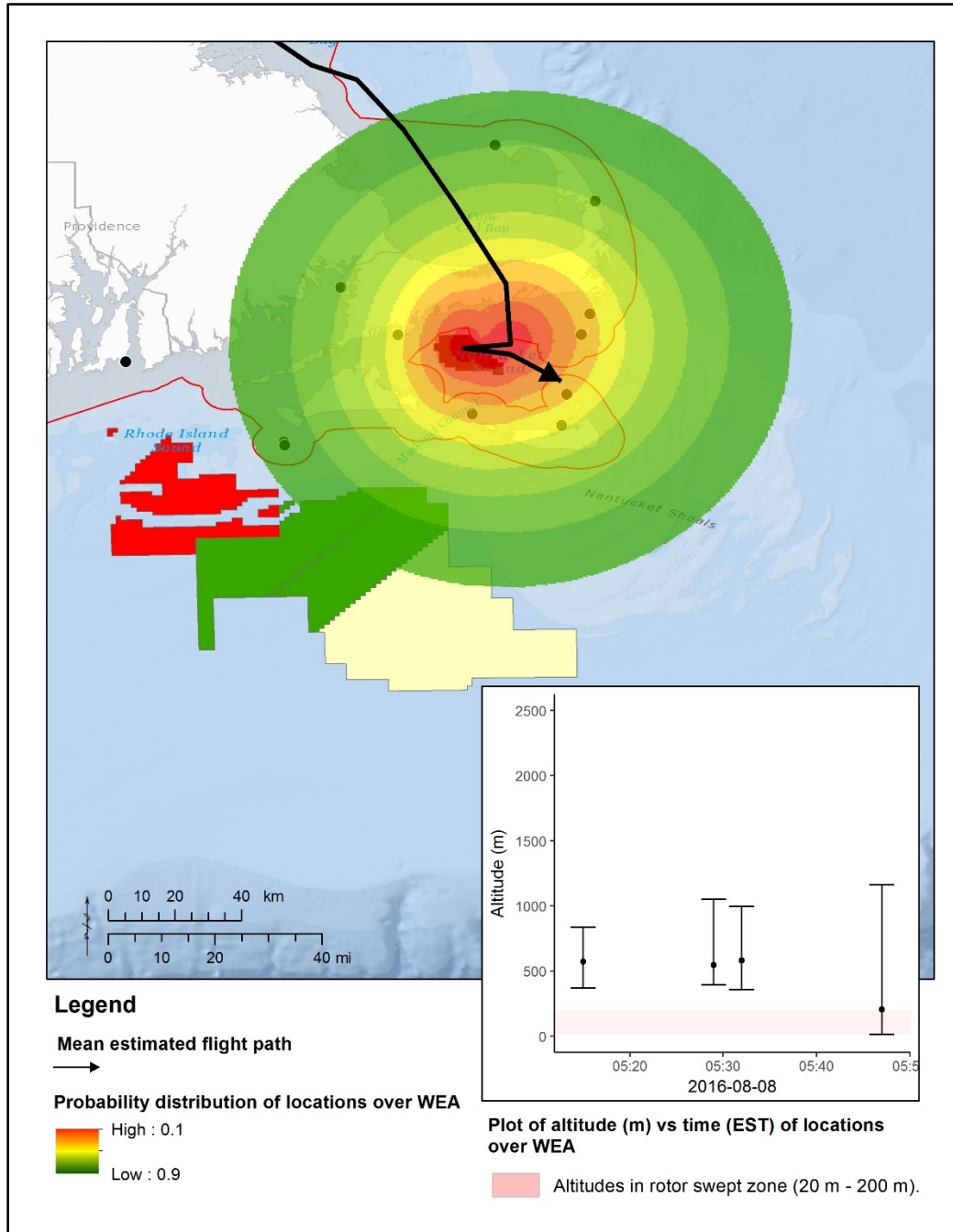


Figure E-4. Estimated flight path of Red Knot ID 169 (AHY, unknown sex), tagged in Delaware Bay, USA during May 2016.

Probability bands show spatial error around locations during estimated exposure to BOEM Lease Area RI / MA OCS-A 0486 on Aug 8, 2016.



Department of the Interior (DOI)

The Department of the Interior protects and manages the Nation's natural resources and cultural heritage; provides scientific and other information about those resources; and honors the Nation's trust responsibilities or special commitments to American Indians, Alaska Natives, and affiliated island communities.



Bureau of Ocean Energy Management (BOEM)

The mission of the Bureau of Ocean Energy Management is to manage development of U.S. Outer Continental Shelf energy and mineral resources in an environmentally and economically responsible way.

BOEM Environmental Studies Program

The mission of the Environmental Studies Program is to provide the information needed to predict, assess, and manage impacts from offshore energy and marine mineral exploration, development, and production activities on human, marine, and coastal environments. The proposal, selection, research, review, collaboration, production, and dissemination of each of BOEM's Environmental Studies follows the DOI Code of Scientific and Scholarly Conduct, in support of a culture of scientific and professional integrity, as set out in the DOI Departmental Manual (305 DM 3).